NOTE TO USERS

Page(s) missing in number only; text follows. Page(s) were scanned as received.

iii

This reproduction is the best copy available.

UMI®

DISSERTATION

EFFECTS OF LOW INTENSITY PULSED ULTRASOUND (LIPUS) AND LONGITUDINAL CORTICAL ALLOGRAFT PERFORATION (LAP) ON ALLOGRAFT HEALING: A BIOMECHANICAL AND HISTOLOGICAL INVESTIGATION

Submitted by

Brandon Santoni

Department of Mechanical Engineering

In partial fulfillment of the requirements

For the Degree of Doctor of Philosophy

Colorado State University

Fort Collins, CO

Summer 2006

COLORADO STATE UNIVERSITY

April 3, 2006

WE HEREBY RECOMMEND THAT THE DISSERTATION PREPARED UNDER OUR SUPERVISION BY BRANDON G. SANTONI ENTITLED EFECTS OF LOW INTENSITY PULSED ULTRASOUND (LIPUS) AND LONGITUDINAL CORTICAL ALLOGRAFT PERFORATION (LAP) ON ALLOGRAFT HEALING: A BIOMECHANICAL AND HISTOLOGICAL INVESTIGATION BE ACCEPTED AS FULLFILLING IN PART REQUIREMENTS FOR THE DEGREE OF DOCTOR OF PHILOSOPHY.

Committee on Graduate Work

Nicole E. Ehrhart

A. Simon Turner

Raoul F. Reiser II

Susan P. James, Co-Advisor

Donna L. Wheeler, Co-Advisor

Department Head/Director

ABSTRACT OF DISSERTATION

EFECTS OF LOW INTENSITY PULSED ULTRASOUND AND LONGITUDINAL CORTICAL ALLOGRAFT PERFORATION ON ALLOGRAFT HEALING

Massive cortical bone allografting suffers from a number of clinical complications including chronic infection, non-union, and fracture all due to a limited degree of graft remodeling within the host, even after extended periods of time *in vivo*. Despite being the preferred biologic alternative to autograft in cases where structural capacity is a clinical necessity, novel means that improve graft healing are significantly lacking. This project was established to investigate the effects of an exogenous, low-intensity pulsed ultrasound signal (LIPUS) either alone or in combination with increased graft cortical porosity (LAP) on allograft healing after four months *in vivo*. Results from this exploratory study will provide preliminary information on the mechanical and biologic response of limbs reconstructed with massive bone allograft using these therapies.

The first part of this study (Chapter 2) was designed to evaluate improvements in the torsional capacity of 12 ovine hindlimbs reconstructed with 5 cm intercalary allografts. Treatment groups included reconstruction with allograft only (-)CTL and autograft only (+)CTL both with no adjuvant therapy, LIPUS, LAP, and LIPUS+LAP. Graft perforation was accomplished by creating 16, 500 μm diameter conduits that extended 10 mm into the cortical endplates. Following euthanasia, the experimental and contralateral

control limbs were harvested and tested to failure in torsion. Reconstructed limbs exposed daily to LIPUS resulted in a 30% increase in ultimate torque to failure ($p=0.229$) and stiffness ($p=0.162$) and promoted the development of 50% more callus with a radiodensity twice that quantified in the negative control limbs. Limbs reconstructed with perforated grafts demonstrated improved torsional capacity though to a lesser degree than LIPUS therapy. Combination therapy (LIPUS+LAP) was not statistically synergistic from a purely biomechanical standpoint but did improve reconstruction stiffness by 40% ($p=0.063$). (+)CTL limbs were completely healed at the four-months time point as demonstrated biomechanically.

In the second part of the study (Chapter 3), decalcified and undecalcified histologic indices of allograft healing were quantified following exposure to LIPUS and LAP and compared to untreated controls. LIPUS and LAP therapies, alone and in combination, resulted in increases in periosteal callus formation and significantly greater bone formation rates (BFR) in this region of interest ($p<0.01$). LIPUS therapy appeared to accelerate endochondral bone formation in the callus producing a stronger, stiffer reconstruction after four months *in vivo*. Longitudinal perforations filled to varying degrees with appositional new bone that extended the length of the 10 mm conduit and demonstrated the efficacy of such a therapy at improving graft revitalization.

The third and final portion of this study (Chapter 4) evaluated the effects of the longitudinal perforations on the structural integrity of the graft prior to transplantation. Uniaxial (n=13 pairs of limbs) and diametral compression tests (n=48 specimens)

revealed insignificant changes in graft integrity as a result of LAP. Specifically, LAP modification reduced the compressive load to failure by approximately 6.7% ($p=0.339$) in uniaxial compression relative to non-perforated grafts. The same form of modification in diametral compression resulted in an 11.1% decrease in ultimate force to failure ($p>0.05$). Within the same diametral compression set-up, transversely perforated grafts (TAP) failed at 80% of the ultimate loads of their non-perforated controls and illustrated the deleterious effects of such a form of graft modification on integrity prior to transplantation.

Overall, this exploratory study has demonstrated the potential of LIPUS and LAP as novel therapies to improve allograft healing. Biomechanics revealed no *statistically* significant improvements relative to the negative control at the =0.05 level, but 30%-40% increases in stiffness may be *clinically* meaningful. This was the first study to show that longitudinal perforations can improve graft revitalization without adversely affecting the integrity of the graft and the only study to date that has illustrated the potential of LIPUS as a stand-alone therapy to accelerate callus formation and graft incorporation without eliciting an adverse cellular response. Future studies are warranted to confirm the trends and significant findings of this pilot study.

Brandon G. Santoni
Department of Mechanical Engineering
Colorado State University
Fort Collins, CO 80523
Summer 2006

ACKNOWLEDGEMENTS

Several individuals and organizations were instrumental in the development and performance of this study.

I would first like to acknowledge my graduate committee, especially my advisor Dr. Donna Wheeler for her confidence in me to independently pursue a relatively unstudied area of research. I would also like to thank Drs. Nicole Ehrhart and Simon Turner for their surgical time and clinical expertise and Drs. Sue James, Raoul Reiser and Christian Puttlitz for their guidance and words of wisdom throughout this process. The histopathological input of Dr. Norrdin and Dr. E.J. Ehrart are also greatly appreciated.

This project would not have been possible without funding provided by the Musculoskeletal Transplant Foundation (MTF). I would like to extend an emphatic thank you to Dr. Hans Burchardt of the MTF for his expert input during the initial grant-writing portion of this study and his continued involvement throughout. I would also like to acknowledge Drs. Neill Pounder and Richard Pearce of Smith&Nephew for their review of the grant and donation of the ultrasound devices.

Several individuals were essential in helping with this study. Jon Kushner and Amy Lyons were instrumental in almost every aspect of this project and I can't thank you both

enough for your tireless efforts. I would also like to thank Millets, Dr. Tatiana Motta, DJ, Scooter, Martini, Kovach and Dr. Chad Lewis for being wonderful friends and co-workers during these last few years. You made the OBRL a wonderful place to learn.

I would like to thank my family: Terry, Todd, Parker, Chloe and my late father, Gary. Without you I wouldn't be the person I am today. Finally, I would like to thank Mindy Barritt. Without your support, I would have never attempted this endeavor. I feel fortunate to have shared my life with you. Thank you.

THIS WORK IS DEDICATED TO GARY AND MINDY

For the things we have to learn before we can do them,
we learn by doing them.

Aristotle

TABLE OF CONTENTS

PREFACE

Replacement of lost bone stock due to tumor resection, arthroplasty revision, sustained trauma or congenital defects remains a common problem in the orthopaedic community. Though autograft remains the gold standard for osseous augmentation, its relative scarcity within the patient prevents it from being used in cases where massive reconstruction concomitant with structural capacity are a clinical and functional necessity. Bone allograft has become a common graft material for use in such cases, though the long-term clinical outcome associated with such grafts leaves much to be desired. Clinical failures in limbs reconstructed with massive allograft result from chronic infection, non-union, and fracture and often necessitate revision surgeries employing additional allografts, megaprostheses, and sometimes amputation. Though bone allograft transplantation has been employed as an orthopaedic intervention for over a century, novel modalities that improve the long-term clinical outcome following allografting are just being realized. These interventions, such as the use of exogenous biophysical stimuli and increasing graft porosity, hold the key to furthering the field of bone allograft transplantation science and may promote a clinical prognosis that far exceeds that which has been achieved to date.

CHAPTER 1. REVIEW OF PERTINENT LITERATURE

ALLOGRAFT TRANSPLANTATION SCIENCE AND THE POTENTIAL ROLE OF EXOGENOUS, BIOPHYSICAL STIMULI AND INREASED CORTICAL POROSITY IN PROMOTING IMPROVED ALLOGRAFT INCORPORATION AND REVITALIZATION

1.1 Allograft Tissue Transplantation.

1.1.1. The Basics.

Allograft tissue transplantation has become commonplace in clinical orthopaedics. By definition, an allograft is a graft of tissue obtained from a donor of the same species as, but with a different genetic make-up from, the recipient into which the tissue is transplanted. Prior to transplantation into a recipient, bone allograft typically undergoes one or more processing steps to minimize the transmission of infection from donor to recipient as well as to attenuate the immunogenicity of transplanted bone. Bone allografts can be used as fresh, deep frozen or freeze-dried grafts, or in a demineralized form. Freezing, lyophilizing (freeze-drying), irradiating, or exposing the graft to harsh chemical treatments limits, if not completely eliminates, the viability of the tissue and therefore bone allograft does not impart osteogenesis but does provide for osteoconduction (Table 1.1). Limited amounts of growth factors, including members of the bone morphogenetic protein (BMP) family, are still present within the allograft producing a potentially osteoinductive matrix.

Conversely, bone autograft is graft material taken from one skeletal location within a patient and transplanted to a separate skeletal site within the same individual. It remains

the "gold standard" method of bone grafting and provides bone-producing cells for osteogenesis (new bone development). Transplanted autograft bone also behaves as an osteoconductive scaffold and results in osteoinductive transformation of cells into osteoblasts. Problems with autograft include donor site morbidity in approximately 25% of all patients lasting up to five years as well as limited supply, as it is typically harvested from the iliac crest, rib, or fibula [45, 102].

Table 1.1. Biologic Comparison of Allograft and Autograft Bone

	Autograft	Allograft
Immunogenicity	-	+
Osteogenesis	+	-
Osteoconduction	+	+
Osteoinductoin	++	+/-
Union	Rapid	Slow
Donor Site	Donor Site	-
Quantity	Limited	Unlimited

Orthopaedic surgical procedures involving the use of allograft range from soft tissue replacement to reconstruct knee damage or severed ligaments to cortical allograft bone struts and corticocancellous chips employed for reestablishing lost bone stock in total joint reconstructions. In fact, the main use of transplanted bone in orthopaedic surgery today is replacement of extensive bone loss associated with failed joint replacement or tumor surgery [87]. From one bone bank over a 10-year period, 83% of all bone graft was used in revision arthroplasties, 12% in fracture treatment, 2% in tumor surgery and 3% in orther orthopaedic procedures [86]. Massive allograft bone, used as either an osteochondral graft or an intercalary graft (Figure 1.1), is the primary source of bone graft material for use in limb salvage procedures after oncological tumor resection.

Currently, more than 975,000 musculoskeletal allograft procedures including transplantation of soft tissues occur each year in the United States [55]. Bone is the second most transplanted tissue after blood and constitutes over 200,000 of the tissue transplantation procedures in the U.S. annually [35]. However, the risks of bone transplantation are well documented and the biology of allograft incorporation remains unpredictable and poorly understood. Cortical allograft bone has been found to incorporate slowly into host bone resulting in allograft susceptibility to non-union, fracture, infection and fatigue failure [32, 33, 45, 79]. Complications associated with these types of structural allografts have become all too frequent with the majority of such complications occurring within the first three to four years following intervention beyond which the graft appears to become a relatively stable, competent system [71]. Such early complication rates have caused surgeons to

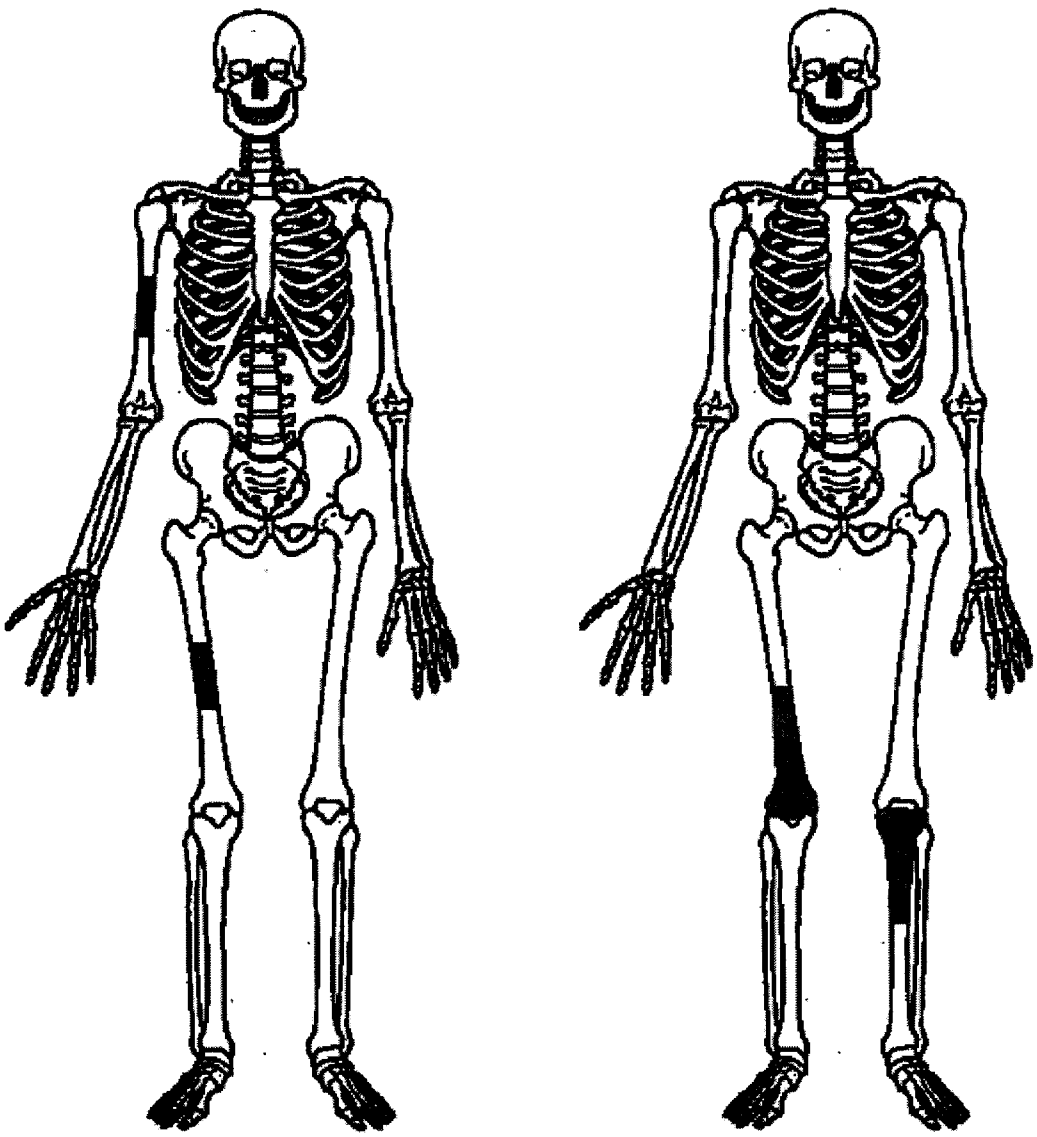

a.) Intercalary Allograft

b.) Osteochondral Allograft

Figure 1.1. Massive allograft bone used to reconstruct a limb following oncologic tumor resection is primarily utilized as either (a) an intercalary allograft replacing the mid-diaphysis of a long bone (in this case the humerus or the femur), or (b) an osteochondral allograft replacing the distal or proximal portion of a long bone (in this case the distal femur or the proximal tibia). Intercalary allografts consist of osseous tissue only, while osteochondral allografts are comprised of both osseous tissue and cartilage that serves to maintain the function of the adjacent joint.

abandon allograft use following tumor resection in favor of large metal prostheses for skeletal reconstruction. Despite exhibiting low initial complication rates, however, these prostheses tend to fail with time [13, 14, 53].

1.1.2. The Biology of Bone Allograft Incorporation.

Clinical studies have shown that massive allograft bone has a 50% to 75% success rate at 10 years [15, 41, 81], while other orthopaedic implants, such as total hips and knees have a 10-year success rate of approximately 90% and a 20-year success rate approaching 80% [1]. Tumor recurrence, non-union of the allograft bone with the host, infection, and severe immune reaction all lead to mechanical failure of the allograft and serve to illustrate the inherent biologic variability of these transplants within the host [16, 32, 33, 41, 58, 70, 79, 80]. Antigenic incompatibility between donor and host and the subsequent immune response remains a significant but poorly understood problem and often manifests within a few months of implantation. Reports on the outcomes and complications associated with long-term osseous reconstruction using structural allografts have indicated fracture rates ranging from 10.4% to 19% [32, 33, 41, 70, 71]. This is seen most often in structural allografts that are effectively alloimplants because they do not incorporate fully with the host. Fracture or non-union failures most frequently arise within several years after implantation [70, 71] and fatigue failures have recently been reported to be the result of an increase in microfracture density within the host[112].

Several studies have been performed on retrieved allografts to determine the degree of radiological or histological incorporation of the graft by the host. Graft incorporation is defined as the biological interaction between the graft material and the host resulting in bone formation providing adequate mechanical properties [86]. The aforementioned studies show varying degrees of bone remodeling [32, 33, 49] and immunological responses [32, 33, 58]. It has been shown that there are a few potential histological outcomes following bone transplantation [12]. In the first and most common outcome, the graft is accepted somewhat reluctantly despite antigenic incompatibility between the host and the donor. This case is characterized biologically by limited remodeling of the graft and modest periosteal new bone formation. Such grafts generally proceed to a satisfactory clinical outcome. More often, however, the allograft is rejected because of strong genetic disparity leading to an adverse immune response and ensuing graft resorption.

The first biologic process observed after bone transplantation is hematoma formation followed by an early inflammatory phase largely at the periphery of the graft and peaking at 14 days post-implantation [10]. Lymphocytes continue to proliferate and over the next eight weeks the allograft is enveloped by a fibrovascular stroma that permits osteogenic precursor cells to be delivered to the graft. The preliminary result is osteoclastic activation and graft resorption with a concomitant decrease in graft mass with increasing graft porosity [36]. Remodelling commences as the graft is revascularized and new bone formation is the end result. Modern allograft processing renders the allograft non-viable with few intact cells and little osteoinductive protein [100]. Vascular infiltration and subsequent new bone development within the graft occurs to a very limited degree and

only superficially [33]. Barring severe and chronic immune response, tumor recurrence, or other clinical complications, union at the host-allograft junction occurs at about 12 months post-transplantation [32]. If incorporation is inhibited during this initial period, the host is unable to integrate with the allograft and the chances of mechanical failure are greatly increased. Non-union, by definition, is a mechanical failure. Structural allografts such as intercalary and osteochondral allografts have very limited biologically activity and hence function largely in a passive load-bearing capacity.

1.1.3. Allograft Immunogenicity.

Orthopaedists have understood for decades that bone allografts elicit transplantation immunity and that this immunogenicity may cause higher failure rates of such grafts [37, 44]. Cortical allografts have traditionally functioned poorly and unless they are modified, they usually invoke an extensive immune response that enhances bone resorption and may ultimately lead to mechanical failure Curtiss et al. [26] and Herndon and Chase [52], in early attempts to reduce the immunogenicity of transplanted allograft, incorporated freezing or freeze drying of the tissue prior to transplantation. Advances in transplantation immunology and a growing interest in bone allografts have resulted in more advanced means by which to measure the elicited immunogenicity of such grafts and its relationship to particular techniques of preservation. Cytotoxicity assays for the humoral (antibody-based immunity) and cell-mediated (cell-based immunity) immune responses have indicated that freeze-drying and deep-freezing of bone allografts markedly reduce their ability to evoke an immune response in the graft recipient [11, 20, 51]. Stevenson [101]

demonstrated with canine osteochondral allografts of the proximal radius that freezing of the graft had a marked effect on reducing humoral antibody titers and cell mediated immunity in the graft recipients, though throughout the 42 week study period, both arms of the immune response were still detectable. Burchardt and Enneking [18] as well as Friedlaender [37] have also confirmed that though the relative success of frozen bone allograft is due to reduced immunogenicity, the frozen bone itself is still somewhat immunogenic.

A corollary to freezing the allografted tissue is an almost complete loss of cellular viability in the specimen. Though such a processing technique has shown promise at reducing immunogenicity, even frozen implants have been reported to fail approximately 25% of the time [45]. Despite the preservation technique, human cortical allografts, like fresh cortical allograft, remain significantly weaker than cortical autografts for at least six months after transplantation due to an initial resporptive phase, the degree of which seemingly dependant on the immunogenicity of the transplanted tissue. Beyond this critical stage, new bone deposition occurs, but at a much slower rate that in cortical autografts [45]. Transplanted bone must be clean, sterile, and free from infection with preservation of its natural biological and biomechanical properties. Aseptic processing requires the graft to be handled in a sterile manner in a controlled environment. It involves thorough debridement and cleansing of grafts and the use of antibiotics and treatment solutions. Terminal sterilization relies on chemicals, gamma-irradiation, gas or autoclaving to achieve sterility. Gamma irradiation is widely used and a dose of approximately 40kGy has been reported necessary to sterilize HIV in bone. However,

adverse effects on graft biomechanics have been reported, with decreases of *in vivo* torsional strength of up to 60% relative to non-irradiated controls [43].

1.1.4. Effects of Local Mechanical Environment on Allograft Healing.

In addition to biologic factors that have proven to be deleterious to the healing progression of allograft tissue, fixation technique and the resulting local mechanical environment of the reconstructed limb have also been cited as factors that may have significant impact on the clinical outcome. Fixation of long bones following massive tumor resection and reconstruction with allograft is accomplished via one of two methods: intramedullary (IM) fixation via nailing or compression plating. Clinical reports have implicated that traditional method of fixation with plates results in a poorer clinical outcome, whereas intramedullary nailing has been reported to have fewer clinical failures. Specifically, Vander Griend [105] reported significantly higher rates of allograft fracture following plate fixation in eighty-three patients whom had undergone tumor resection in the femur, tibia, or humerus compared to those limb reconstructed with intramedullary nailing. The presence of the screw holes (stress concentrations) in the non-viable graft promote graft fracture. Furthermore, in many instances, intramedullary nailing provides for superior clinical stability, especially immediately following the surgical procedure, to bone plates in the treatment of complex long bone fractures. With regard to the degree of allograft incorporation and healing, Benevenia et al. [8] reported that despite eliciting less torsional stability immediately following allograft reconstruction, plating resulted in clinically superior degrees of healing as measured via

radiographic, mechanical, and histomorphometric analyses using a bilateral canine model employing both IM nailing and plating. These authors concluded that a less stable form of fixation may be preferred to promote callus formation and the ensuing allograft incorporation by the host.

1.1.5. Graft Modification as a Means to Promote Allograft Incorporation.

Seeking a means of improving allograft incorporation, researchers first looked to increase the cortical porosity and exposed surface area of cortical allograft so as to provide increased access to surrounding vasculature and the host of cells responsible for inducing the reparative cascade. Tarsoly et al. [60, 104] first reported considerable histological enhancement of cortical allograft incorporation after drilling numerous 1 mm diameter holes perpendicular to the longitudinal axis of 20 cm canine femoral allografts. At two weeks following transplantation, the perforated grafts showed considerably more vascularized granulation tissue penetrating the graft via the drill holes compared to contralateral, non-perforated controls. By four weeks, the holes were filled with a network of thick bone trabeculae while non-perforated controls qualitatively exhibited increased cortical resorption. At the eight-week end point of this study, the perforated grafts had nearly been completely substituted with new bone.

Burchardt et al. [17], using perforated, autologous canine fibular transplants, reported rapid deposition of trabecular bone within the transverse conduits, but found no evidence of accelerated spatial and temporal repair as a result of the graft preparations. These initial

findings indicated the potential of cortical perforations at accelerating the incorporation and remodeling processes, but no clinical studies came out of these early reports.

Researchers have since applied to the appendicular skeleton partial demineralization combined with laser perforation of bone used in maxillofacial applications to improve the osteoconductivity of the tissue. *In vivo* animal studies have shown that partial cortical demineralization combined with laser perforations perpendicular to the long axis of the allograft have beneficial effects in terms of incorporation and remodeling [66-68, 42, 78], presumably by further increasing the cortical porosity relative to perforations alone. However, such surface modifications render the allograft less mechanically stable. It has been demonstrated that such treatments reduce the flexural rigidity to 60% of the rigidity of original tissue [65]. In contrast, laser perforation alone perpendicular to the long axis of the cortical allograft has been established to have only minimal effects in terms of altered flexural rigidity of whole bone and compressive mechanical performance, but the beneficial biological response seen with partial cortical demineralization was lost.

Recently, a large animal study [66, 67] evaluated IM fixed allografts that underwent either no processing (control), transverse perforation of the graft, or partial demineralization combined with transverse laser perforation inducing the formation of 300 μm holes. It was found that animals with partial demineralization exhibited a large degree of resorption as indicated by the formation of persistent resorption lacunae, whereas transplanted demineralized and laser-perforated allografts exhibited almost complete incorporation into the host at the study's nine-month endpoint. The actual mechanism

through which partial demineralization combined with laser perforation enhances the biologic response is still under investigation, but may be associated with an increased exposed surface area and increased porosity allowing access to surrounding vasculature.

Though it does appear that the osteogenic effects of laser perforation perpendicular to the long axis of the allograft depend on the degree of cortical demineralization, perforation along the longitudinal axis would provide a more direct access for bone remodeling cell infiltration and may not be dependent on cortical demineralization. Longitudinal perforations extending a few millimeters into the cortical shell would appear to provide direct access of bone cells for creeping substitution of reparative tissue while minimally affecting the overall strength of the implanted allograft.

1.2 Mechano-regulation & Adaptation of the Skeletal System. The Role of Biophysical Surrogates to Mechanical Force Loading.

Skeletal health requires appropriate mechanical stimuli (strain) that have been hypothesized to act via mechanotransduction pathways within native bone tissue [25]. Such mechanosensory mechanisms, which have been demonstrated in osteoblasts [27], osteoclasts [76] and osteocytes [19, 92, 110], thereby maintain the form and architecture of the surrounding tissue and modulate the remodeling responses exhibited during normal ambulation, or after sustained skeletal trauma, be it in the form of fracture or the augmentation of lost host bone stock due to oncological tumor resection with cortical allograft. Several authors [25, 47, 63, 69, 84, 95, 96] have provided some insight into the possible mechanisms involved in bone's response to physiological mechanical force-loading,

contended by some to have been initially introduced by Wolff [113] and known as Wolff's Law, including the stimulation of vascular activity [106]. Specifically, force-loading has been shown in numerous studies to produce micromechanical strains in living tissue that result in biochemical events at the cellular level. These elicited events moderate the physiological response and ultimately promote healing.

This healing progression is a complex biological process that involves the spatial and temporal orchestration of numerous cell types and genes, combined with the organization of an extracellular matrix, all working in unison towards restoring the bone's structural integrity and rapid return to full function. Much thought has been devoted to finding a way to accelerate or augment these reparative processes that have developed over millions of years of vertebrate evolution. Of the six million fractures that occur annually in the United States, the healing progression in 10% is delayed (i.e. not healed in three months) and a significant subpopulation of these delayed unions do not heal by nine months, and are thus characterized as non-unions. Though the exact mechanism through which the healing progression becomes impaired is unknown, several disciplines of bioengineering and biotechnology are currently involved in efforts to augment and accelerate the fracture repair process.

The osteobiologic approach to fracture augmentation includes autogenous or allogeneic bone graft supplementation, artificial materials (i.e. hydroxyapatites) used as bone graft substitutes, and the use of purified or recombinant molecules like rhBMP-2 and –7 (i.e. OP-1) with osteoinductive potentials. The combination of biomaterials like the calcium

phosphates with proteins such as OP-1 has provided the physician with a new tool in the form of an orthopaedic tissue engineered device that is both osteoconductive and osteoinductive and has been shown to regenerate bone in cases of trauma, tumor resection, arthroplasty, and spine fusion [22, 40].

The biophysical approach to aid fracture healing includes such strategies as controlling fixator stiffness to passively regulate the biomechanical environment of the fracture healing process [115] to the exogenous application of physical forces in the biological range in the form of pulsed electromagnetic fields (PEMF) [2, 75], low intensity ultrasound [29, 48], high frequency, low magnitude mechanical stimuli [90, 91, 93, 94] and direct electric current [34, 72]. The scientific underpinning for the biophysical approach is that they serve as non-invasive, exogenous surrogates for the regulatory signals normally arising through functional loading of the skeleton (Wolff's Law) that have become absent because of the sustained trauma.

The first modern case of healing using direct current stimulation was reported in 1971 in treating non-unions of the medial malleolus [34]. This means of electrical stimulation has since been utilized as an adjunct to spinal fusion [62] as well as in the treatment of congenital pseudoarthrosis of the tibia [82] and osteonecrosis of the femoral head [99]. One such direct current stimulator, EBI's® OsteoGen -D™, has been deemed appropriate for high-risk fractures as an adjunct for bone graft surgery by supplying 20 μA of current through a titanium mesh cathode to the host bone and the graft material. This device is

surgically implanted to assure patient compliance and provides continuous treatment 24 hours per day for up to 6 months [2].

Inductive coupling stimulators induce a current in tissue by generating a time-varying magnetic field around them. Such stimulators come in two types. The first uses an on-off pulse of power delivered in "bursts" at 15 Hz and is known as PEMF. The other type of stimulator, known as CMF (combined magnetic field) delivers a time-varying signal in a sinusoidal manner at 76 Hz and is superimposed on a constant magnetic field. PEMF was first used in the treatment of non-unions in the 1970s [5], and since that time, most clinical publications relating to the use of PEMF have dealt with their efficiency at healing delayed or full non-unions in the tibia, femur and scaphoid [6, 9, 39]. Unlike direct current stimulators, inductive coupling stimulators are not implanted but instead stimulate healing in an exogenous fashion. Modern PEMF and direct current stimulators (Figure 1.2) are manufactured by EBI® and Orthofix® and can require up to 10 hours of continuous stimulation to produce the desired effect[2].

1.3 Ultrasound Based Bone Healing: An Assessment of the Evidence.

Ultrasound, a form of mechanical energy that can be transmitted in organisms as high frequency acoustical pressure waves, has been used widely in medicine as a therapeutic, operative and diagnostic tool. Conventional therapeutic and some levels of operative ultrasound use intensities as high as 1 to 5 W/cm^2 and can cause considerable heat and necrosis in living tissues as evidenced by the first reports of the effects of such intensities

on bone tissue [3, 28]. Despite the adverse effects of using such intensities on bone, such heat production has proven beneficial for physical therapists to decrease joint stiffness, reduce pain and muscle spasms, and improve muscle mobility [30]. Ultrasound at intensity levels ranging from 5-300 W/cm^2 has found use as a surgical instrument to fragment calculi, ablate diseased tissues such as cataracts, and remove polymethylmethacrylate bone cement during revision arthroplasty [111]. At the other end of the intensity spectrum, much lower magnitudes in the range of 1-50 mW/cm^2 are used to drive diagnostic tools to image peripheral blood flow, vital organs, fetuses, and metabolic disorders such as osteoporosis [59]. Coincidentally, the same intensities have been used to evaluate fracture callus during healing [73, 74]. Such low intensities induce minimal heating in tissue and are therefore considered nonthermal and nondestructive.

By definition, ultrasound is a form of mechanical energy that is transmitted through and into biological tissues as an acoustic pressure wave at frequencies above the limit of human hearing. Presumably, these acoustic pressure waves mimic a mechanical signal that takes full advantage of bone tissue's sensitivity to low-level physical signals [91, 93]. However, this acoustically driven mechanical signal induces peak strains ($<1\mu\varepsilon$) several orders of magnitude lower than those generated by functional load bearing [96], while the rates of loading induced by ultrasound are several orders of magnitude higher. Nevertheless, extremely low-level, high frequency mechanical signals persist in functionally loaded bone [38] and represent strong regulatory signals to skeletal tissue [54] even during fracture healing [46].

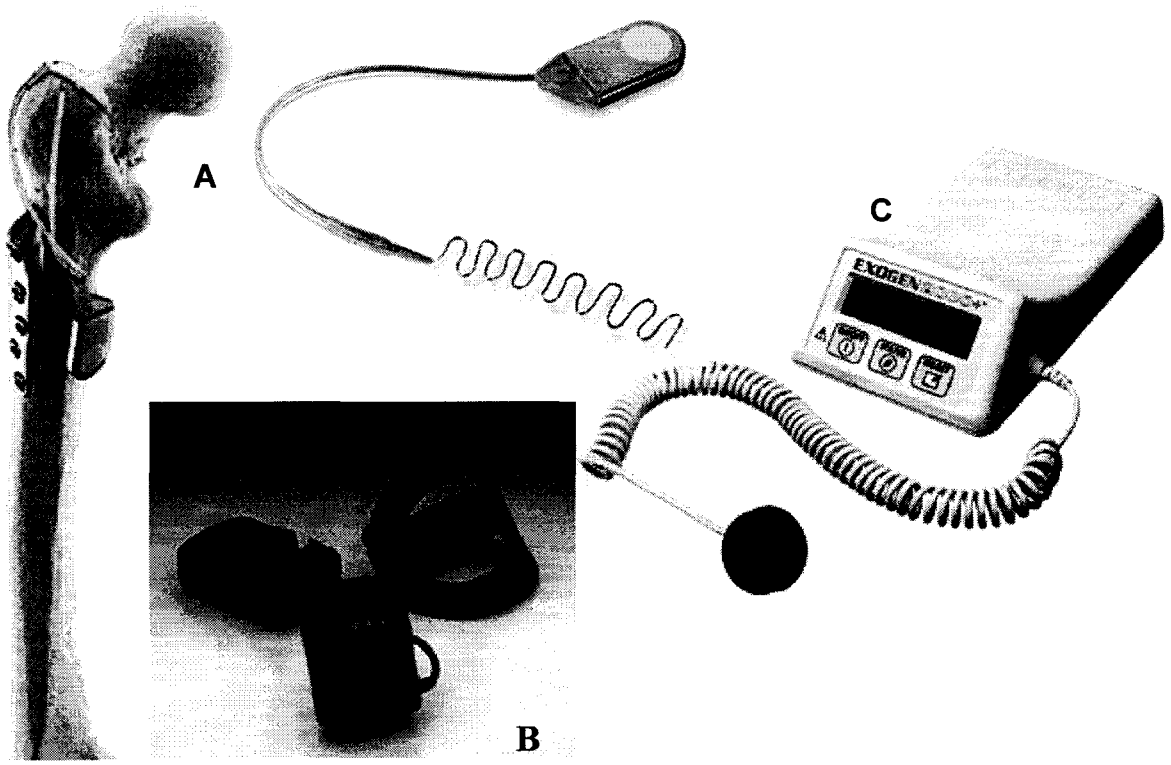

Figure 1.2. (A) EBI's® OsteoGen™ is a surgically implanted bone growth stimulator for the treatment of long bone nonunions and is a useful adjunct for the treatment of nonunions when surgery is already planned or when patient compliance may be a concern. Because the OsteoGen® is totally surgically implanted, patients are assured of therapeutic treatment directly at the nonunion site 24 hours a day for up to 6 months. The OsteoGen® bone growth stimulator is compatible with bone graft surgery in the surgical treatments (internal and external fixation) commonly used for the management of nonunions. (B) EBI's® PEMF Bone Healing System® is used as an adjunctive treatment alternative in the treatment of nonunions, failed fusions, and congenital pseudarthroses in the appendicular system. (C) The EXOGEN 2000+ device provides a non-invasive therapy for the healing of nonunion or the acceleration of fresh fracture healing that the patient administers at home for 20 minutes daily until a physician determines the fracture to be sufficiently healed to discontinue device use. The device transmits a low intensity ultrasound signal to the fracture site through coupling gel. Ultrasound is high frequency sonic pressure waves. The device provides low intensity ultrasound of 30 mW/cm^2, which is comparable to the diagnostic ultrasound intensities used in sonogram (fetal monitoring) procedures, and is 1% to 5% of the intensities used in conventional therapeutic ultrasound.

The complexity in elucidating how low-level acoustic signals interact with bone and connective tissue lies in the complex response of living tissue to these high-frequency ultrasonic stimuli. On passing through the tissue, the ultrasonic energy is absorbed at a rate proportional to the density of the tissue. Thus, the radical changes in density inherent in a healing callus, due to the various tissue types present, may well establish gradients of mechanical strain which, as already mentioned, are recognized as strong determinants of bone-remodeling [47]. Absorption of the ultrasound signal also results in energy conversion to heat and while this effect is extremely small (<1°C) enzymes such as MMP-1, a collagenase known to be present during healing, are extremely sensitive to small variations in temperature. Ultrasound, therefore, may serve to reestablish or normalize the effective metabolic temperatures in areas where blood flow has been compromised such as those in the immediate vicinity of a fracture. Though this effect may seem somewhat insignificant it may be biologically profound. Furthermore, at interfaces of distinct densities, such as at bone-callus surfaces, much of the incident radiation energy will be reflected, resulting in complex gradients of acoustic pressure through the tissue.

The differential energy absorption of ultrasound also induces the movement of fluid across surfaces, a phenomenon know as acoustic streaming (Figure 1.3), particularly in regions where major quantities of bulk fluid are found [7, 89]. This acoustic streaming and the resultant fluid flow stimulate a dynamic physical environment and may mechanistically advance signal-transduction pathways, a process referred to as mechanotransduction. At its most basic mechanical level, the enhanced movement of

fluid increases nutrient delivery and waste removal and may well serve as a conduit for pluripotent cell lineages that ultimately play a role in the healing progression. It is likely that the acoustic signal is recognized and is strongly influential in the biology of bone cells and their progenitors. Regardless of its form, ultrasound results in mechanical perturbations of the tissues within its path and inextricably links ultrasound to Wolff's law, the "form follows function" foundation of orthopaedics.

The initial studies investigating the potential effects of ultrasound on bone healing were performed back in the 1950's and reported mixed results ranging from high degrees of tissue necrosis as a result of exposure to a continuous 5-20 W, 800kHz signal [3, 28], to enhanced bone callus formation in a controlled, paired study of radial fractures in rabbits [23]. The first clinical use of ultrasound to stimulate fracture healing was reported only a few years later by Italian authors in a study of eight patients where daily treatment resulted in an increase in periosteal callus formation [24]. Thirty years later, in a study of

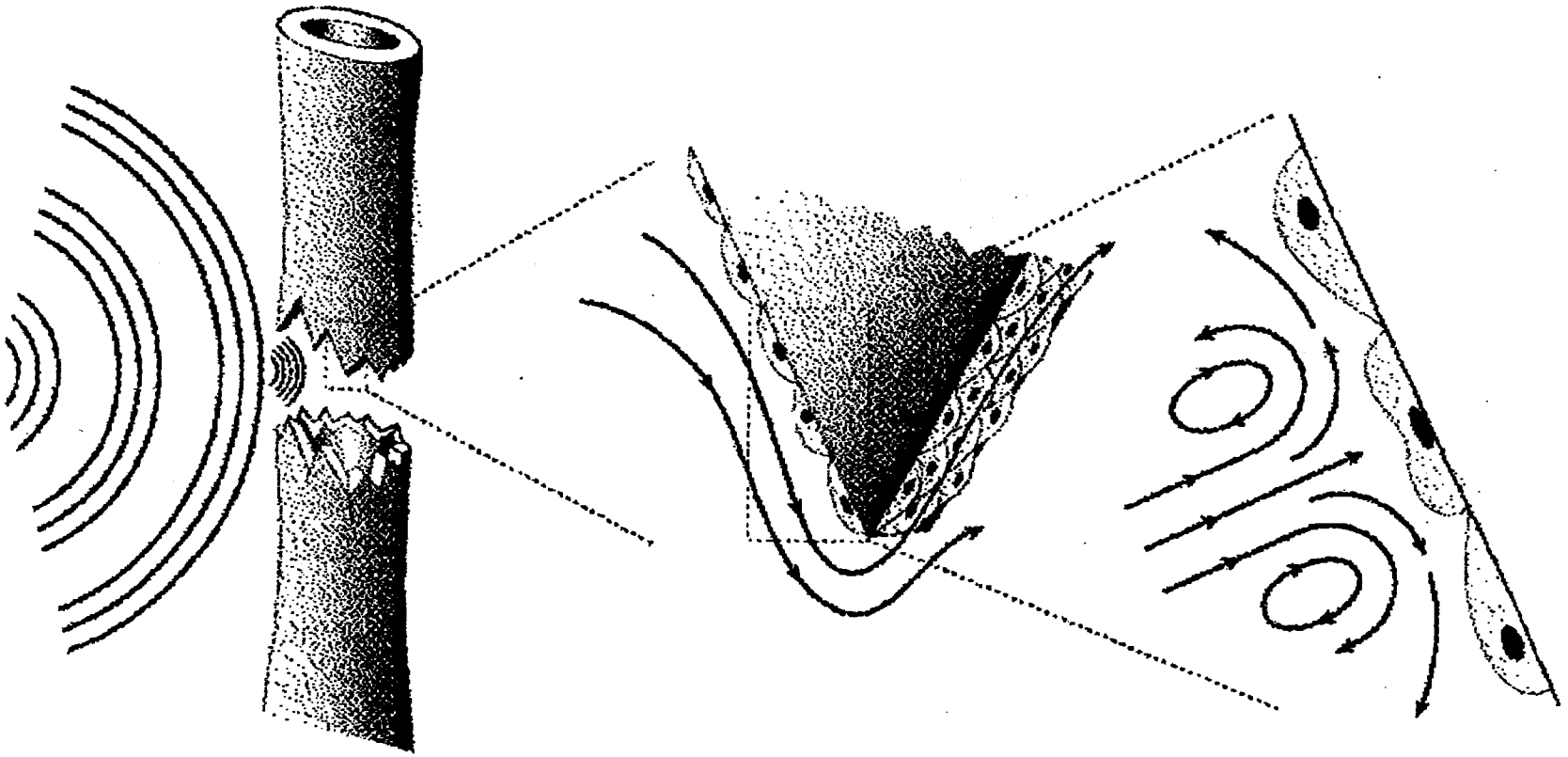

Figure 1.3. Illustration of ultrasonic pressure wave propagation at the gross fracture level (left), the interfragmentary level (middle) and the cellular level (right); due to the high density of the bone relative to the fracture gap and surrounding soft tissues, the ultrasonic pulse (left) is localized to the relatively low density fracture gap; the pressure waves stream across the surfaces of the fracture's jagged edge (Middle), mechanically stimulating the proliferating and differentiating fibroblasts, chondroblasts, and osteoblasts; the physical interaction with the cells can influence their metabolism through various means (right) including direct deformation and shear of the cell, and acoustically mediated streaming of the fluids adjacent to the cell population; illustration adapted from Hadjiargyrou et al.[48]

bilateral fibular fractures in rats, Dyson et al. [30] demonstrated accelerated fracture healing during the early stages of the healing progression with a pulsed 500 mW/cm^2 signal. About the same time, Xavier and Duarte [116], in a pioneering article, reported a 70% healing rate in twenty-six recalcitrant non-unions after a brief exposure (20 minutes/day) to a very low intensity pulsed ultrasound (30 mW/cm^2) signal. Such a therapy was initially pursued as a means of mechanically stimulating the fracture site without the need for actual weight-bearing. Initial studies undertaken to optimize ultrasound signal parameters were performed by Duarte [29] and indicated that pulsed ultrasound intensities of 49.6 mW/cm^2 and 57 mW/cm^2 successfully accelerated cortical bridging across the site of a fibular osteotomy in rabbits by 28% compared to untreated controls and also confirmed the non-thermal nature of the signal intensity used in human studies (30 mW/cm^2). These early studies prompted the development of what is now Smith and Nephew's commercially available Exogen 2000+ Sonic Accelerated Fracture Healing System (Figure 2C), which is currently prescribed for 25,000 fractures annually in the United States.

Using mechanical integrity as a critical endpoint in a rabbit fibular osteotomy model, Pilla et al. [83] reported that biomechanical healing in the stimulated group (200 μs burst of 1.5 MHz sine waves repeated at 1 kHz for 20 minutes daily) was accelerated by a factor of 1.7 relative to non-treated contralateral controls (i.e. biomechanical integrity was achieved in the stimulated group in half the time as usual). Wang et al. [108], in a similar study using a rat femoral fracture model, showed that daily ultrasound treatment

significantly increased the treated fracture strength (i.e. maximum torque to failure) by 22% compared to intact contralateral controls.

Tissue selectivity to specific parameters in the ultrasound signal is supported additionally by data from Ito et al. [56] and Jinguishi et al. [57]. These investigators used the rat femoral fracture model to show that low intensity pulsed ultrasound treatment increased bone mineral content and density, peak torque and stiffness and accelerated the overall endochondral ossification process. These studies also evaluated the pulse width and repetition frequency parameters of the ultrasound, and found that a pulse width of 200 μs has a significantly greater effect on fracture healing than that of 100 or 400 μs pulses, and that a 1 kHz repetition rate is more conducive to the healing process than 2 kHz. These findings support earlier reports that a 200 μs pulse width and a 1 kHz repetition rate are optimal for the healing of fractures (Figure 1.4).

Numerous studies (Table 1.2) have been undertaken to identify the exact biological mechanisms by which therapeutic levels of pulsed ultrasound accelerate the remodeling response after sustained trauma. Studies dating back to the early 1980's identified a change in the rate of influx and efflux of potassium ions in thymocytes [21], and Ryaby et al. [97] later reported that ultrasound increased calcium incorporation in differentiating cartilage and bone cell-cultures. More recent cell-culture experiments have illustrated that daily exposure to LIPUS promotes the osteoblastic phenotype as evidenced by increased production of TGF-β, alkaline phosphatase, osteonectin and osteopontin, while concomitantly down-regulating the osteoclastic response[98, 103]. The documented pro-

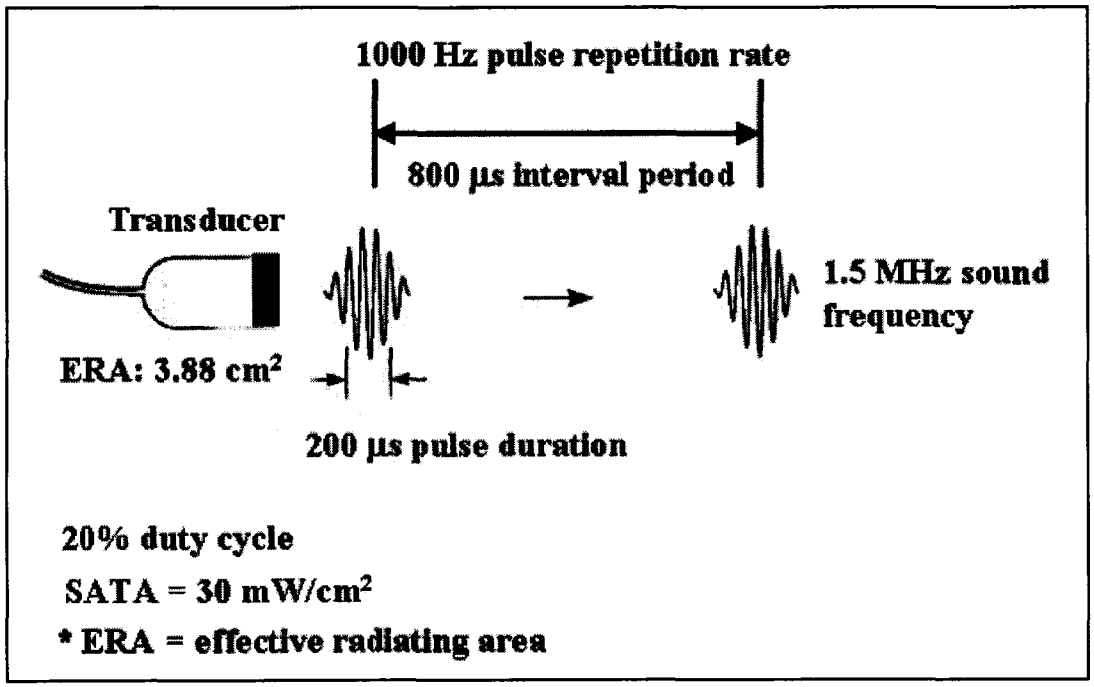

Figure 1.4. LIPUS signal specifications. These signal characteristics are consistent with those currently used for the treatment of fresh fractures and non-unions in approximately 25,000 clinical cases annually.

osteoblastic and anti-osteoclastic findings have prompted recent efforts that employ LIPUS to mitigate the onset of osteoporosis in patients with spinal cord injuries [109].

Low-intensity pulsed ultrasound has also been shown to affect the expression of genes involved in the inflammation and remodeling stages of fracture repair. Wu et al. [114] showed an increase in aggrecan gene expression following exposure of cultured chondrocytes to LIPUS. During chondrogenesis, this large chondroitin-sulfate molecule aggregates with hyaluronan, decorin, and biglycan, creating key proteoglycan scaffolding elements for Type-II collagen. Even when only this specific gene is considered, ultrasound accelerates and ultimately augments the process of callus formation, thereby augmenting endochondral ossification and increasing the mechanical strength and overall repair of the fractured bone. Thus, ultrasound acts as a non-invasive surrogate to the mechanical forces at work in Wolff's law without raising an element of structural risk to the wound-healing process.

Such intensities of ultrasound have been shown in numerous clinical studies to have a strong positive influence on each of the three key stages of the healing process, namely inflammation, repair, and remodeling, because it enhances angiogenic, chondrogenic and osteogenic activities [4, 108]. Heckman et al. [50], in a prospective, randomized, placebo-controlled, double-blind study, reported that low intensity pulsed ultrasound (LIPUS) treatment for 20 minutes/day at 30 mW/cm^2 resulted in a significant 24% reduction in the time required for clinical healing of closed or grade I open tibial fractures. Additionally, Kristiansen et al. [61] reported a 38% shorter time until union for patients treated with

Table 1.2. Stimulatory effects of LIPUS - *in vivo*

Study	Fracture Model/Cell Type	Intensity	Observed Effects
in vivo			
Duarte (1983)	Rabbit fibular osteotomy and femoral drill hole defect	49, 57 mW/cm^2	> callus formation
Xavier and Duarte (1983)	Human nonunions	30 mW/cm^2	> initiation of healing
Pilla et al. (1990)	Rabbit fibular osteotomy	30 mW/cm^2	> biomechanical strength
Wang et al. (1994)	Rat femoral fracture model	30 mW/cm^2	> biomechanical strength
Yang et al.(1996)	Rat femoral fracture model	50, 100 mW/cm^2	> aggrecan mRNA expression
Hadjiargyrou et al. (1998)	Rat femoral fracture model	30 mW/cm^2	> osteopontin mRNA
Rawool et al. (1998)	Dog ulnar osteotomy	30 mW/cm^2	> blood flow
Jinguishi et al. (1998)	Rat femoral fracture model	30 mW/cm^2	> maximal torque/bone mineral density
Nolte et al. (2001)	Human tibial, radial/ulnar, femoral, scaphoid nonunions	30 mW/cm^2	86% healing rate in 22 weeks
Tsumaki (2004)	Human tibial osteotomy	30 mW/cm^2	> callus BMD in treated limbs after 8 weeks
Leung et al. (2004)	Human tibial fractures	30 mW/cm^2	> clinical/radiographic/biochemical healing
Azuma et al. (2001)	Rat femoral fracture model	30 mW/cm^2	> biomechanical strength
Emami et al. (1999)	Human tibial fractures	30 mW/cm^2	no effect
Mayr et al. (2000)	Human nonunions	30 mW/cm^2	91% overall healing rate in 152 days
Raso et al. (2005)	Sciatic nerve crush in rats	400 mW/cm^2	20% > in sciatic function index
Cook et at. (2001)	Rabbit osteochondral defect	30 mW/cm^2	> histologic quality of repaired cartilage
Sparrow et al. (2004)	Rabbit bilateral MCL transection	300 mW/cm^2	> type I collagen and structural properties

Table 1.2 (cont.). Stimulatory effects of LIPUS - *in vitro*

Study	Fracture Model/Cell Type	Intensity	Observed Effects
in vitro			
Chapman et al. (1980)	Thymocytes	0.5-3 W/cm^2	< cellular K+ ion content
Ryaby et al. (1989)	Differentiated cartilage, bone cell cultures	200 mW/cm^2	> Ca^{2+} ion incorporation
Ryaby et al. (1991, 1992)	MC3T3 and TE85 osteoblasts	20, 30, 45 mW/cm^2	> adenylate cyclase/ >TGF-β
Wu et al. (1996)	Chondrocytes	50, 120 mW/cm^2	> aggragan mRNA expression
Parvizi et al. (2002)	Chondrocytes	50-500 mW/cm^2	> intracellular Ca^{2+} release
Kokubu et al. (1999)	MC3T3 osteoblastic cell-line	30 mW/cm^2	> PGE_2/COX-2 expression
Ito et al. (2000)	SaOS-2 osteoblastic cell-line, HUVEC endothelial cells	30 mW/cm^2	> PDGF-AB expression
Sun et al. (2001)	Rat alveolar mononuclear cell-calvaria ostaoblast co-culture	68 mW/cm^2	> alkaline phosphatase and TNF-α expression
Nolte et al. (2001)	Fetal mouse metatarsal rudiments	30 mW/cm^2	> length of calcifed diaphysis
Warden et al.	UMR-106 bone forming cells	30 mW/cm^2	> ALP and OC mRNA expression
Korstjens et al. (2004)	Fetal mouse metatarsal rudiments	30 mW/cm^2	> bone collar volume & % calcified cartilage
Li et al. (2003)	Rat calvarial osteoblasts	600 mW/cm^2	> TGF- β1, < IL-6 & TNF-α (<osteoclast fxn.)
Sena et al. (2005)	Rat bone marrow derived stromal cells	30 mW/cm^2	> c-jun,c-myc, COX-2, osteopontin,osteonectin
Sant'Anna (2005)	Rat bone marrow derived stromal cells	30 mW/cm^2	> ALP, osteopontin, BMP-7, TGF- β1
Naruse et al. (2000)	ST2 stromal cells	30 mW/cm^2	> IGF, osteocalcin, bone sialoprotein mRNA

ultrasound compared to those treated with placebo in a multicenter clinical trial of dorsally angulated fractures of the distal radius. A more recent study undertaken by Nolte et al. [77] confirmed the earlier findings of Xavier and Duarte and reported an 86% healing rate in non unions of the tibia, femur, radius/ulna, scaphoid, humerus, metatarsal, and clavicle in an average treatment time of 22 weeks. Leung et al. [64], in a study of thirty complex tibial fractures fixed with either an intramedullary interlocking nail (n=11) or an external fixator (n=19), showed that LIPUS-treated fractures healed significantly better as demonstrated by clinical, radiological, densitometric, and biochemical assessments. Despite the number of clinical studies indicating statistically significant healing effects of LIPUS on complex fractures as well as non-unions, one study performed by Emami et al. [31] has indicated no significant effect of ultrasound on the healing of complex tibial fractures.

In addition to those mechanistic events that occur at the molecular level, Rawool et al. [85] demonstrated that LIPUS stimulated a greater degree of vascularity at the site of ulnar osteotomies in dogs. In fact, these investigators showed that ultrasound not only increased blood flow to the trauma site during treatment, but increased blood flow at the fracture site for an extended period of time following removal of the stimulus. This blood flow was paralleled by greater callus formation and markedly improved blood-flow distribution around the fracture.

These and other studies indicate that in addition to modulating gene expression, ultrasound may increase blood flow through the dilation of capillaries and promote neo-

angiogenesis within the fracture callus[88, 107]. It is generally believed that blood flow serves as a principal factor in the acceleration of fracture healing and wound repair and that enhancing its presence may promote quicker healing. Definitely, one of the most important biological goals of the inflammatory response is to reestablish blood flow to the injured area. The corollary to this observation is that anything that diminishes blood flow or oxygenation of the fracture site will potentially suppress the healing response. Therefore, a major benefit of ultrasound may be that it biologically and biophysically optimizes healing processes and promotes an idealized environment that is conducive to repair.

1.4 Objectives and Specific Aims.

The objectives of this research were to evaluate the biological and mechanical responses of healing allograft bone when exposed to low-intensity pulsed ultrasound and longitudinal perforations in an ovine model. The LIPUS and LAP adjuvant treatments were compared with natural healing of allograft and autograft in the same model. Objectives include:

1. Quantification of mechanical (Chapter 2) and histological (Chapter 3) effects of the following treatments on short term (4 months) healing of allograft bone:

    a.) No adjuvant treatment to allograft (-CTL)
    b.) Low-Intensity Pulsed Ultrasound (LIPUS) to allograft
    c.) Longitudinal Allograft Perforations (LAP)
    d.) LIPUS+LAP treatment to allograft
    e.) No adjuvant treatment to autograft (+CTL)

2. Comparison of results of longitudinal perforation to those published for transverse perforations with and without partial demineralization.

3. Quantification of the effects of longitudinal perforation on mechanical strength of allograft bone prior to implantation (Chapter 4);

1.5 Hypotheses.

It was hypothesized that the combined LIPUS and LAP treatments would significantly improve osteointegration and revitalization of the allograft bone after 4 months of healing compared to the untreated negative control, LIPUS only and LAP only. The hypothesis is based on the documented stimulatory cellular effects of LIPUS on bone healing (both through mechanical mechanisms and molecular mechanisms) and the increased porosity and surface area generated by LAP providing a conduit for host cellular infiltration into the allograft. In order to test this hypothesis, the following specific aims were accomplished:

1. Quantification of biomechanical properties of the treated and untreated allograft bone prior to and after healing.
    a. Torsional biomechanics
    b. Structural and material properties
2. Quantification of histomorphometric indices of bone incorporation and revitalization of allograft bone
    a. Allograft revitalization depth and % allograft revitalized
    b. Mineral apposition rate, mineralizing surface and bone formation rate in allograft
    c. Callus or reactive region
    d. Porosity of allograft bone

1.6. Significance.

Low-intensity pulsed ultrasound has a proven track record of clinical success in accelerating the time to healing following fracture healing and ultimately reducing the rate of fracture non-union. More importantly, these low level mechanical signals are non-invasive and therefore do not necessitate surgical intervention. Also, graft porosity has been proven to improve the tissue's osteoconductive properties. The effects of LIPUS and LAP could potentially improve both the short-term and long-term clinical outcomes of patients receiving massive cortical allograft following tumor resection by minimizing the documented biological variability in graft incorporation and revitalization while at the same time promoting an idealized environment that is optimal for repair. These proposed treatments might have a large impact on transplantation science by reducing the rate of fracture and accelerating the remodeling and revitalization processes of the allograft.

1.7 References

1. NIH Consensus Statement on total knee replacement December 8-10, 2003. J Bone Joint Surg Am. 86-A:1328-1335, 2004.

2. Anglen J: The clinical use of bone stimulators. J South Orthop Assoc. 12(2):46-54, 2003.

3. Ardan NI, Jr., Janes JM, Herrick JF: Ultrasonic energy and surgically produced defects in bone. J Bone Joint Surg Am. 39-A:394-402, 1957.

4. Azuma Y, Ito M, Harada Y, et al.: Low-intensity pulsed ultrasound accelerates rat femoral fracture healing by acting on the various cellular reactions in the fracture callus. J Bone Miner Res. 16(4):671-680, 2001.

5. Bassett CA, Pawluk RJ, Pilla AA: Acceleration of fracture repair by electromagnetic fields. A surgically noninvasive method. Ann N Y Acad Sci. 238:242-262, 1974.

6. Bassett CA, Schink-Ascani M, Lewis SM: Effects of pulsed electromagnetic fields on Steinberg ratings of femoral head osteonecrosis. Clin Orthop. 246:172-188, 1989.

7. Beck BR, Qin YX, McLeod KJ, et al.: On the relationship between streaming potential and strain in an *in vivo* bone preparation. Calcif Tissue Int. 71(4):335-343, 2002.

8. Benevenia J, Zimmerman M, Keating J, et al.: Mechanical environment affects allograft incorporation. J Biomed Mater Res. 53:67-72, 2000.

9. Bigliani LU, Rosenwasser MP, Caulo N, et al.: The use of pulsing electromagnetic fields to achieve arthrodesis of the knee following failed total knee arthroplasty. A preliminary report. J Bone Joint Surg Am. 65(4):480-485, 1983.

10. Bonfiglio M, Jeter WS: Immunological responses to bone. Clin Orthop Relat Res. 87:19-27, 1972.

11. Bos GD, Goldberg VM, Powell AE, et al.: The effect of histocompatibility matching on canine frozen bone allografts. J Bone Joint Surg Am. 65(1):89-96, 1983.

12. Bos GD, Goldberg VM, Zika JM, et al.: Immune responses of rats to frozen bone allografts. J Bone Joint Surg Am. 65:239-246, 1983.

13. Bradish CF, Kemp HB, Scales JT, Wilson JN: Distal femoral replacement by custom-made prostheses. Clinical follow-up and survivorship analysis. J Bone Joint Surg Br. 69:276-284, 1987.

14. Brien EW, Terek RM, Healey JH, Lane JM: Allograft reconstruction after proximal tibial resection for bone tumors. An analysis of function and outcome comparing allograft and prosthetic reconstructions. Clin Orthop Relat Res. 116-127, 1994.

15. Brostrèom LA, Nilsonne U, Nilsson OS: Survival of frozen bone allograft. Ann Chir Gynaecol. 77(2):85-89, 1988.

16. Burchardt H: The biology of bone graft repair. Clin Orthop. 174:28-42, 1983.

17. Burchardt H, Busbee GA, 3rd, Enneking WF: Repair of experimental autologous grafts of cortical bone. J Bone Joint Surg Am. 57(6):814-819, 1975.

18. Burchardt H, Enneking WF: Transplantation of Bone. Surg Clin N Am. 58:403-427, 1978.

19. Burger EH: Experiments on cell mechanosensitivity: Bone cells as mechanical engineers. In Cowin SC (eds). Bone Mechanics Handbok. New York, CRC Press 2001.

20. Burwell RG: Fate of Freeze-Dried Bone Allografts. Transplant P. 8:95-111, 1976.

21. Chapman IV, MacNally NA, Tucker S: Ultrasound-induced changes in rates of influx and efflux of potassium ions in rat thymocytes *in vitro*. Ultrasound Med Biol. 6(1):47-58, 1980.

22. Cook SD: Preclinical and clinical evaluation of osteogenic protein-1 (BMP-7) in bony sites. Orthopedics. 22:669-671, 1999.

23. Corradi C, Cozzolino A: [Effect of ultrasonics on the development of osseous callus in fractures.]. Arch Ortop. 66:77-98, 1953.

24. Corradi C, Cozzolino A: [Ultrasound and bone callus formation during function]. Arch Ortop. 66:77-98, 1953.

25. Cowin SC, Moss ML: Mechanosensory mechanisms in bone. In Cowin SC (eds). Bone Mechanics Handbook. New York, CRC Press 2001.

26. Curtiss PH, Powell AE, Herndon CH: Immunological Factors in Homogenous-Bone Transplantation.3. The Inability of Homogenous Rabbit Bone to Induce Circulating Antibodies in Rabbits. J Bone Joint Surg Am. 41:1482-1488, 1959.

27. Damien E, Price JS, Lanyon LE: Mechanical strain stimulates osteoblast proliferation through the estrogen receptor in males as well as females. J Bone Miner Res. 15(11):2169-2177, 2000.

28. Deforest RE, Herrick JF, Janes JM, Krusen FH: Effects of ultrasound on growing bone. Archives of physical medicine and rehabilitation. 21-30, 1958.

29. Duarte LR: The stimulation of bone growth by ultrasound. Arch Orthop Trauma Surg. 101(3):1983.

30. Dyson M: Therapeutic applications of ultrasound. In Ziskin MC (eds). Biological Effects of Ultrasound. New York, Churchill Livingstone 121-133, 1985.

31. Emami A, Petrâen-Mallmin M, Larsson S: No effect of low-intensity ultrasound on healing time of intramedullary fixed tibial fractures. J Orthop Trauma. 13(4):252-257, 1999.

32. Enneking WF, Campanacci DA: Retrieved human allografts: a clinicopathological study. J Bone Joint Surg Am. 83-A(7):971-986, 2001.

33. Enneking WF, Mindell ER: Observations on massive retrieved human allografts. J Bone Joint Surg Am. 73(8):1123-1142, 1991.

34. Friedenberg ZB, Harlow MC, Brighton CT: Healing of nonunion of the medial malleolus by means of direct current: a case report. J Trauma. 11(10):883-885, 1971.

35. Friedlaender GE: Bone allografts: the biological consequences of immunological events. J Bone Joint Surg Am. 73:1119-1122, 1991.

36. Friedlaender GE: Bone grafts. The basic science rationale for clinical applications. J Bone Joint Surg Am. 69:786-790, 1987.

37. Friedlaender GE, Strong DM, Sell KW: Studies on the antigenicity of bone. I. Freeze-dried and deep-frozen bone allografts in rabbits. J Bone Joint Surg Am. 58(6):854-858, 1976.

38. Fritton SP, McLeod KJ, Rubin CT: Quantifying the strain history of bone: spatial uniformity and self-similarity of low-magnitude strains. J Biomech. 33(3):317-325, 2000.

39. Frykman GK, Taleisnik J, Peters G, et al.: Treatment of nonunited scaphoid fractures by pulsed electromagnetic field and cast. J Hand Surg [Am]. 11(3):344-349, 1986.

40. Gao TJ, Lindholm TS, Kommonen B, et al.: Enhanced healing of segmental tibial defects in sheep by a composite bone substitute composed of tricalcium phosphate cylinder, bone morphogenetic protein, and type IV collagen. J Biomed Mater Res. 32:505-512, 1996.

41. Gebhardt MC, Flugstad DI, Springfield DS, Mankin HJ: The use of bone allografts for limb salvage in high-grade extremity osteosarcoma. Clin Orthop. 270:181-196, 1991.

42. Gendler E: Perforated demineralized bone matrix: a new form of osteoinductive biomaterial. J Biomed Mater Res. 20(6):687-697, 1986.

43. Godette GA, Kopta JA, Egle DM: Biomechanical effects of gamma irradiation on fresh frozen allografts *in vivo*. Orthopedics. 19:649-653, 1996.

44. Goldberg VM, Powell A, Shaffer JW, et al.: Bone grafting: role of histocompatibility in transplantation. J Orthop Res. 3(4):1985.

45. Goldberg VM, Stevenson S: Natural history of autografts and allografts. Clin Orthop. 225:7-16, 1987.

46. Goodship AE, Lawes T, Rubin CT: Low magnitude high frequency mechanical stimulation of endochondral bone repair. Transactions of the Orthopaedic Research Soceity. 22:234, 1997.

47. Gross TS, Edwards JL, McLeod KJ, et al.: Strain gradients correlate with sites of periosteal bone formation. J Bone Miner Res. 12(6):982-988, 1997.

48. Hadjiargyrou M, McLeod K, Ryaby JP, et al.: Enhancement of fracture healing by low intensity ultrasound. Clin Orthop. 355 Suppl:S216-229, 1998.

49. Hamer AJ, Suvarna SK, Stockley I: Histologic evidence of cortical allograft bone incorporation in revision hip surgery. J Arthroplasty. 12(7):785-789, 1997.

50. Heckman JD, Ryaby JP, McCabe J, et al.: Acceleration of tibial fracture-healing by non-invasive, low-intensity pulsed ultrasound. J Bone Joint Surg Am. 76(1):26-34, 1994.

51. Heiple KG, Chase SW, Herndon CH: A Comparative Study of the Healing Process Following Different Types of Bone Transplantation. J Bone Joint Surg Am. 45:1593-1616, 1963.

52. Herndon CH, Chase SW: The Fate of Massive Autogenous and Homogenous Bone Grafts Including Articular Surfaces. Surg Gynecol Obstet. 98:273-290, 1954.

53. Horowitz SM, Glasser DB, Lane JM, Healey JH: Prosthetic and extremity survivorship after limb salvage for sarcoma. How long do the reconstructions last? Clin Orthop Relat Res. 293:280-286, 1993.

54. Huang RP, Rubin CT, McLeod KJ: Changes in postural muscle dynamics as a function of age. J Gerontol A Biol Sci Med Sci. 54(8):B352-357, 1999.

55. Irvine G: Musculoskeletal allograft procedures in the year 2001. American Association of Tissue Banks. 2004.

56. Ito M, Azuma Y, Harada Y, et al.: Low intensity pulsed ultrasound accelerates fracture healing in a rat femoral fracture model. Transactions of the Orthopaedic Research Society, 732, 1998

57. Junguishi S, Azuma Y, Ito M: Effects of non-invasive pulsed low-intensity ultrasound on rat femoral fractures. Third World Congress of Biomechanics, 1998

58. Kandel RA, Pritzker KP, Langer F, Gross AE: The pathologic features of massive osseous grafts. Hum Pathol. 15(2):141-146, 1984.

59. Kaufman JJ, Einhorn TA: Ultrasound assessment of bone. J Bone Miner Res. 8:517-525, 1993.

60. Kondrai G, Tarsoly E: [On the increase of the incorporation ability of Kiel hard bone preparations]. Acta Chir Acad Sci Hung. 7:201-210, 1966.

61. Kristiansen TK, Ryaby JP, McCabe J, et al.: Accelerated healing of distal radial fractures with the use of specific, low-intensity ultrasound. A multicenter, prospective, randomized, double-blind, placebo-controlled study. J Bone Joint Surg Am. 79(7):961-973, 1997.

62. Kucharzyk DW: A controlled prospective outcome study of implantable electrical stimulation with spinal instrumentation in a high-risk spinal fusion population. Spine. 24(5):465-468, 1999.

63. Lanyon LE: Functional strain as a determinant for bone remodeling. Calcif Tissue Int. 36 Suppl 1:897-905, 1984.

64. Leung KS, Lee WS, Tsui HF, et al.: Complex tibial fracture outcomes following treatment with low-intensity pulsed ultrasound. Ultrasound Med Biol. 30(3):389-395, 2004.

65. Lewandrowski KU, Bonassar L, Uhthoff HK: Mechanical properties of perforated and partially demineralized bone grafts. Clin Orthop. 238-246, 1998.

66. Lewandrowski KU, Schollmeier G, Ekkemkamp A, et al.: Incorporation of perforated and demineralized cortical bone allografts. Part II: A mechanical and histologic evaluation. Biomed Mater Eng. 11(3):209-219, 2001.

67. Lewandrowski KU, Schollmeier G, Ekkemkamp A, et al.: Incorporation of perforated and demineralized cortical bone allografts. Part I: radiographic and histologic evaluation. Biomed Mater Eng. 11(3):197-207, 2001.

68. Lewandrowski KU, Tomford WW, Schomacker KT, et al.: Improved osteoinduction of cortical bone allografts: a study of the effects of laser perforation and partial demineralization. J Orthop Res. 15(5):748-756, 1997.

69. Luo G, Cowin SC, Sadegh AM, et al.: Implementation of strain rate as a bone remodeling stimulus. J Biomech Eng. 117(3):329-338, 1995.

70. Mankin HJ, Gebhardt MC, Jennings LC, et al.: Long-term results of allograft replacement in the management of bone tumors. Clin Orthop. 324:86-97, 1996.

71. Mankin HJ, Springfield DS, Gebhardt MC, Tomford WW: Current status of allografting for bone tumors. Orthopedics. 15(10):1147-1154, 1992.

72. Meril AJ, Garland Orthopedic Clinic T: Direct current stimulation of allograft in anterior and posterior lumbar interbody fusions. Spine. 19(21):2393-2398, 1994.

73. Moed BR, Kim EC, van Holsbeeck M, et al.: Ultrasound for the early diagnosis of tibial fracture healing after static interlocked nailing without reaming: histologic correlation using a canine model. J Orthop Trauma. 12:200-205, 1998.

74. Moed BR, Subramanian S, van Holsbeeck M, et al.: Ultrasound for the early diagnosis of tibial fracture healing after static interlocked nailing without reaming: clinical results. J Orthop Trauma. 12:206-213, 1998.

75. Nelson FR, Brighton CT, Ryaby J, et al.: Use of physical forces in bone healing. J Am Acad Orthop Surg. 11(5):344-354, 2003.

76. Noble BS, Peet N, Stevens HY, et al.: Mechanical loading: biphasic osteocyte survival and targeting of osteoclasts for bone destruction in rat cortical bone. Am J Physiol Cell Physiol. 284(4):C934-943, 2003.

77. Nolte PA, van der Krans A, Patka P, et al.: Low-intensity pulsed ultrasound in the treatment of nonunions. J Trauma. 51(4):693-702, 2001.

78. O'Donnell RJ, Deutsch TF, Flotte RJ, et al.: Effect of Er:YAG laser holes on osteoinduction in demineralized rat calvarial allografts. J Orthop Res. 14(1):108-113, 1996.

79. Ortiz-Cruz E, Gebhardt MC, Jennings LC, et al.: The results of transplantation of intercalary allografts after resection of tumors. A long-term follow-up study. J Bone Joint Surg Am. 79(1):97-106, 1997.

80. Ottolenghi CE: Massive osteo and osteo-articular bone grafts. Technic and results of 62 cases. Clin Orthop. 87:156-164, 1972.

81. Parrish FF: Allograft replacement of all or part of the end of a long bone following excision of a tumor. J Bone Joint Surg Am. 55(1):1-22, 1973.

82. Paterson DC, Simonis RB: Electrical stimulation in the treatment of congenital pseudarthrosis of the tibia. J Bone Joint Surg Br. 67(3):454-462, 1985.

83. Pilla AA, Mont MA, Nasser PR, et al.: Non-invasive low-intensity pulsed ultrasound accelerates bone healing in the rabbit. J Orthop Trauma. 4(3):1990.

84. Qin YX, Kaplan T, Saldanha A, et al.: Fluid pressure gradients, arising from oscillations in intramedullary pressure, is correlated with the formation of bone and inhibition of intracortical porosity. J Biomech. 36(10):1427-1437, 2003.

85. Rawool D, Goldberg B, Forsberg F, et al.: Power doppler assessment of vascular changes during fracture treatment with low -intensity ultrasound. Transactions of the Radiological Society of North America. 1998:1185, 1998.

86. Rees DC, Haddad FS: Bone transplantation. Hosp Med. 64:205-209, 2003.

87. Rees DC, Haddad FS, Royal National Orthopaedic Hospital SM: Bone transplantation. Hosp Med. 64(4):205-209, 2003.

88. Reher P, Doan N, Bradnock B, et al.: Effect of ultrasound on the production of IL-8, basic FGF and VEGF. 11:416-423, 1999.

89. Rubin C, Bolander M, Ryaby JP, Hadjiargyrou M: The use of low-intensity ultrasound to accelerate the healing of fractures. J Bone Joint Surg Am. 83-A(2):259-270, 2001.

90. Rubin C, Pope M, Fritton JC, et al.: Transmissibility of 15-hertz to 35-hertz vibrations to the human hip and lumbar spine: determining the physiologic feasibility of delivering low-level anabolic mechanical stimuli to skeletal regions at greatest risk of fracture because of osteoporosis. Spine. 28(23):2621-2627, 2003.

91. Rubin C, Recker R, Cullen D, et al.: Prevention of postmenopausal bone loss by a low-magnitude, high-frequency mechanical stimuli: a clinical trial assessing compliance, efficacy, and safety. J Bone Miner Res. 19(3):343-351, 2004.

92. Rubin C, Sun YQ, Hadjiargyrou M, et al.: Increased expression of matrix metalloproteinase-1 in osteocytes precedes bone resorption as stimulated by disuse: evidence for autoregulation of the cell's mechanical environment? J Orthop Res. 17(3):354-361, 1999.

93. Rubin C, Turner AS, Mèuller R, et al.: Quantity and quality of trabecular bone in the femur are enhanced by a strongly anabolic, noninvasive mechanical intervention. J Bone Miner Res. 17(2):349-357, 2002.

94. Rubin CT: Peak microstrains induced by LIPUS. 2004.

95. Rubin CT: Skeletal strain and the functional significance of bone architecture. Calcif Tissue Int. 36 Suppl 1:S1-8, 1984.

96. Rubin CT, Lanyon LE: Regulation of bone formation by applied dynamic loads. J Bone Joint Surg Am. 66(3):397-402, 1984.

97. Ryaby JP, Bachner EJ, Bendo JA, et al.: Low intensity pulsed ultrasound increases calcium incorporation on both differentiating cartilage and bone cell cultures. Transactions of the Orthopaedic Research Soceity. 14:15, 1989.

98. Sena K, Leven RM, Mazhar K, et al.: Early gene response to low-intensity pulsed ultrasound in rat osteoblastic cells. Ultrasound Med Biol. 31:703-708, 2005.

99. Steinberg ME, Brighton CT, Corces A, et al.: Osteonecrosis of the femoral head. Results of core decompression and grafting with and without electrical stimulation. Clin Orthop Relat Res. 249:199-208, 1989.

100. Stevenson S: Biology of bone grafts. Orthop Clin North Am. 30:543-552, 1999.

101. Stevenson S: The immune response to osteochondral allografts in dogs. J Bone Joint Surg Am. 69(4):573-582, 1987.

102. Summers BN, Eisenstein SM, Department for Spinal Disorders RJ, Agnes Hunt Orthopaedic Hospital OE: Donor site pain from the ilium. A complication of lumbar spine fusion. J Bone Joint Surg Br. 71(4):677-680, 1989.

103. Sun JS, Hong RC, Chang WH, et al.: *In vitro* effects of low-intensity ultrasound stimulation on the bone cells. J Biomed Mater Res. 57(3):449-456, 2001.

104. Tarsoly E, Ostrowski K, Moskalewski S, et al.: Incorporation of lyophilized and radiosterilized perforated and unperforated bone grafts in dogs. Acta Chir Acad Sci Hung. 10(1):287-292, 1969.

105. Vander Griend RA: The effect of internal fixation on the healing of large allografts. J Bone Joint Surg Am. 76(5):657-663, 1994.

106. Wallace AL, Draper ER, Strachan RK, et al.: The vascular response to fracture micromovement. Clin Orthop. 301:281-290, 1994.

107. Wang FS, Kuo YR, Wang CJ, et al.: Nitric oxide mediates ultrasound-induced hypoxia-inducible factor-1alpha activation and vascular endothelial growth factor-A expression in human osteoblasts. Bone. 35:114-123, 2004.

108. Wang SJ, Lewallen DG, Bolander ME, et al.: Low intensity ultrasound treatment increases strength in a rat femoral fracture model. J Orthop Res. 12(1):40-47, 1994.

109. Warden SJ, Bennell KL, Matthews B, et al.: Efficacy of low-intentisy pulsed ultrasound in the precention of osteoporosis following spinal cord injury. Bone. 2:431-436, 2001.

110. Weinbaum S, Cowin SC, Zeng Y: A model for the excitation of osteocytes by mechanical loading-induced bone fluid shear stresses. J Biomech. 27(3):339-360, 1994.

111. Wells PNT: Surgical applications of ultrasound. In Ziskin MC (eds). Biological Effects of Ultrasound. New York, Churchill Livingstone 157-167, 1985.

112. Wheeler DL, Enneking WF: Allograft Bone Decreases in Strength *In vivo* over Time. 435:36-42, 2005.

113. Wolff J: The law of bone remodeling. Berlin, Hirshwald 17-35,1892

114. Wu C, Lewallen DG, Bolander ME, et al.: Exposure to low intensity ultrasound stimulates aggrecan gene expression by cultured chondrocytes. Transactions of the Orthopaedic Research Soceity. 21:622, 1996.

115. Wu JJ, Shyr HS, Chao EY, Kelly PJ: Comparison of osteotomy healing under external fixation devices with different stiffness characteristics. J Bone Joint Surg Am. 66:1258-1264, 1984.

116. Xavier CAM, Duarte LR: Ultrasonic stimulation of Bone Callus. Rev. Brazil Orthop. 18:73-80, 1983.

CHAPTER 2. TORSIONAL BIOMECHANICS & RADIOAGRAPHICAL ANALYSIS

BIOMECHANICAL EFFECTS OF LOW INTENSITY PULSED ULTRASOUND (LIPUS) AND LONGITUDINAL ALLOGRAFT PERFORATION (LAP) ON OVINE HINDLIMBS RECONSTRUCTED WITH INTERCALARY ALLOGRAFT

2.1. Introduction

Massive segmental bone defects caused by trauma or tumor resection have been reconstructed with autogenous bone[16], metallic megaprostheses[26], or allograft[31]. Stabilization of the bone ends and subsequent bone grafting with non-vascularized or vascularized bone grafts is the most common repair method after traumatic segmental bone loss. Bone autograft harvested locally or from the iliac crest, rib, or fibula is frequently used to elicit healing in such cases yet the usefulness of such grafting is limited by the amount that is available for structural restoration, the necessity of a second operation, and the risk of complications at the donor site[43, 52]. Massive bone allograft is an attractive alternative to autogenous graft because it supports bone formation, its supply is virtually unlimited, and restorations where structural integrity is a clinical necessity are possible. Unfortunately, even after extended periods, allografts typically do not fully incorporate with the host[24], presumably due to a lack of osteogenic capacity and osteoinductivity relative to autogenous bone[19]. Allografts typically demonstrate only superficial incorporation, revascularization, and limited bone remodeling that may result in non-union or fracture of the allograft-host bone junctions[5] and graft fatigue failures

due to increases in microfracture density concomitant with the bone's inability to remodel[50]. Graft healing is further attenuated if the adjacent host has been irradiated as may be the case when pre- or post-operative radiation therapy is employed[14]. Such post-operative complications have resulted in allograft success rates of only 60% at ten years[20].

Improving incorporation of the allograft is key to a successful reconstruction and improving long-term clinical outcome[15]. Though the field of bone allograft transplantation has been around for nearly a century[30], novel strategies that aim to improve graft incorporation are lacking. With the discovery of bone morphogenetic proteins (BMPs), recent efforts have involved augmenting the host-allograft bone junctions with osteogenic protein-1 (OP-1) and rhBMP-2 which have demonstrated improved graft incorporation and healing using these potent biomolecules [11, 35].

Increasing graft porosity via perforating the bony cortex perpendicular to the long axis of the graft has received considerable attention as a means to improve graft incorporation by the host, though these graft modifications have been reported to have mixed results[7, 28, 29, 45]. Lewandrowski et al.[28, 29] reported increased resorption and little evidence of incorporation of 3 cm intercalary sheep allografts containing multiple 300 μm perforations after 9 months. Combining the transverse perforations with extensive cortical demineralization improved the biologic response of the host to the graft and resulted in almost complete graft incorporation[28, 29], but at the expense of graft

mechanical integrity. It was determined that the flexural properties of the perforated and demineralized graft decreased by approximately 40%[28]. Since cortical allografts are repaired initially by increased osteoclastic activity paralleled by decreased osteoblastic activity that decreases the mass and radiodensity of the material and concomitantly increases its internal porosity[6], transplanting a graft with significantly reduced structural properties may potentiate early mechanical failure within the host.

The orientation of perforations within the bony cortex has yet to be evaluated. Past research indicates transverse perforations increase allograft porosity but improve graft healing only when the cortical shell is additionally demineralized. The significantly reduced load-bearing capacity of the perforated and demineralized grafts has lead to accelerated mechanical failure and caused orthopaedists to abandon this form of graft modification[36]. Longitudinal perforations, as opposed to those oriented perpendicular to the long axis of the graft, may provide more direct access for bone remodeling cell infiltration and effects on graft revitalization may not be dependent on cortical demineralization. Introducing conduits that run parallel to the long axis of the graft would provide direct access to bone cells for creeping substitution of reparative tissue while minimally affecting the overall strength of the implanted allograft.

During the first six months following limb reconstruction with a bone allograft, the transplanted tissue is weakened by approximately 40% due to the initial resorptive phase paralleled by little new bone deposition within the graft[6]. Beyond this six-month period,

the fate of the graft is unpredictable. Host-graft bridging is accomplished via a periosteal callus that originates on the host tissue and apposes periosteally onto the grafted tissue thereby promoting mechanical integrity of the reconstructed limb[6, 17]. A process which could upregulate the osteoblastic response of the adjacent host and promote callus formation while at the same time attenuating osteoclastogenesis and graft resorption may reduce the risk of long-term graft failure. Ultrasound, administered at intensities consistent with those used for diagnostic procedures (1 to 50 mW/cm^2), has been demonstrated in both animal[3, 22, 25, 48] and human clinical studies[27, 33] to have strong osteogenic potentials, and, more recently, anti-osteoclastic capabilities[40, 44]. Animal studies have shown an increase in callus tissue formation and maturation[3, 39] that translated directly into return to full biomechanical integrity in half the time as non-stimulated fractures[34]. Low-intensity pulsed ultrasound (LIPUS) has demonstrated positive effects in fresh fractures as well as established non-unions through high-frequency, acoustic pressure waves that cause low-level micromechanical strains on the bone tissue. These micromechanical strains induce piezoelectric potentials [12] and acoustic streaming[21, 38] in ossifying tissue which have been suggested by some to behave as highly anabolic stimuli, even in skeletal sites where the repair process has stopped completely (i.e., non-union).

The highly anabolic stimulus induced by exogenous, biophysical stimuli, such as LIPUS and PEMF (pulsed electromagnetic fields), has been applied to areas other than fresh fracture and non-union healing. Recent studies have suggested beneficial effects of

LIPUS and PEMF in accelerating spinal fusion[1, 2, 13], soft tissue healing[41, 10], osteointegration of biomaterials[18], and as countermeasures for osteopenia following spinal cord injury[49]. However, only one study to date has investigated the effects of a biophysical stimulus on allograft healing following tumor resection. Campana et al.[8] demonstrated significantly better radiographic and clinical healing following ten hours of daily PEMF stimulation compared to untreated limbs. LIPUS has yet to be evaluated as an adjuvant therapy to improve allograft healing but requires only 20 minutes of daily stimulation to produce similar anabolic effects as PEMF[1].

Therefore, the goal of this exploratory study was to examine the potential of daily stimulation of the host-allograft bone junctions with low-intensity pulsed ultrasound in limbs reconstructed in an ovine tibial intercalary defect with longitudinally perforated or non-perforated fresh, frozen allograft. The LIPUS and LAP adjuvant treatments will be compared with natural healing of allograft and autograft in the same model.

2.3. Material and Methods
2.3.1. Study Design

Fifteen animals were systematically assigned to five experimental groups based on intercalary graft type and treatment: +CTL, -CTL, LIPUS, LAP, LIPUS+LAP. The +CTL animals (n=3) received a tibial ostectomy with immediate replacement of the resected autologous graft. The –CTL group (n=3) received fresh frozen ovine tibial allografts. Both the +CTL and –CTL groups did not receive LAP or LIPUS treatments. The LIPUS treatment group (n=3), following grafting with fresh frozen ovine tibiae, received low-intensity pulsed ultrasound for 20 minutes/day, 5 days/week, for the duration of the healing period. The LAP treatment group received fresh frozen ovine allografts with 500 μm longitudinal perforations. The LIPUS+LAP treatment group received both LIPUS and LAP treatments. The power of this exploratory study with n=3 per treatment group was 0.5. All animals were euthanized four months following intercalary allograft/autograft transplantation for radiographic, biomechanical, and histological analysis. An overview of the study design is presented in Table 2.1 and Figure 2.1.

Table 2.1. Experiemental Study Design

Treatment	# of Sheep Survival Time	End Point Assays
Allograft only, (-Control, -CTL)	3/4 mos.	Torsional Biomechanics Radiography Decalcified Histology Undecalcified Histology
Allograft + LIPUS (LIPUS)	3/4 mos.	
Allograft + LAP (LAP)	3/4 mos.	
Allograft + LIPUS +LAP (LIPUS + LAP)	3/4 mos.	
Autograft only (+Control, +CTL)	3/4 mos.	

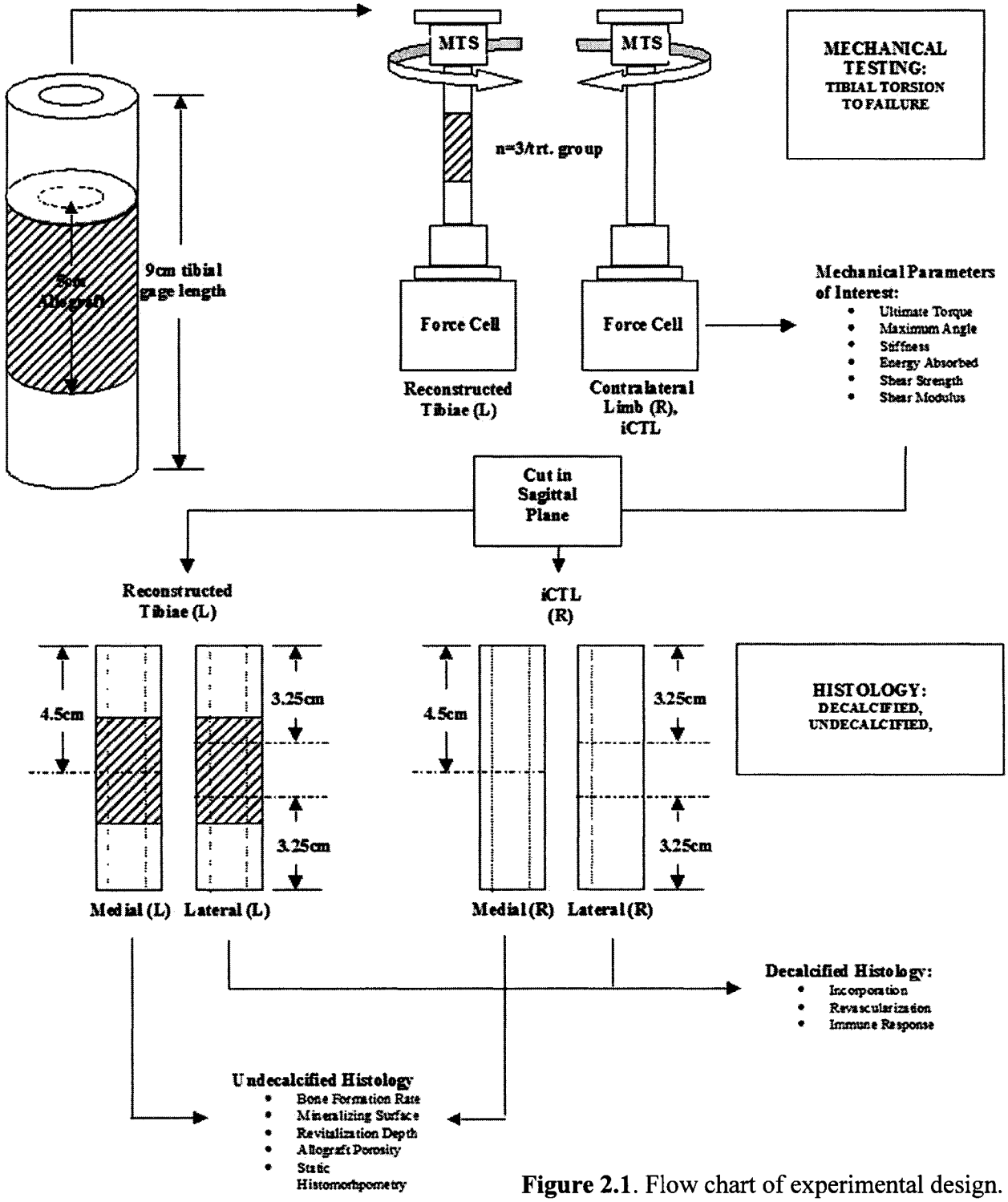

Figure 2.1. Flow chart of experimental design.

2.3.2. Preparation of Grafts.

Tibial allografts for the study were aseptically harvested from twelve skeletally mature, female sheep. A separate donor was used for each experimental graft except for the animals in the +CTL treatment group. Wool was removed from the left limbs and the skin aseptically prepared and draped in a surgical suite (Figure 2.2, A&B). The diaphyseal region of each tibia was palpated and a small medial incision was made overlying the mid-diaphyseal region of the tibia. A 5 cm diaphyseal ostectomy was created with a standard oscillating bone saw. Those grafts assigned to the –CTL and LIPUS groups were immediately wrapped in sterile saline/antibiotic solution soaked gauze and frozen to -80°C.

Following ostectomy, the LAP and LIPUS+LAP grafts were placed in 20 cc of 0.9% sodium chloride (NaCl) solution containing polymyxin B sulfate (500,000 units/l), neomycin (1 gram), and ampicillin (3 GM) saline/antibiotic solution. These grafts received multiple cortical perforations along the longitudinal axis of the graft using a micro-drill bit approximately 500 μm in diameter. Prior to drilling, the allograft was removed from the bone preservative solution and both proximal and distal cortical end plates were dried with sterile gauze. A pattern of points was marked on both end plates. The first four marks were placed at approximately the 12, 3, 6, and 9 o'clock positions and the remaining 90-degree increments were filled with an additional three marks for a total of 16 points identified for drilled perforations. The stenciled allograft was wrapped in sterile gauze and secured between the faces of a stainless steel vice. The clamped

allograft was placed in a sterile saline bath to minimize additional tissue necrosis during drilling. Fresh saline was used for each allograft preparation. A 500 μm diameter steel bit (Cleveland Tools, Cleveland, OH) and a rotary tool affixed to a drilling press (Dremel, Racine, WI) were used to create longitudinal perforations to a depth of approximately 10 mm (Figure 2.2, C-G). Similar to the LIPUS and –CTL grafts, perforated grafts were rinsed with saline/antibiotic solution, wrapped in sterile saline/antibiotic solution-soaked gauze, placed in sealed plastic bags, and frozen for at least 4 weeks at -80°C.

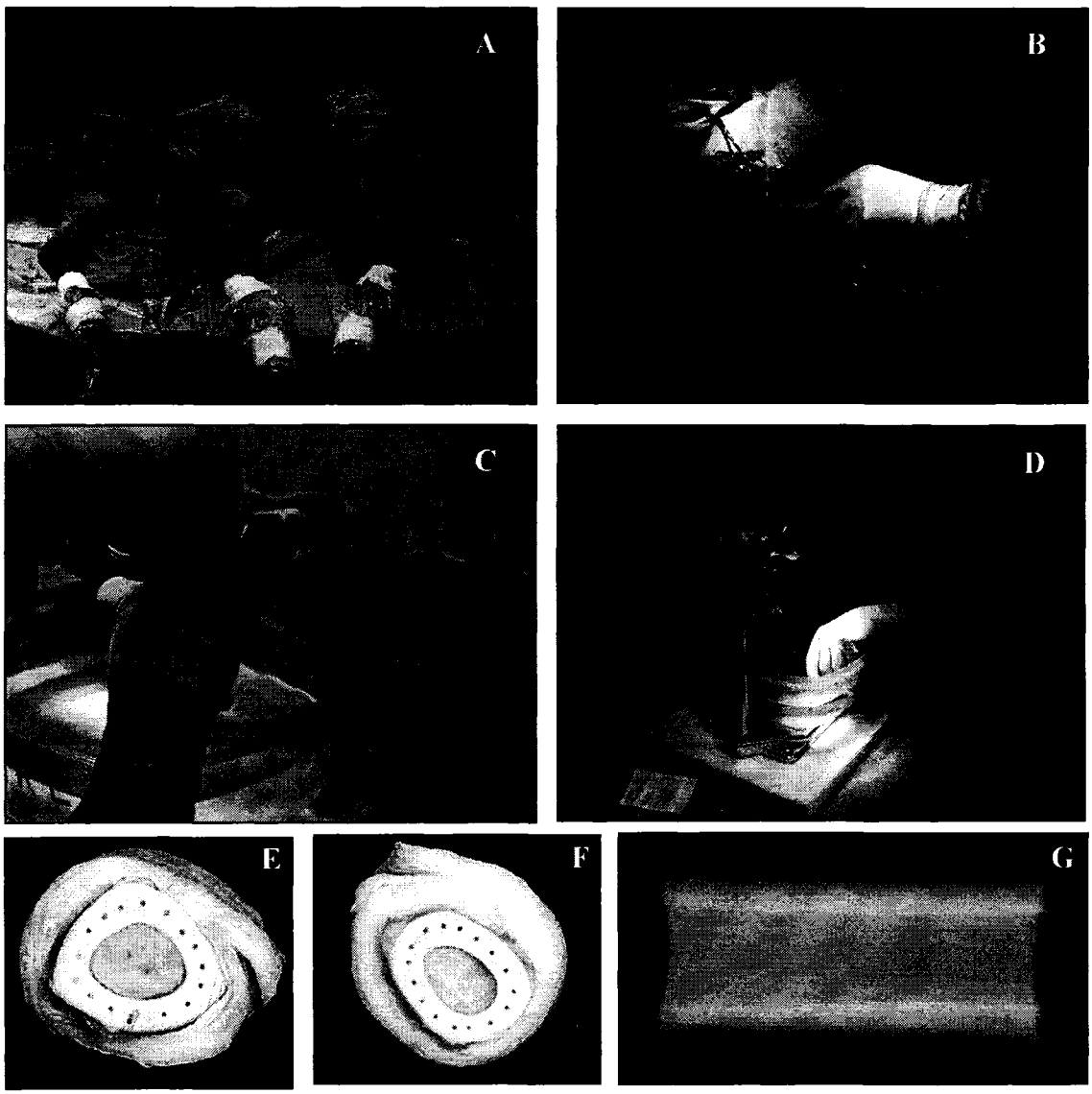

Figure 2.2. (A) Draped ovine hindlimbs prepared for allograft harvest; (B) 5 cm cranial incision in mid-diaphyseal region of tibia; (C) wrapped specimen secured in stainless steel vice; (D) dremel tool and press used for perforating cortical end plates; (E&F) Proximal and distal end plates of 5 cm perforated allografts; (G) contact radiograph illustrating the consistency of cortical end plate penetration.

2.3.3. Animal Model & Surgical Procedure

The animal model and surgical procedure were approved by the local IACUC committee. Prior to insertion into the defect, the 5 cm bone segments were debrided of all soft tissues (periosteum removed and the medullary canal completely curetted and flushed of all marrow) and subsequently thawed in bone preservation fluid. Skeletally mature, female sheep were prepared for tibial ostectomy using standard aseptic techniques and general anesthesia. With the sheep in dorsal recumbancy, a 12-cm skin incision was made from the left knee (stifle) joint to the ankle to expose the tibia and ostectomy site. An 8.0 mm intramedullary nail (Innovative Animal Products, Rochester, MN) was inserted antegrade using an entry portal in the craniomedial aspect of the tibial plateau. Then, a 5 cm defect was created using an oscillating saw and measurement jig under constant cooling with saline. The allograft was inserted, aligned so as to maximize the degree of proximal and distal congruency, and stabilized with proximal and distal interlocking screws (Synthes, Paoli, PA). Intraoperative characterization of proximal and distal congruency was recorded based on the percentage of graft-host contact at the cranial, caudal, medial and lateral interfaces. Lateral radiographs were taken immediately postoperatively (Figure 2.3 & 2.4).

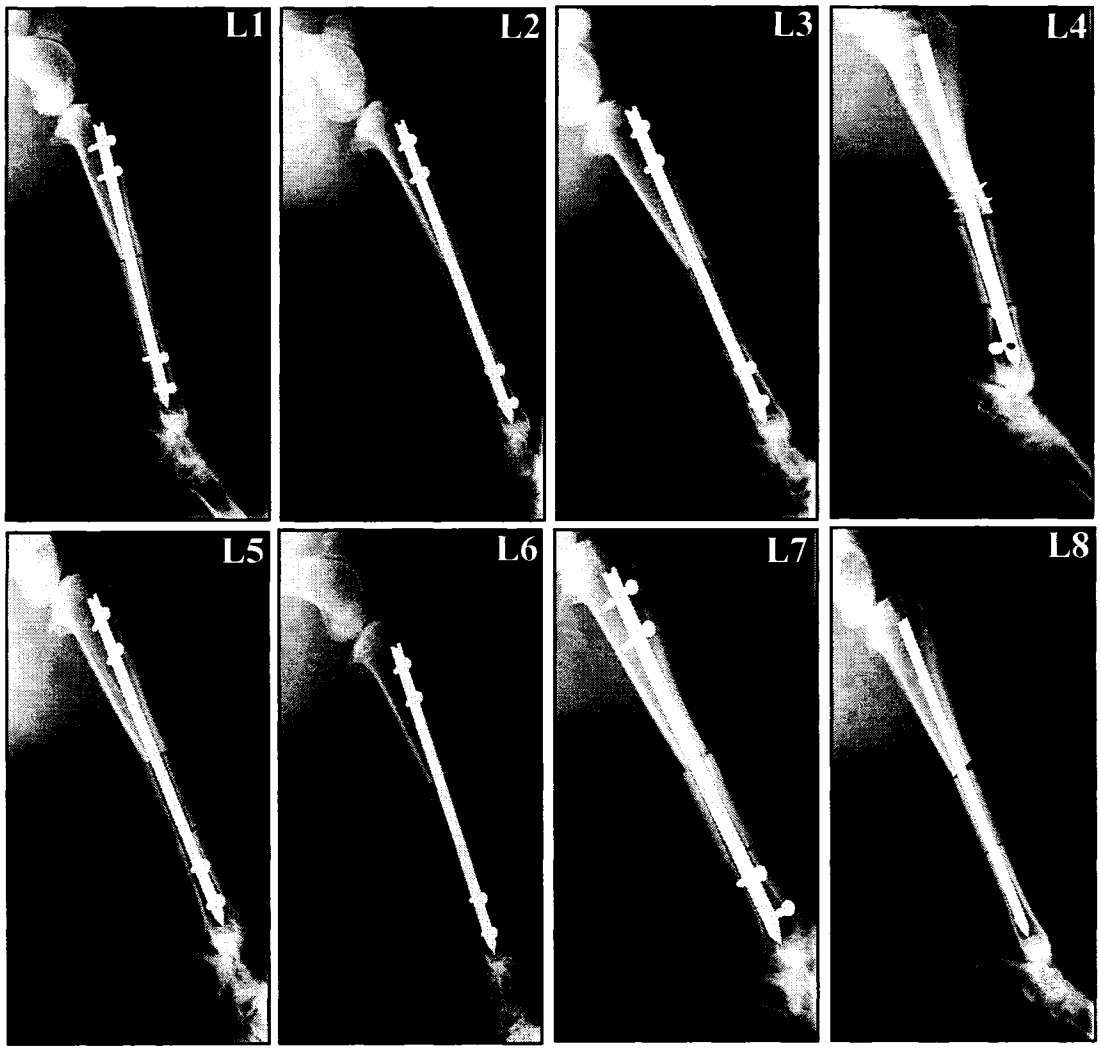

Figure 2.3. Post-operative lateral/medial radiographs of the left tibiae of sheep #1-8. Sheep #4 was euthanized due to missing the most distal of the screw holes.

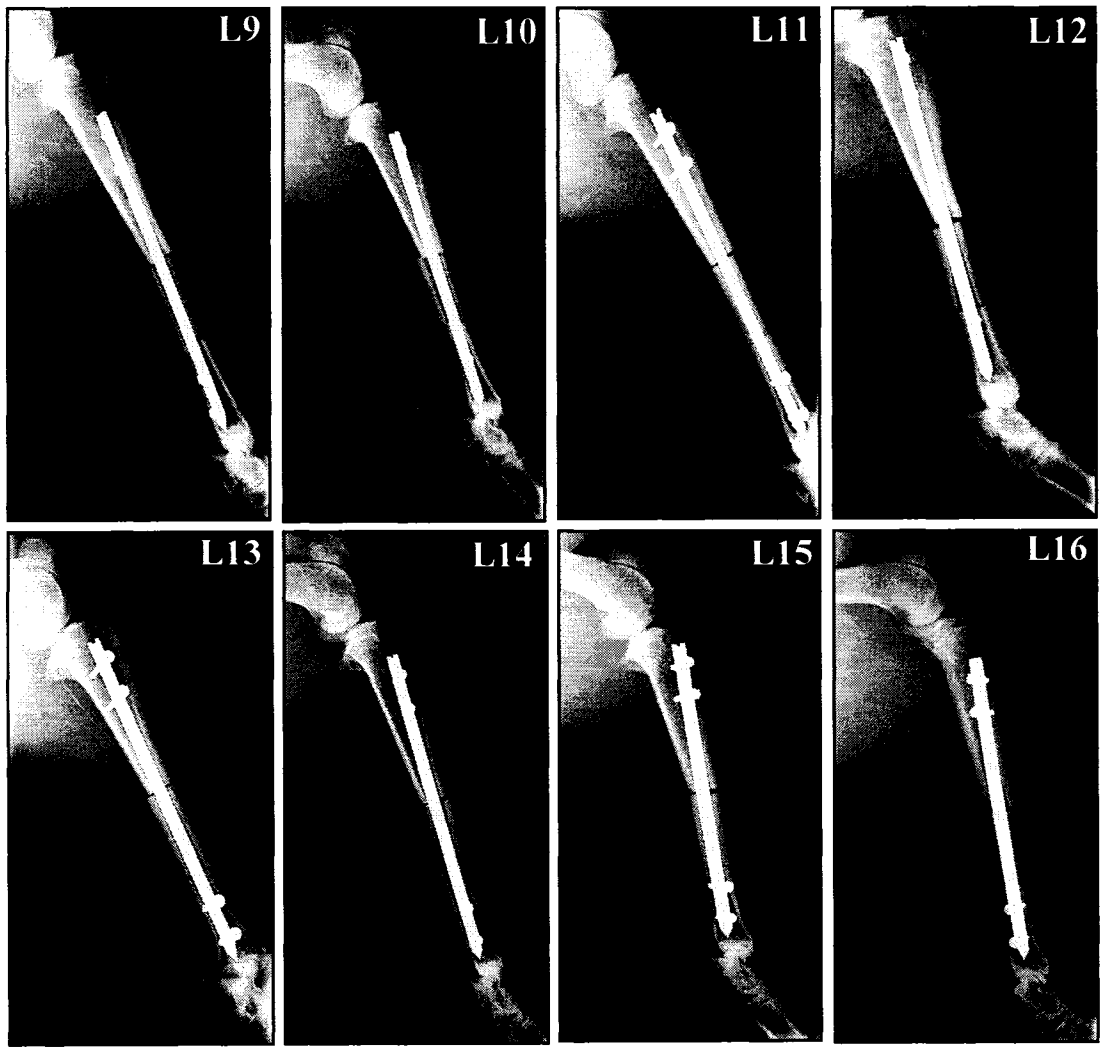

Figure 2.4. Post-operative lateral/medial radiographs of sheep #9-16. Sheep #16 replaced sheep #4 (Figure 2.3).

2.3.4. LIPUS Signal & Duration of Treatment.

Animals in the LIPUS and LIPUS+LAP groups were prepped and fitted with two ultrasound transducers (Figures 2.5 & 2.6) within 72 hours following surgery. Ultrasound gel was applied to the experimental limb on the cranial/medial aspect the tibia at both the proximal and distal graft-host junctions and the transducers were affixed using a custom retaining and alignment strap (Figure 2.6). The 1.5 MHz ultrasound signal generated by an Exogen 2000+ SAFHS device (Exogen Inc., Piscataway, NJ) consisted of a 200 μs burst sine wave repeating at a frequency of 1.0 kHz at a signal intensity of 30 mW/cm^2. Ultrasound exposure was 20 minutes/day for 5 days/week for the duration of the healing period.

2.3.5. Radiography and Hard Callus at the Proximal and Distal Host-Graft Junctions

Allograft healing was assessed by post-euthanasia medial/lateral and cranial/caudal digital radiographs using a standard image analysis system (NIH Image J, NIH, Bethesda, MD, USA). Radiographs were calibrated by a density phantom during acquisition. The total periosteal callus area was quantified and further categorized into high density (equivalent to adjacent cortical bone) and low density callus. Measurement regions extended throughout the length of the allograft and 1 cm into the host bone.

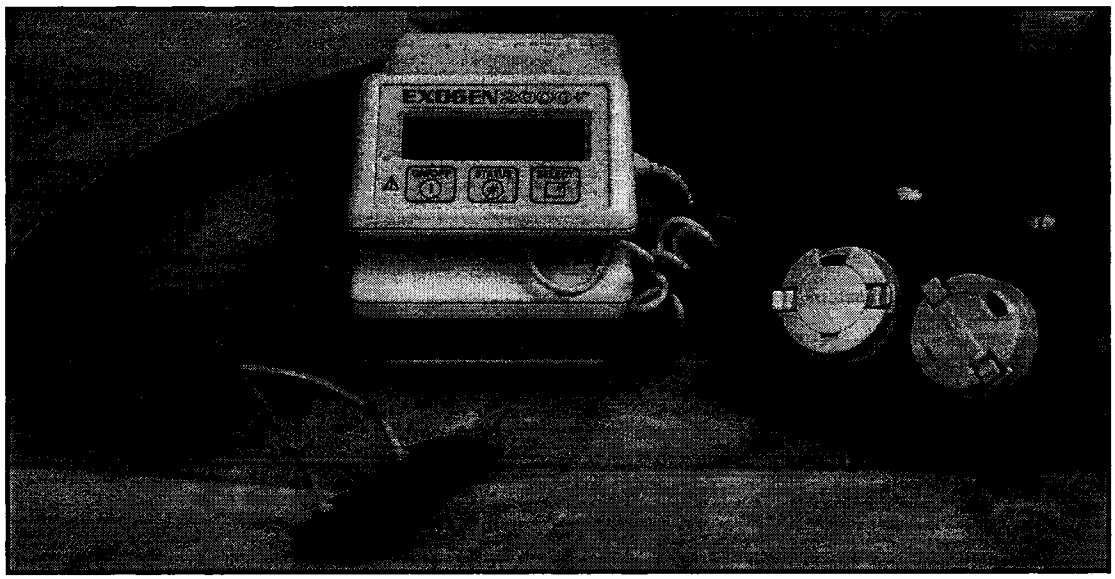

Figure 2.5. Exogen 2000+ system used for delivery of LIPUS consisting of (A) dual PZT (lead zirconia titanate) transducers for simultaneous stimulation of the proximal and distal host-graft junctions, (B) main operating units and (C) modified retaining and alignment fixture (RAF) that maintained transducer separation of 5cm (center to center).

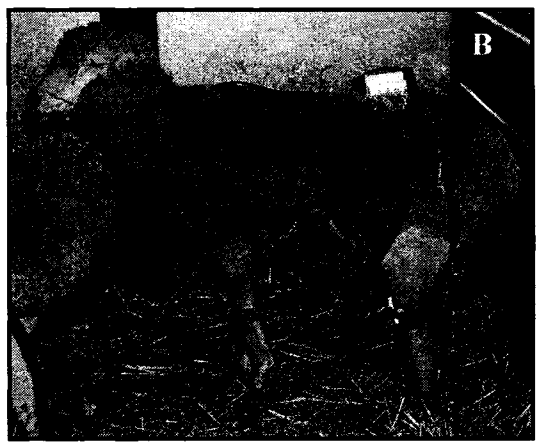

Figure 2.6. RAF application to left tibia of LIPUS sheep (A); proximal and distal transducers were coated with a generous amount of coupling gel prior to application; illustration of restraining harness and cranial/medial positioning of transducers (B).

2.3.6. Biomechanical Testing

Following euthanasia, the tibiae were dissected and the surgical hardware carefully removed without disturbing the callus. Specimens were wrapped in saline soaked gauze sponges until testing. After removal of the surgical hardware, the tibiae were cut to a standard length to maintain a consistent gauge length during torsional testing. The proximal and distal ends of the tibia were potted in specially designed boxes using high strength potting resin (Dynacast potting material #960DTGU-Green, Kindt-Collins Co, Cleveland, OH). The resin was allowed to set for at least 2 hours prior to testing. The contralateral intact control limbs (iCTL) were prepared in the same manner as the experimental tibiae. The gauge length and cross-sectional geometry at the central region of defect or central gauge length were measured using a digital micrometer and recorded.

Within 12 hours of death, the specimens were mechanically tested in torsion at a rate of 12 degree/sec until failure (Figure 2.7)[4]. Right limbs were torqued clockwise and left limbs were torqued counterclockwise to maintain external rotational moments for all tibiae. Torque and angular displacement data were collected at 100 Hz during testing. Tibial geometry was modeled as that of a hollow, thin-walled ellipse (Fig 2.8). Digital photographs of the specimens prior to and following failure were taken to document gross appearance, failure mode, fracture pattern, and failure location. Digital calipers were used to take rough measurements of the outside diameter and cortical thickness of the tibia at the site of failure in the cranial/caudal plane and the medial/lateral plane. The following variables were calculated from torque and angular displacement data: cross

sectional area, polar moment of inertia, torsional strength (Eqn. 2.1, 2.5)*, shear modulus (Eqn. 2.2), energy absorbed at failure and torsional stiffness.

$$\tau = \frac{Tb}{J} \quad \text{(General Equation of Shear Stress)} \qquad \textbf{Equation 2.1}$$

$$G = \frac{Tl}{\theta K} = Stiffness * \frac{l}{K} \qquad \textbf{Equation 2.2}$$

where

$$K = \frac{4\pi^2 t * \left[(a - \frac{1}{2}t)^2 * (b - \frac{1}{2}t)^2 \right]}{U} \qquad \textbf{Equation 2.3}$$

and

$$U = \pi(a + b - t)\left[1 + 0.258 \frac{(a-b)^2}{(a+b-t)^2} \right] \qquad \textbf{Equation 2.4}$$

where θ is the angle of twist, T is the applied torque, l is the length of the unembedded bone (i.e. gage length), τ is the shear stress, b is the minor radius of the bone diameter (elliptical), G is the shear modulus and J is the polar moment of inertia. Stiffness was calculated as the slope of the linear portion of the torque/angular displacement curve and K is the shape dependant factor for a hollow ellipse. Taking the elliptical geometry into account, shear stress in a cortical cross section was calculated as follows [51]:

$$\tau = \frac{T}{2\pi * t * (a - \frac{1}{2}t) * (b - \frac{1}{2}t)} \qquad \textbf{Equation 2.5*}$$

*The mechanics principles used to derive Equation 2.5 can be traced back to advanced theories that describe the deformation and shear stresses induced in non-circular members exposed to torsional loading proposed by St. Vennant and Prandtl; the K formula as well as the stress formula are based on rigorous mathematical analyses but are approximate; their accuracy depends upon how nearly the actual section conforms to the geometrical assumptions and geometrical uniformity.

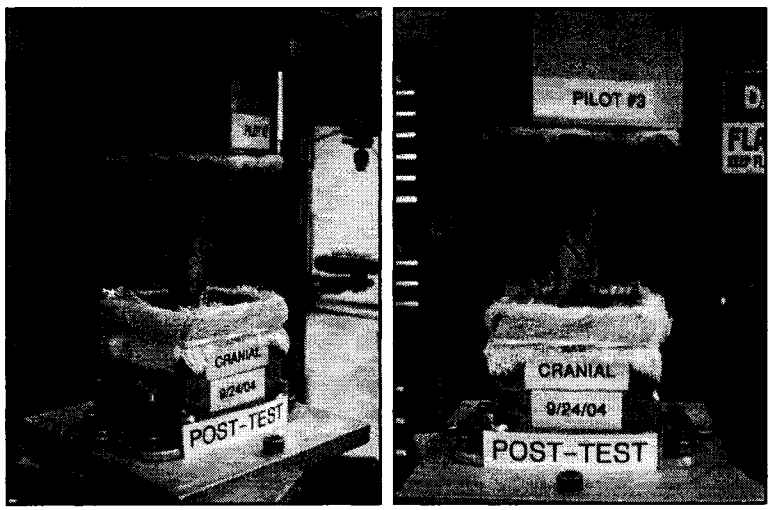

Figure 2.7. Gross images of biomechanical testing set-up illustrating consistent gage length, potting boxes and orientation of tibiae within the MTS machine.

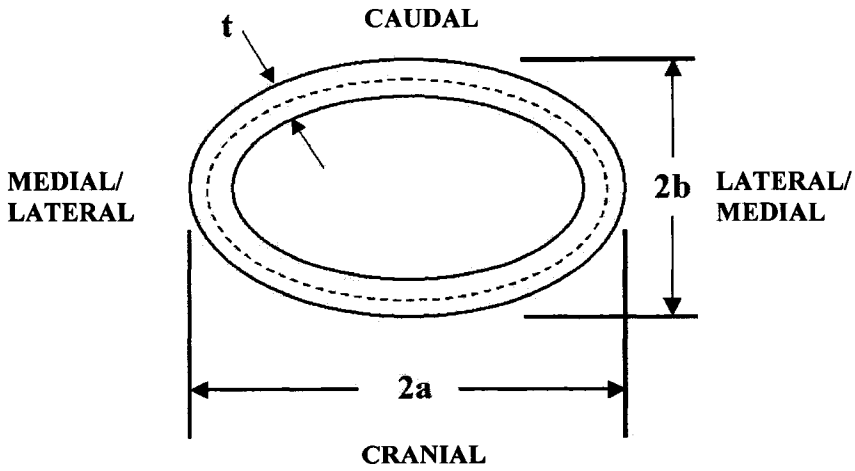

Figure 2.8. Hollow, thin-walled section of uniform thickness used to model geometry of mid-diaphyseal ovine tibias exposed to torsional loading. Dashed line used to calculate U (defined above), which is used in calculating the shape factor.

All biomechanical data were normalized to the value of the iCTL (intact contralateral control). Normalization was accomplished by calculating the difference between the torsional property for the intact limb and the experimental limb (LIPUS, LAP, LIPUS+LAP, -CTL, +CTL) for each animal. The response variable statistically evaluated was this difference in the torsional property. Normalization was performed to minimize the inherent variability in torsional properties between animals. Although statistical comparisons between treatments were performed on normalized torsional values, descriptive statistics and graphical representation are illustrated using the true torsional value (not normalized) in order to provide practical data. After testing the specimens were bisected in the sagittal plane and fixed for histological evaluation (Figure 2.1).

2.3.7. uCT Analysis.

One animal from each treatment group was randomly chosen to receive micro-computed tomography (μCT) scans. After mechanical testing, tissue debridement and immersion in formalin, the distal section (2.5 cm x 1 cm) of the lateral half of the allograft-host junction underwent μCT scanning at a resolution of 30 μm (Scanco Medical uCT 40, ScanCo USA, Southeastern, PA). This 2.5 cm region of interest (ROI) contained 1.0 cm of host bone and a 1.5 cm section of allograft. The μCT images were used to qualitatively visualize cortical bone bridging, callus formation and the degree of bone penetration into the longitudinal perforations for the LAP and LAP+LIPUS groups. Bone penetration was quantified by measuring the diameter of the perforation relative to the

initial drill size. After μCT scans, the specimens continued through the decalcification process and embedding for histopathological assessments.

2.3.8. Statistical Analysis

The effects of LIPUS, LAP, LIPUS+LAP on cortical, intercalary allograft healing after 16 weeks of healing were determined using a 1-way ANOVA followed by a Dunnett's post hoc multiple comparison procedure with the allograft only treatment group serving as the control. Biomechanical response variables of interest included: ultimate torque at failure, maximum angle at failure, torsional stiffness, energy absorbed at failure, ultimate shear stress, and shear modulus.

Given the small n and associated power with this study, Cohen's d values for treatment effects were also calculated. Whereas statistical tests of significance provide information as to the likelihood that experimental results differ from chance expectations, effect-size (ES) measurements provide information as the relative magnitude of the experimental treatment. Cohen's d was computed as an estimate of effect size on all significant/insignificant findings using the means and pooled standard deviations. A large effect size is considered when $d \geq 0.8$, medium when $d \geq 0.5$, and small when $d \geq 0.2$.

Radiographic results of total callus area and total callus area with equivalent cortical density between treatment groups were analyzed in a similar fashion. Additionally, a

correlation analysis was performed to investigate the biological effects of ultrasound and increased cortical perforation (i.e. hard callus area quantification through Image J analysis) to the mechanical findings (i.e. ultimate torque, stiffness, etc.). An additional correlation analysis was performed to determine the effect of allograft congruency with adjacent proximal and distal host tissue and quantified callus area. All statistical analyses were conducted using SAS statistical software (SAS Institute, Cary, NC) at a significance level of α=0.05.

2.4. Results

2.4.1. Surgical Procedure

Intraoperative assessments of proximal and distal host/graft congruencies are tabulated in Table 2.2. There were three post-operative complications, two of which occurred within 72 hours of surgery. Both animals were humanely sacrificed and replaced for inclusion in the study. The third complication occurred 13 weeks postoperatively when one animal sustained a left metatarsal fracture. This animal was euthanized immediately and the reconstructed limb and intact, contralateral control limb were harvested and stored at -20°C for inclusion in the biomechanical, radiographic and histological analyses. Despite three complications, all other sheep were ambulatory within 24 hours following surgery.

2.4.2. Post-Operative Radiography and Gross Appearance:

After 4 months of healing, radiolucent lines were radiographically observed at the proximal graft-host junctions in all treatment groups. However, 8 of the 15 distal graft-host junctions (53.3%) were radiographically united after the healing period. All animals receiving autologous intercalary grafts (+CTL) were united at the distal junction after 4 months. None of the –CTL (allograft only) were either radiographically or grossly united. Gross images of representative reconstructions from each of the four treatment groups are provided in Figure 2.9.

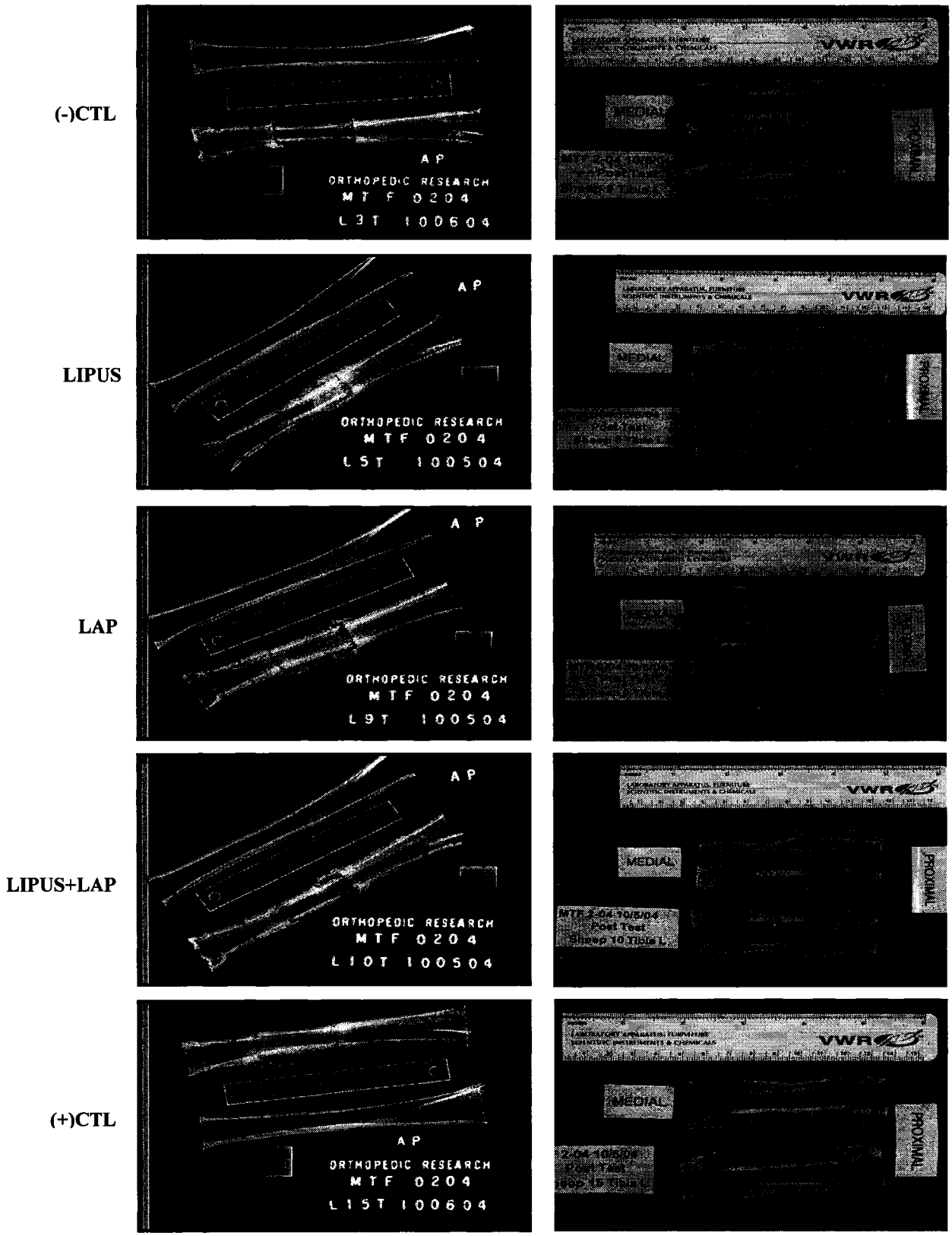

Figure 2.9. From left to right for each treatment group: Four-month c/c radiographs, pre-test reconstructed limb (L) and the iCTL (R), and experimental limbs cut in sagittal plane to reveal gross appearance of the allograft/autograft within the host tissue.

Table 2.2. Operative Summary

Sheep Number/ Treatment Group	Congruency (%)		Congruency (Average %)	
	Proximal	Distal	Proximal	Distal
1/(-)CTL	75	75		
2/(-)CTL	95	95	87	90
3/(-)CTL	90	100		
4/LIPUS	50	100		
5/LIPUS	50	65	87	90
6/LIPUS	100	80		
7/LAP	85	85		
8/LAP	50	90	70	75
9/LAP	75	50		
10/LIPUS+LAP	95	95		
11/LIPUS+LAP	95	95	73	97
12/LIPUS+LAP	30	100		
13/(+)CTL	75	90		
14/(+)CTL	50	100	73	96
15/(+)CTL	50	100		

2.4.3. Structural & Mechanical Properties.

Biomechanical failures of all reconstructions occurred at the proximal host/graft junction. LIPUS, LAP, and LIPUS+LAP treated limbs exhibited increased torque, stiffness, and structural energy absorbed at failure compared to –CTL yet the differences were not statistically significant (Figure 2.10). On average, the +CTL tibiae had structural properties equivalent to intact tibia. Cohen's *d* values for effect size (ES) indicated large treatment effects relative to the negative control for ultimate torque (LIPUS: d=1.45; LAP: d=1.14; LIPUS+LAP: d=2.11) and stiffness (LIPUS: d=1.96; LAP: d=1.80; LIPUS+LAP: d=1.98).

No significant differences between LIPUS, LAP, and LIPUS+LAP treatment groups were noted for ultimate torsional strength or shear modulus (Table 2.3). Relative to the –CTL (allograft only), +CTL exhibited a 21.3% increase in ultimate torsional strength and a 23.5% increase in shear modulus (p=0.004 and p=0.018. respectively). However, +CTL torsional properties were only 29% that of the contralateral intact tibiae at four months. The ultimate strength and shear modulus of LIPUS, LAP, and LIPUS+LAP treated tibia were less than 10% that of their intact tibial controls.

Table 2.3. Summary of Mechanical Data.*

	Torsional Strength (N/mm^2)			Shear Modulus (N-mm/deg)		
Group	Treatment Limb		% iCTL	Treatment Limb		% iCTL
(-) CTL	4.532 ±	0.358	7.70	1.429 ±	0.264	5.17
LIPUS	4.585 ±	0.119	8.29	2.222 ±	0.844	7.17
LAP	3.191 ±	0.827	5.72	0.917 ±	0.136	4.15
LIPUS+LAP	5.506 ±	1.923	10.10	1.812 ±	0.769	7.60
(+) CTL	12.983 ±	5.001	28.70	5.650 ±	1.336	28.69

*Results presented as Mean ± SEM

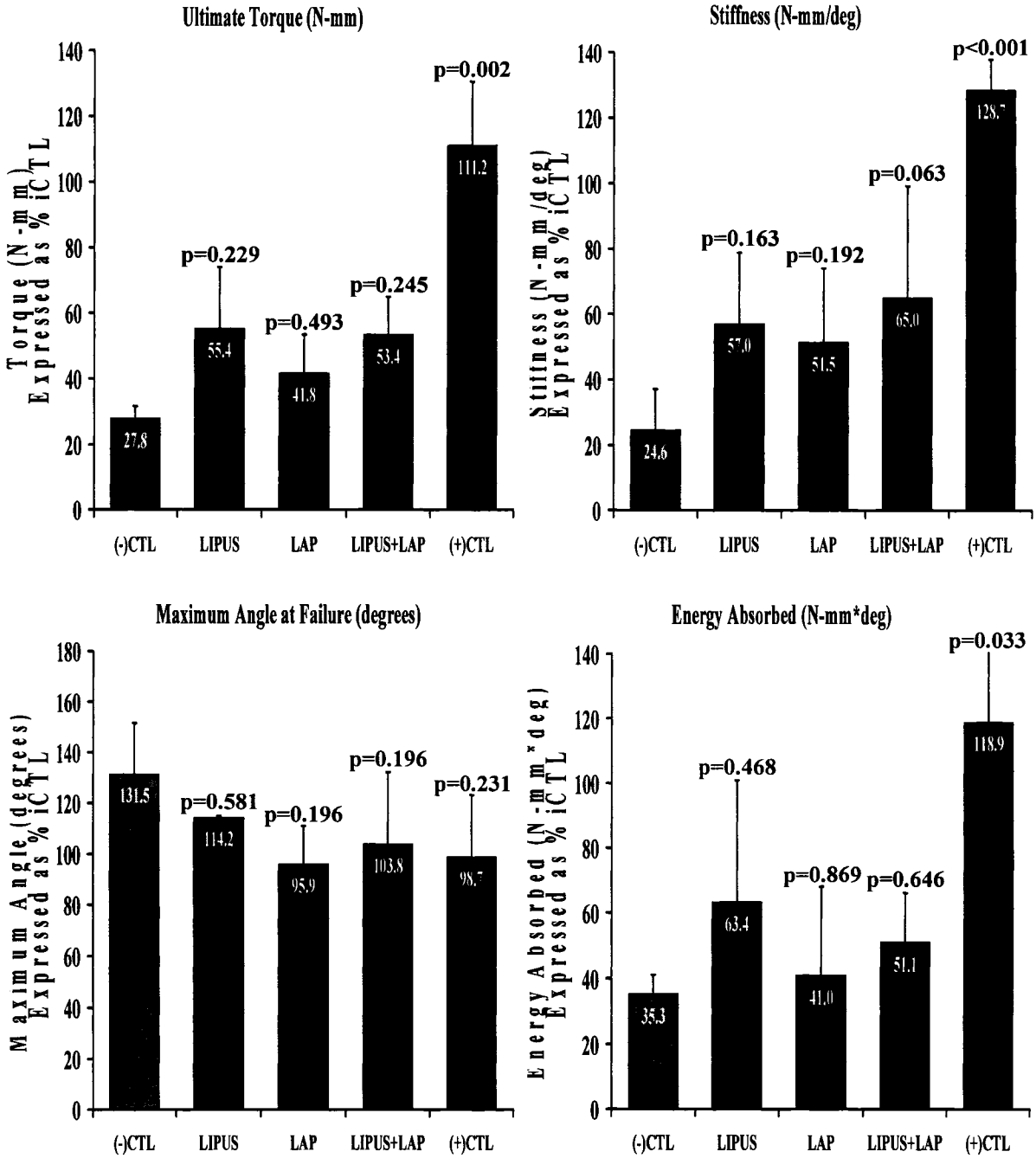

Figure 2.10. Summary of structural properties (Mean ± SEM); though experimental treatment comparisons to the (-)CTL were not significant ($p>0.05$), limbs reconstructed with 5 cm intercalary allografts and exposed to LIPUS exhibited approximately 30% increases in ultimate torque to failure and stiffness ($p=0.229$ and $p=0.163$, respectively); limbs reconstructed with perforated grafts exhibited similar trends relative to the negative control but to a lesser extent that daily stimulation with LIPUS; combined therapy effects on structural properties were not statistically significant at the four-months time point, but did show a trend of increased stiffness relative to individual therapies; (+)CTL limbs displayed structural properties similar to the iCTL.

2.4.2 Hard Callus Area Quantification.

A graphical summary of total callus formed around the healing allografts is presented in Figure 2.11. Periosteal callus formation was greatest in the LAP treatment group exhibiting 75% more callus area than –CTL (p=0.054). The LIPUS and LIPUS+LAP treatment groups also had greater total callus area than –CTL (p=0.206 and p=0.075, respectively). The +CTL had less callus than the LAP, LIPUS and LIPUS+LAP yet slightly higher periosteal callus area than -CTL (p=0.389). The portion of periosteal callus with a density equivalent to the adjacent host cortical bone in the LIPUS, LAP, and LIPUS+LAP treatment groups were nearly double that found in the –CTL group (Figure 2.12) yet these differences were not significant (p=0.221, p=0.229, p=0.210, respectively). The +CTL treatment group exhibited more high density callus than the –CTL group (p=0.190) but less total callus area than LAP, LIPUS, and LAP+LIPUS treatments.

No correlations were noted between graft/host congruency and total periosteal callus (Proximal: r = -0.132, p=0.644; Distal: r = -0.376, p=0.168). However, strong positive correlations were found between percentage of high-density callus as quantified in the LIPUS, LAP, LAP+LIPUS, and +CTL treatment groups and ultimate torque and stiffness (ultimate torque: r = 0.436, p=0.105; stiffness: r = 0.509, p=0.053). Raw data is available for reference in Appendix 1.

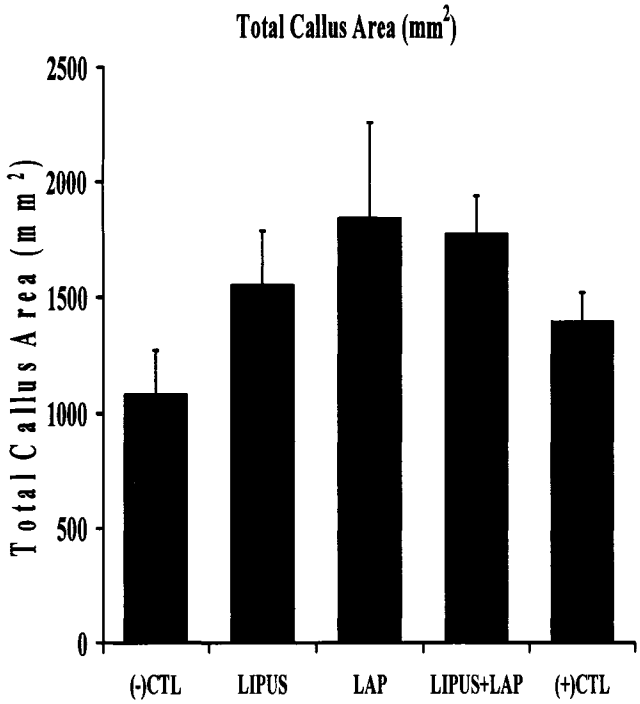

Figure 2.11. Total callus area quantified from 4 months post-operative cranial/caudal and medial/lateral radiographs; periosteal callus formation was greatest adjacent to perforated grafts (LAP, p=0.054, *d*=1.36) followed by limbs reconstructed with perforated grafts and exposed to LIPUS (LIPUS+LAP, p=0.075, *d*=2.26); callus formation was at a minimum in the limbs reconstructed with allograft only (-CTL); results are expressed as Mean ± SEM.

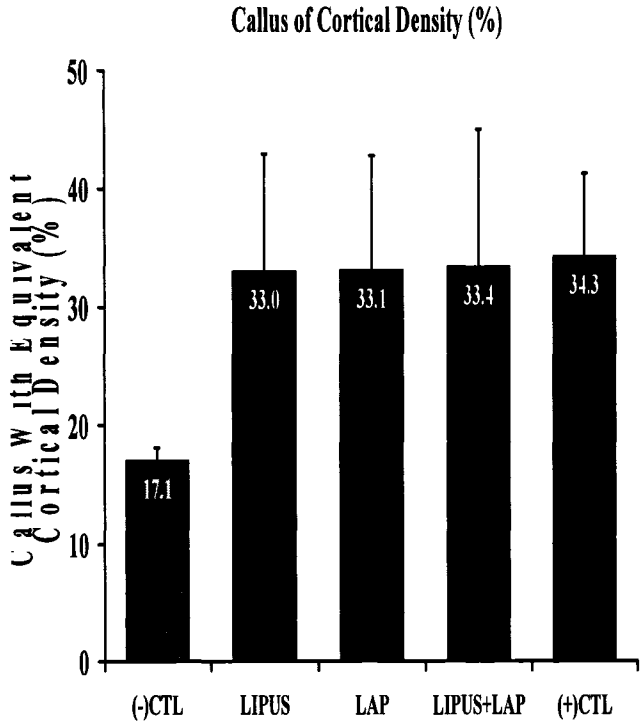

Figure 2.12. Amount of total callus area with density equivalent to cortical bone; experimental treatment groups (LIPUS, LAP, LIPUS+LAP) exhibited twice as much callus with equivalent cortical density relative to the (-)CTL, though this finding was not significant after four months *in vivo* (p>0.210); periosteal callus formation adjacent to autologous graft exhibited a similar trend; results are expressed as Mean ± SEM.

2.4.3 μCT Analysis and Qualitative Analysis.

Transverse μCT slices through the bulk allograft and allograft with longitudinal perforations from the LAP treatment group are presented in Figure 2.13. Figures 2.13B-D show appositional callus surrounding the allograft at three levels. A cross-sectional image within the region of the longitudinal perforations is shown in Figure 2.13D. The ossified callus formation between all treatment groups was similar. Osseous tissue appeared to be deposited within the longitudinal perforations of both the LAP and LIPUS+LAP treatment groups showing a decrease in perforation diameter of 21.6% and 23.5%, respectively.

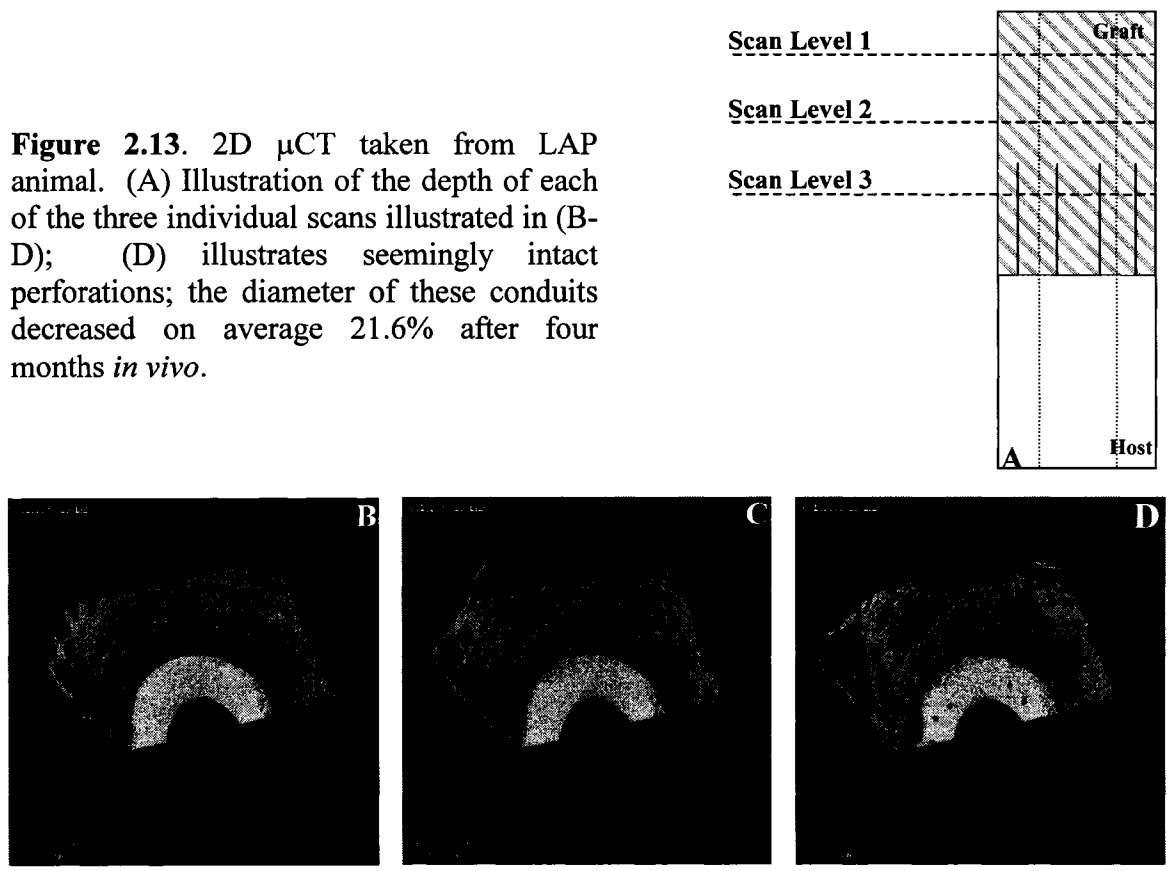

Figure 2.13. 2D μCT taken from LAP animal. (A) Illustration of the depth of each of the three individual scans illustrated in (B-D); (D) illustrates seemingly intact perforations; the diameter of these conduits decreased on average 21.6% after four months *in vivo*.

2.5. Discussion.

The present study demonstrated the potential of low-intensity pulsed ultrasound therapy, delivered for 20 minutes daily to the proximal and distal host-allograft junctions, as a potential exogenous intervention, to improve the biomechanical integrity of ovine tibiae reconstructed with 5 cm intercalary allografts. Though not statistically significant, daily LIPUS stimulation resulted in 28% and 32% increases in limb ultimate torque to failure and stiffness, respectively, after 4 months *in vivo* relative to limbs reconstructed with fresh frozen allograft only and not exposed to the exogenous, biophysical stimulus. Additionally, graft modification with the LAP therapy demonstrated beneficial effects on mechanical integrity, though not to the same degree as LIPUS stimulation. Micro-CT analysis provided indirect evidence that the longitudinal perforations served as conduits for new appositional bone formation as demonstrated by a 22% decrease in conduit diameter after four months *in vivo*.

Fracture of massive intercalary allograft is a common complication that may arise years after initial graft transplantation[31, 50]. Internal stabilization of the proximal and distal host-allograft junctions employing rigid bone plates would provide for direct compression across these interfaces, however screw holes in the allograft increase the risk of fracture[46, 47], and plate placement may prevent circumferential treatment of the host/graft junction. Pressure waves generated by the LIPUS signal that would normally

be incident on the healing tissue could be scattered, if not completely reflected, by an internal plate obscuring the defect site thus reducing the therapeutic dose. In the present research, ovine tibiae were stabilized with an intramedullary, interlocking nail (IN) after transplanting the intercalary graft. Given its intraosseous location, IM nailing provides adequate stabilization without the increased risk of allograft fracture and allows the LIPUS signal to interact directly with the defect site and prevents the radiation from being directly reflected at the periosteal surface. Despite the favorable qualities associated with IM nailing with regard to this study, nails prohibit endosteal callus formation and do not provide for compression across the host/graft interfaces, which has been suggested by some[42] to be of significant importance in promoting allograft incorporation. In addition, IM nails do not confer absolute torsional and flexural rigidity to the reconstructions. Future studies should evaluate the effect of the LIPUS and LAP therapies at promoting allograft healing using a more stable form of internal fixation, such as with a dynamic compression plate.

In successful clinical cases, massive allograft incorporation proceeds in neovascularized areas by the gradual periosteal resorption of the graft by osteoclastic cutting cones followed by new bone deposition by osteoblasts[6]. Adequate stabilization of the graft within the host must be achieved for primary bone healing (direct cortico-cortical union) to occur and optimal graft incorporation. Limb stabilization with IM nailing does not confer absolute rigidity to the reconstruction[4]. Healing of IM-fixed intercalary defects depend on robust callus formation and callus ossification to stabilize the limb and

minimize micromotion at the host-graft interface. Periosteal callus formation in limbs reconstructed with allograft only (-CTL) exhibited minimal callus formation, which translated into minimal structural integrity (27% and 25%, respectively, of the ultimate torque to failure and stiffness of the contralateral intact control limbs). The larger periosteal callus formed with equivalent cortical density in limbs exposed to LIPUS and/or reconstructed with a perforated graft conferred the stability necessary to augment allograft incorporation. Autogenous grafts proceeded to an even higher level of graft incorporation. Though periosteal callus formation was less relative to that quantified in the experimental treatment groups, autologous grafts exhibited more primary graft healing as indicated by the lack of radiolucent lines in post-operative radiographs. Direct cortico-cortical union as well as ossified callus conferred mechanical stability to autografted limbs that exceeded the structural properties of the iCTL. Primary healing of the proximal host-allograft junctions was not achieved in any of the experimental treatment groups and the negative control as indicated by radiolucent lines at the interface. However, the five of twelve (42%) distal host graft junctions in the experimental treatment groups and three of three distal junctions in the +CTL group healed through primary union and periosteal callus formation. This discrepancy may be explained by increased micromotion proximally than distally which may be the result of both a slight degree of curvature in the proximal tibia as well as the internal diameter of the tibia being larger than the external diameter of the IM nail at this interface. The resulting lack of a tight fit in this region may have allowed for excessive micromotion that promoted greater callus formation that had ossified to a lesser degree. This finding

may suggest that a 5 cm intercalary defect is too large a defect in this animal model. Future studies should consider either moving the same size of defect further distally, or consider using a smaller defect size.

Periosteal callus formation increased by 50% to 75% depending upon experimental treatment relative to limbs reconstructed with non-perforated allograft only. A large callus increases the diameter of the bone and distributes the load-bearing tissue away from the neutral axis of the tibia resulting in a higher cross-sectional area and polar moments of inertia over which the applied load can be distributed. The stimulation of callus formation therefore explains the increases in structural properties of experimental limbs exposed to LIPUS. The improvement in biomechanical integrity agrees with those reported previously in fresh fractures in animal[3, 34, 48] and human clinical studies[23, 27]. Interestingly, simple graft modification (LAP) promoted the largest degree of callus formation *in vivo*. Although 20% more callus formed for the LAP group, this tissue did not confer the same degree of structural integrity as limbs exposed to LIPUS, a finding that may be attributed to ultrasound's reported effects on accelerating the endochondral ossification process[25, 32]. Since torsional strength and shear modulus are inversely related to cross sectional area, increases in callus formation also explain why the mechanical properties of the tested limbs were at a minimum relative to the iCTL limbs. The findings that the +CTL was completely healed after four months *in vivo* can be attributed to the osteogenic and osteoinductive qualities of this form of graft. Without adjuvant treatment, the –CTL limbs exhibited structural properties of only 20% relative to normal,

seemingly confirming the lack of osteogenic capacities of such grafts and perhaps implicating the immunogenicity of fresh frozen allografts at impeding healing. The findings that the –CTL progressed to a minimal level of healing as quantified biomechanically is consistent with other large animal studies employing intercalary allografts[35].

The results of this study suggest that LIPUS delivered for twenty minutes daily alone or in combination with a perforated allograft enhanced healing of the junction between a cortical allograft and host bone stabilized internally with an IM nail. LIPUS therapy and LIPUS+LAP combined therapy nearly doubled the treated limb's torsional capacity and torsional stiffness after four months *in vivo* even in the presence of relatively unstable form of fixation. Interestingly, simple modification of the cortical allograft (LAP) resulted in increased structural properties relative to the –CTL, though does not appear to be as proficient as LIPUS therapy at improving limb integrity. However, this study did provide indirect evidence that the longitudinal conduits do accommodate creeping substitution of reparative tissue and promote appositional bone formation within the perforations. Since no graft failures were documented during the four-month healing period, it appears as though the LAP treatment can promote graft revitalization without severely affecting the structural properties of the transplanted tissue. Concomitant histological studies will confirm these biomechanical and radiographic observations that LAP improved graft revitalization and may better ascertain the cumulative effects of LAP and LIPUS.

The results of this study are clinically relevant, as exogenous intervention with LIPUS may improve healing, reduce revision procedures, and obviate the need for autologous bone grafting with it associated morbidity[43]. LIPUS may also be combined with biological interventions such as the introduction of growth factors, to amplify the effects of these potent proteins while reducing the efficacious dose. However, the effects of growth factors on healing are limited to the time they remain at the local site which is often less than a day[9, 37]. LIPUS can be administered immediately post-operatively and continue indefinitely until graft incorporation is determined via clinical examination and radiography.

Although the results presented here are encouraging, future investigations are warranted to determine the effects of LIPUS on malignant cells that may remain following local tumor resection. Though no clinical graft failures were documented in this study, future *ex vivo* investigations are needed to quantify the effects of LAP treatment on graft integrity prior to transplantation *in vivo*. Though only statistical trends were reported here, the clinical significance of 30-40% increases in reconstruction stiffness and ultimate torque to failure following adjuvant LIPUS and/or LAP therapies cannot be understated. Given the large effect size (ES) as quantified by Cohen's *d* values, the lack of statistical significance is thought to be the result of low sample size per treatment group (n=3) and low power (post-hoc biomechanical power = 0.54). Future studies with larger sample sizes (n=8, power=0.77) may substantiate with statistical significances the large effect sizes and statistical trends quantified in this exploratory biomechanical investigation.

2.6 References.

1. Anglen J: The clinical use of bone stimulators. J South Orthop Assoc. 12(2):46-54, 2003.

2. Aynaci O, Onder C, Piðskin A, et al.: The effect of ultrasound on the healing of muscle-pediculated bone graft in spinal fusion. Spine. 27(14):1531-1535, 2002.

3. Azuma Y, Ito M, Harada Y, et al.: Low-intensity pulsed ultrasound accelerates rat femoral fracture healing by acting on the various cellular reactions in the fracture callus. J Bone Miner Res. 16(4):671-680, 2001.

4. Benevenia J, Zimmerman M, Keating J, et al.: Mechanical environment affects allograft incorporation. J Biomed Mater Res. 53:67-72, 2000.

5. Berrey BH, Jr., Lord CF, Gebhardt MC, Mankin HJ: Fractures of allografts. Frequency, treatment, and end-results. J Bone Joint Surg Am. 72:825-833, 1990.

6. Burchardt H: The biology of bone graft repair. Clin Orthop. 174:28-42, 1983.

7. Burchardt H, Busbee GA, 3rd, Enneking WF: Repair of experimental autologous grafts of cortical bone. J Bone Joint Surg Am. 57(6):814-819, 1975.

8. Capanna R, Donati D, Masetti C, et al.: Effect of electromagnetic fields on patients undergoing massive bone graft following bone tumor resection. A double blind study. Clin Orthop. 306:213-221, 1994.

9. Cook SD, Rueger DC: Osteogenic protein-1: biology and applications. Clin Orthop Relat Res. **324**:29-38, 1996.

10. Cook SD, Salkeld SL, Popich-Patron LS, et al.: Improved cartilage repair after treatment with low-intensity pulsed ultrasound. Clin Orthop Relat Res. S231-243, 2001.

11. Cullinane DM, Lietman SA, Inoue N, et al.: The effect of recombinant human osteogenic protein-1 (bone morphogenetic protein-7) impregnation on allografts in a canine intercalary bone defect. J Orthop Res. 20(6):1240-1245, 2002.

12. Duarte LR: The stimulation of bone growth by ultrasound. Arch Orthop Trauma Surg. 101(3):1983.

13. Eck JC, Hodges SD, Humphreys SC: Techniques for stimulating spinal fusion: efficacy of electricity, ultrasound, and biologic factors in achieving fusion. Am J Orthop. 30(7):535-541, 2001.

14. Ehrhart NP, Eurell JA, Constable PD, et al.: The effect of host tissue irradiation on large-segment allograft incorporation. Clin Orthop Relat Res. 435:43-51, 2005.

15. Enneking WF, Campanacci DA: Retrieved human allografts: a clinicopathological study. J Bone Joint Surg Am. 83-A(7):971-986, 2001.

16. Enneking WF, Eady JL, Burchardt H: Autogenous cortical bone grafts in the reconstruction of segmental skeletal defects. J Bone Joint Surg Am. 62:1039-1058, 1980.

17. Enneking WF, Mindell ER: Observations on massive retrieved human allografts. J Bone Joint Surg Am. 73(8):1123-1142, 1991.

18. Fini M, Giavaresi G, Setti S, et al.: Current trends in the enhancement of biomaterial osteointegration: biophysical stimulation. Int J Artif Organs. 27(8):681-690, 2004.

19. Garbuz DS, Masri BA, Czitrom AA: Biology of allografting. Orthop Clin North Am. 29(2):199-204, 1998.

20. Gebhardt MC, Flugstad DI, Springfield DS, Mankin HJ: The use of bone allografts for limb salvage in high-grade extremity osteosarcoma. Clin Orthop. 270:181-196, 1991.

21. Hadjiargyrou M, McLeod K, Ryaby JP, et al.: Enhancement of fracture healing by low intensity ultrasound. Clin Orthop. 355 Suppl:S216-229, 1998.

22. Hantes ME, Mavrodontidis AN, Zalavras CG, et al.: Low-intensity transosseous ultrasound accelerates osteotomy healing in a sheep fracture model. J Bone Joint Surg Am. 86-A:2275-2282, 2004.

23. Heckman JD, Ryaby JP, McCabe J, et al.: Acceleration of tibial fracture-healing by non-invasive, low-intensity pulsed ultrasound. J Bone Joint Surg Am. 76(1):26-34, 1994.

24. Heiple KG, Chase SW, Herndon CH: A Comparative Study of the Healing Process Following Different Types of Bone Transplantation. J Bone Joint Surg Am. 45:1593-1616, 1963.

25. Korstjens CM, Nolte PA, Burger EH, et al.: Stimulation of bone cell differentiation by low-intensity ultrasound--a histomorphometric in vitro study. J Orthop Res. 22(3):495-500, 2004.

26. Kotz R, Ritschl P, Trachtenbrodt J: A modular femur-tibia reconstruction system. Orthopedics. 9:1639-1652, 1986.

27. Kristiansen TK, Ryaby JP, McCabe J, et al.: Accelerated healing of distal radial fractures with the use of specific, low-intensity ultrasound. A multicenter, prospective, randomized, double-blind, placebo-controlled study. J Bone Joint Surg Am. 79(7):961-973, 1997.

28. Lewandrowski KU, Schollmeier G, Ekkemkamp A, et al.: Incorporation of perforated and demineralized cortical bone allografts. Part II: A mechanical and histologic evaluation. Biomed Mater Eng. 11(3):209-219, 2001.

29. Lewandrowski KU, Schollmeier G, Ekkemkamp A, et al.: Incorporation of perforated and demineralized cortical bone allografts. Part I: radiographic and histologic evaluation. Biomed Mater Eng. 11(3):197-207, 2001.

30. Lexer E: Substitution of whole or half joints from freshly amputated extremities by free plastic operation. Surg Gynecol Obstet. 6:601-607, 1908.

31. Mankin HJ, Gebhardt MC, Jennings LC, et al.: Long-term results of allograft replacement in the management of bone tumors. Clin Orthop. 86-97, 1996.

32. Nolte PA, Klein-Nulend J, Albers GH, et al.: Low-intensity ultrasound stimulates endochondral ossification in vitro. J Orthop Res. 19(2):301-307, 2001.

33. Nolte PA, van der Krans A, Patka P, et al.: Low-intensity pulsed ultrasound in the treatment of nonunions. J Trauma. 51(4):693-702, 2001.

34. Pilla AA, Mont MA, Nasser PR, et al.: Non-invasive low-intensity pulsed ultrasound accelerates bone healing in the rabbit. J Orthop Trauma. 4(3):246-253, 1990.

35. Pluhar GE, Manley PA, Heiner JP, et al.: The effect of recombinant human bone morphogenetic protein-2 on femoral reconstruction with an intercalary allograft in a dog model. J Orthop Res. 19:308-317, 2001.

36. Rees DC, Haddad FS, Royal National Orthopaedic Hospital SM: Bone transplantation. Hosp Med. 64(4):205-209, 2003.

37. Ripamonti U: Delivery systems for bone morphogenetic proteins. A summary of experimental studies in primate models. Ann Chir Gynaecol Suppl. 207:13-24, 1993.

38. Rubin C, Bolander M, Ryaby JP, Hadjiargyrou M: The use of low-intensity ultrasound to accelerate the healing of fractures. J Bone Joint Surg Am. 83-A(2):259-270, 2001.

39. Sakurakichi K, Tsuchiya H, Uehara K, et al.: Effects of timing of low-intensity pulsed ultrasound on distraction osteogenesis. J Orthop Res. 22(2):395-403, 2004.

40. Sena K, Leven RM, Mazhar K, et al.: Early gene response to low-intensity pulsed ultrasound in rat osteoblastic cells. Ultrasound Med Biol. 31:703-708, 2005.

41. Sparrow KJ, Finucane SD, Owen JR, Wayne JS: The effects of low-intensity ultrasound on medial collateral ligament healing in the rabbit model. Am J Sport Med. 33:1048-1056, 2005.

42. Stevenson S, Executive Director NJVLJCUSAssac: Biology of bone grafts. Orthop Clin North Am. 30(4):543-552, 1999.

43. Summers BN, Eisenstein SM: Donor site pain from the ilium. A complication of lumbar spine fusion. J Bone Joint Surg Br. 71:677-680, 1989.

44. Sun JS, Hong RC, Chang WH, et al.: In vitro effects of low-intensity ultrasound stimulation on the bone cells. J Biomed Mater Res. 57(3):449-456, 2001.

45. Tarsoly E, Ostrowski K, Moskalewski S, et al.: Incorporation of lyophilized and radiosterilized perforated and unperforated bone grafts in dogs. Acta Chir Acad Sci Hung. 10(1):55-63, 1969.

46. Thompson RC, Jr., Pickvance EA, Garry D: Fractures in large-segment allografts. J Bone Joint Surg Am. 75:1663-1673, 1993.

47. Vander Griend RA: The effect of internal fixation on the healing of large allografts. J Bone Joint Surg Am. 76(5):657-663, 1994.

48. Wang SJ, Lewallen DG, Bolander ME, et al.: Low intensity ultrasound treatment increases strength in a rat femoral fracture model. J Orthop Res. 12(1):40-47, 1994.

49. Warden SJ, Bennell KL, Matthews B, et al.: Efficacy of low-intensity pulsed ultrasound in the prevention of osteoporosis following spinal cord injury. Bone. 29:431-436, 2001.

50. Wheeler DL, Enneking WF: Allograft Bone Decreases in Strength In Vivo over Time. Clin Orthop. 435:36-42, 2005.

51. Young WC: Roark's Formulas for Stress & Strain. New York, McGraw-Hill 1989

52. Younger EM, Chapman MW: Morbidity at bone graft donor sites. J Orthop Trauma. 3:192-195, 1989.

CHAPTER 3. DECALCIFIED AND UNDECALCIFIED HISTOLOGICAL ANALYSES

BIOLOGICAL EFFECTS OF LOW-INTENSITY PULSED ULTRASOUND AND INCREASED CORTICAL POROSITY ON ALLOGRAFT INCORPORATION AND REVITALIZATION

3.1 Introduction.

Skeletal healing is a complex biological process that involves the spatial and temporal orchestration of numerous cell types, growth factors and genes working in unison towards restoring the bone's structural integrity and rapid return to full function. Much thought has been devoted to accelerating or augmenting these reparative processes that have developed over millions of years of vertebrate evolution. Biophysical stimulation has been investigated experimentally and clinically as an orthopaedic intervention for several decades and positive results have been reported for fractures, delayed unions and non-unions [22, 23, 43, 47], bone necrosis[5] and integration of intercalary bone grafts[12]. More recently, biophysical stimulation has been reported to have beneficial effects with regard to biomaterial osteointegration[20]. These interventions include the exogenous application of pulsed electromagnetic fields (PEMF)[3, 45], low intensity ultrasound (LIPUS)[17, 29], high frequency, low magnitude mechanical stimuli [58, 59, 55, 57] and direct electric current[22, 44]. The scientific underpinning for these biophysical approaches is that they serve as non-invasive, exogenous surrogates for the regulatory signals normally arising through functional loading of the skeleton that have become absent because of the sustained trauma.

Ultrasound is a form of mechanical energy that is transmitted through and into biological tissues as an acoustic pressure wave at frequencies above the limit of human hearing. From an orthopaedic standpoint, these acoustic pressure waves mimic a mechanical signal that takes full advantage of bone tissue's sensitivity to low-level physical signals[58, 59]. On passing through the tissue, the ultrasonic energy is absorbed at a rate proportional to the tissue density. The radical changes in density inherent in a healing callus, due to the various tissue types present, may well establish gradients of mechanical strain[28]. The differential energy absorption of ultrasound also induces the movement of fluid across surfaces, a phenomenon know as acoustic streaming[6, 56]. The resultant fluid flow stimulates a dynamic physical environment and may mechanistically advance signal-transduction pathways, a process referred to as mechanotransduction.

Since its first clinical use in the 1950s ultrasound, administered at intensities consistent with those used for diagnostic procedures (1 to 50 mW/cm^2), has been demonstrated in both animal[4, 30, 32, 68] and human clinical studies[33, 47] to have strong osteogenic, chondrogenic, and angiogentic potentials that have ultimately been shown to accelerate fracture and non-union healing. Recent *in vitro* work has even demonstrated anti-osteoclastic capabilities[60, 63] of ultrasound as well as an ability to promote soft tissue healing after injury[14, 61].

A number of studies have been undertaken to identify the exact biological mechanisms by which therapeutic levels of pulsed ultrasound accelerate the remodeling response after sustained trauma. Recent cell-culture experiments have illustrated that daily exposure to

LIPUS promotes the osteoblastic phenotype as evidenced by increased production of IL-8 (interleukin-8), basic-FGF (fibroblast growth factor), VEGF (vascular endothelial growth factor), TGF-β (transforming growth factor-β), alkaline phosphatase, osteonectin and osteopontin, while concomitantly down-regulating the osteoclastic response[54, 60, 63, 67]. The temporal sequence of events concomitant with fracture healing documented clinically combined with the *in vitro* findings that LIPUS stimulates VEGF secretion strongly support the possibility that pulsed, low-intensity ultrasound improves callus formation by initiating enhanced angioneogenesis in the developing callus. The documented pro-osteoblastic and anti-osteoclastic findings have prompted recent efforts that employ LIPUS to mitigate the onset of osteoporosis in patients with spinal cord injuries[69].

Though much of the orthopaedic focus with regard to ultrasound therapy has been directed to augmenting fresh fracture repair, no work to date has investigated the healing potential of LIPUS in areas of depleted or absent biology as is the case following tumor resection and replacement with a massive structural bone allograft. Allograft transplantation has become commonplace in clinical orthopaedics yet allograft bone has been found to incorporate slowly resulting in susceptibility to host-graft non-union, fracture, and fatigue failure. These documented findings are a direct result of the lack of osteogenic capacity of the transplanted cadaveric tissue that results following extensive processing and clinical studies have shown that massive allograft bone has a 50% to 75% success rate at 10 years[8, 24, 49], while other orthopaedic implants, such as total hips and knees have a 10-year success rate of approximately 90%[1].

Improving incorporation of the allograft is key to a successful reconstruction and improving long-term clinical outcome[19]. Though the field of bone allograft transplantation has been around for nearly a century, novel strategies that aim to improve graft incorporation are lacking. Recent reports by Cullinane et al.[15], Pluhar et al.[51], and Zabka et al.[70] have attempted to accelerate allograft healing by augmenting the host-graft junctions with osteogenic protein-1 (OP-1) or bone morphogenetic protein-2 (BMP-2) in canine intercalary defects stabilized with IM nails. Their preliminary histological findings suggest enhanced graft incorporation and when allografts were supplemented with these potent biomolecules.

Increasing graft porosity via perforating the bony cortex perpendicular to the long axis of the graft has received considerable attention as a means to improve graft incorporation by the host, though these graft modifications have been reported to have mixed results[11, 38, 39, 64]. Lewandrowski et al.[38, 39] reported increased resorption and little evidence of incorporation of 3 cm intercalary sheep allografts containing multiple 300 μm perforations after 9 months *in vivo*. Combining the transverse perforations with extensive cortical demineralization improved the biologic response of the host to the graft and resulted in almost complete graft incorporation [38, 39] but at the expense of decreasing the flexural properties of the graft by 40%. Since allograft repair proceeds initially by increased osteoclastic activity paralleled by decreased osteoblastic activity that decreases the mass and radiodensity of the material and concomitantly increases its internal porosity[9], transplanting a graft that already has significantly reduced structural properties may potentiate early mechanical failure within the host.

The orientation of perforations within the bony cortex and the ensuing effects on graft revitalization have yet to be quantified. Past research indicates transverse perforations increase allograft porosity but improve graft healing only when the cortical shell is additionally demineralized. The significantly reduced load-bearing capacity of the perforated and demineralized grafts has lead to accelerated mechanical failure and caused orthopaedists to abandon this form of graft modification[53]. Longitudinal perforations, as opposed to those oriented perpendicular to the long axis of the graft, may provide more direct access for bone remodeling cell infiltration and effects on graft revitalization may not be dependent on cortical demineralization. Introducing conduits that run parallel to the long axis of the graft would provide direct access to bone cells for creeping substitution of reparative tissue while minimally affecting the overall strength of the implanted allograft.

This study investigated a novel application of LIPUS therapy either alone or in combination with increased cortical porosity parallel to the long axis of the graft as a means to improve the incorporation and remodeling of a 5 cm intercalary allograft transplanted into a large animal model. Static and dynamic histomorphometric parameters as well as histopathologic parameters were quantified to determine the extent of allograft healing relative to animals not receiving adjuvant treatments.

3.2 Materials and Methods.
3.2.1. Experimental Study Design

Fifteen animals were systematically assigned to five experimental groups based on intercalary graft type and treatment: +CTL, -CTL, LIPUS, LAP, LIPUS+LAP. The +CTL animals (n=3) received a tibial ostectomy with immediate replacement of the resected autologous graft. The –CTL group (n=3) received fresh frozen ovine tibial allografts. Both the +CTL and –CTL groups did not receive LAP or LIPUS treatments. The LIPUS treatment group (n=3), following grafting with fresh frozen ovine tibiae, received low-intensity pulsed ultrasound for 20 minutes/day, 5 days/week, for the duration of the healing period. The LAP treatment group received fresh frozen ovine allografts with 500 μm longitudinal perforations. The LIPUS+LAP treatment group received both LIPUS and LAP treatments. Fluorochrome labels were intravenously administered to all sheep three days (tetracycline at 30 mg/kg IV) and 14 days (calcein green at 20 mg/kg IV) prior to euthanasia. Fluorochrome labels are taken up into actively mineralizing bone matrix and allow for easy detection of allograft turnover and active bone remodeling. All animals were euthanized four months following intercalary allograft transplantation for radiographic, biomechanical, and histological analysis. An overview of the study design is presented in Table 3.1 and Figure 3.1.

Table 3.1. Experiemental Study Design

Treatment	# of Sheep Survival Time	End Point Assays
Allograft only, (-Control, -CTL)	3/4 mos.	Torsional Biomechanics Radiography Decalcified Histology Undecalcified Histology
Allograft + LIPUS (LIPUS)	3/4 mos.	
Allograft + LAP (LAP)	3/4 mos.	
Allograft + LIPUS +LAP (LIPUS + LAP)	3/4 mos.	
Autograft only (+Control, +CTL)	3/4 mos.	

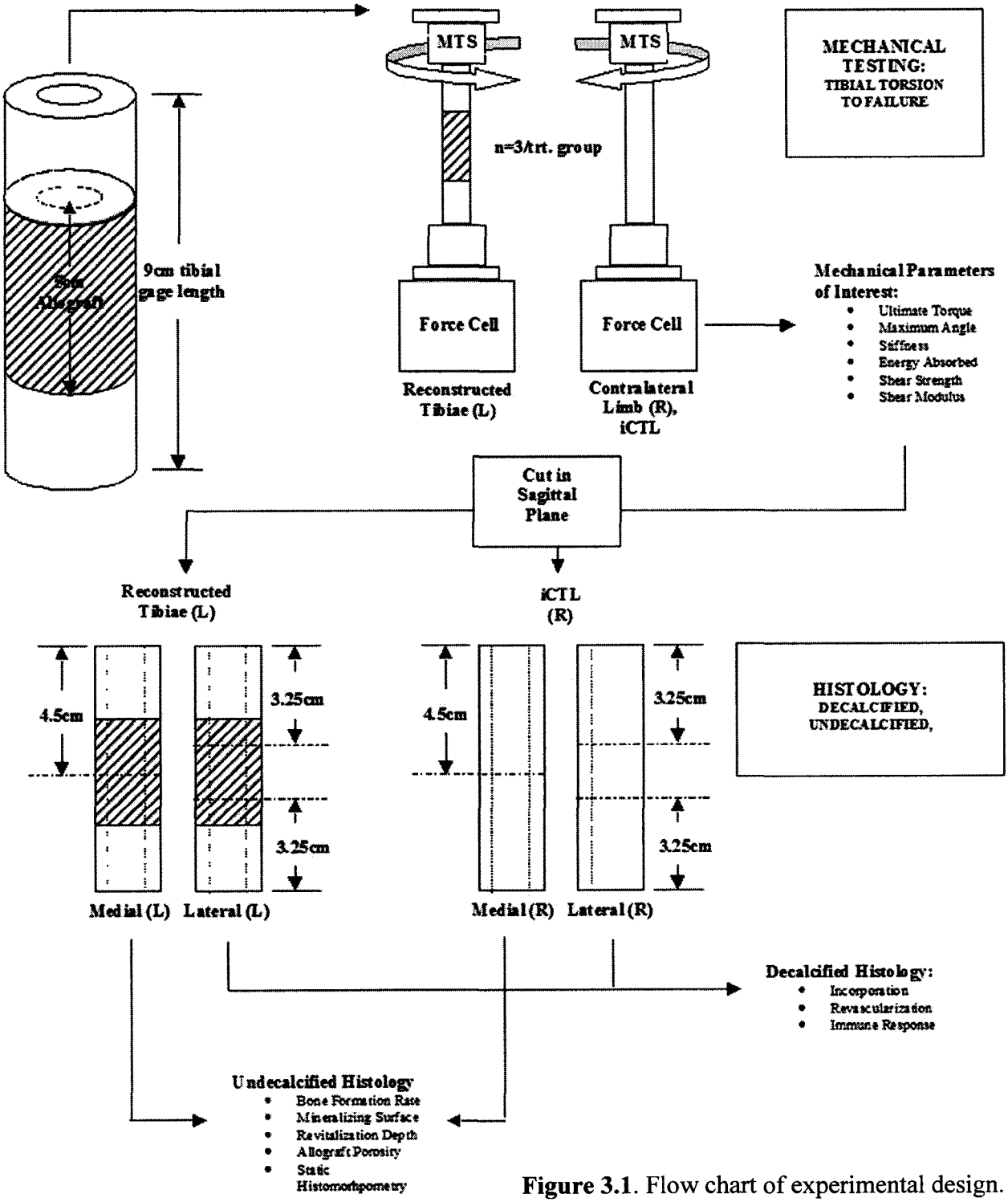

Figure 3.1. Flow chart of experimental design.

3.2.2. Tissue Processing.

Following biomechanical testing, transverse cuts were made to isolate the 5 cm allograft plus 2 cm of proximal and 2 cm of distal host bone (Figure 3.1). The specimens were sectioned immediately in the longitudinal, sagittal plane, creating medial and lateral tibial halves. Sectioning in the sagittal plane was chosen based on the perceived non-homogeneous effects of the ultrasound therapy in this plane due to the cranial placement of the ultrasound transducers over the proximal and distal host/graft junctions.

The medial longitudinal sections were processed for undecalcified histology whereas the lateral longitudinal sections were processed using decalcified histology techniques (Figure 3.1). Briefly, medial halves were sectioned into proximal and distal sections containing approximately 2.5 cm of allograft plus 2 cm of host bone. The proximal and distal specimens were placed in 70% ethyl alcohol (ETOH) for fixation and undecalcified histology. The lateral halves were further sectioned by two transverse cuts creating three tissue specimens: a 3.25 x 1cm distal section (allograft + host bone), a 2.5 x 1cm middle section (allograft only), and a 3.25 x 1cm proximal section (allograft + host bone). Each of the lateral longitudinal sections was placed in 10% neutral formalin for fixation and μCT analysis and decalcified histology.

The contralateral control tibiae were sectioned and processed in an identical fashion to those of the treatment tibiae. However, only the medial section underwent histological analysis. Specifically, the proximal and distal specimens were analyzed for dynamic parameters for comparison to the identical parameters quantified in the reconstructed,

treatment tibia. Such an analysis may provide insight as to any changes in metabolism that occur in the contralateral control limbs relative to the treated limb as a result of the trauma sustained during the surgical intervention, the presence of the cortical allograft, and the delivery of the ultrasonic signal.

3.2.3. Decalcified Histological Analysis.

The formalin fixed tissue specimens were delcalcified in a 12.5% HCl-EDTA solution, dehydrated in graded solutions of ETOH (75%-100%), and cleared with xylene. The specimens were then processed using standard paraffin histology techniques: processed using Citadel 2000 (ThermoShandon), embedded using Histocentre2 (ThermoShandon). Multiple (2-3) 5 μm sections were cut from the specimen block and stained with Hematoxylin and Eosin (H&E) for semi-quantitative evaluation of the degree of allograft revitalization, vascular infiltration, fibrous tissue development and evidence of an elicited immune response. A scoring system was created to evaluate the various parameters considered consistent with allograft healing (Figure 3.2, Appendix II). To quantify treatment effects, of particular relevance to this study were such parameters as the quality and degree of osseous bridging across the host/graft junctions, allograft vascularity, the presence/absence of a chronic immune response, and the degree of callus formation and maturation. In addition, metabolism in the host and graft were quantified as a means to determine treatment effects on the osteoblastic (Ob) and osteoclastic (Oc) activity. The latter was quantified according to an Ob/Oc contimuum score that evaluated the relative contributions of the osteoclasts and osteoblasts to remodeling in the host and the graft (Figure 3.2, Appendix II).

Decalcified histology provided fast turn-around, good cellularity, and general evaluation of morphological features. Digital images were taken of general histological features identified by the H&E stained section.

Histopathological Scoring System

Host-Graft Bridging: 0 ↔ 4
(No bridging ↔ Bridging callus and cortex on two sides)
Callus Tissue Type: 0 ↔ 3 (Fibrous/pseudoarthorosis ↔ Bone)
Host/Graft Direct Interface: 0 ↔ 3 (Fibrous/Pseudoarthrosis ↔ Bone)
Callus (% of Cortical Thickness): 0 ↔ 5 (None ↔ >200%)
Graft Vascularity: 0 ↔ 3 (None ↔ Prolific)
Host Remodeling Continuum: 0 ↔ 6
(No Oc resorption ↔ *Extensive Oc resorption/Extensive Ob presence)*
Graft Remodeling Continuum: 0 ↔ 6
(No Oc resorption ↔ *Extensive Oc resorption/Extensive Ob presence)*
Inflammatory Cell Presence: 0 ↔ 2 (Many ↔ None)

Figure 3.2. Scoring system developed for intercalary allograft healing. For a more detailed explanation of graded parameters, refer to Appendix II.

3.2.4. Undecalcified Histological Analysis.

After fixation, the medial, 4.5 x 1cm proximal and distal sections were placed in fresh 70% ETOH for 1 week then dehydrated in graded solutions of ETOH (70%, 95%, and 100%) and xylene over the course of approximately 5 weeks. The samples were infiltrated with a series of solutions containing methyl methacrylate, dibutyl phthalate, and benzoyl peroxide. The final methyl methacrylate solution was polymerized into a hardened plastic block and kept in the dark until completion of dynamic analysis. One 300 μm section was taken from each specimen block in the sagittal plane using an Exakt diamond blade bone saw (Exakt Technologies, Oklahoma, OK). All sections were ground to 100 μm thickness using an Exakt microgrinder. The sections remained unstained until after dynamic histomorphometric analyses (Figure 3.3), then were stained using Sanderson's rapid bone stain (Surgipath, Richmond, IL) and counterstained with acid fuchsin to provide color differentiation between tissue types for semi-automatic image analysis. This stain displays bone as a vivid red, while soft tissue stains blue/green and cartilage is purple.

High-resolution digital images were acquired for unstained (fluorescent) and stained sections using an Image Pro Imaging system (Media Cybernetics, Silver Spring, MD) and a Nikon E800 microscope (AG Heinze, Lake Forest, CA), Spot digital camera (Diagnostic Instruments, Sterling, Heights, MI), and a pentium IBM-based computer with expanded memory capabilities (Dell Computer Corp., Round Rock, TX). Images were acquired by microscopic field and a composite digital image with multiple fields was reconstructed to represent the region of interest. All histomorphometric measurements

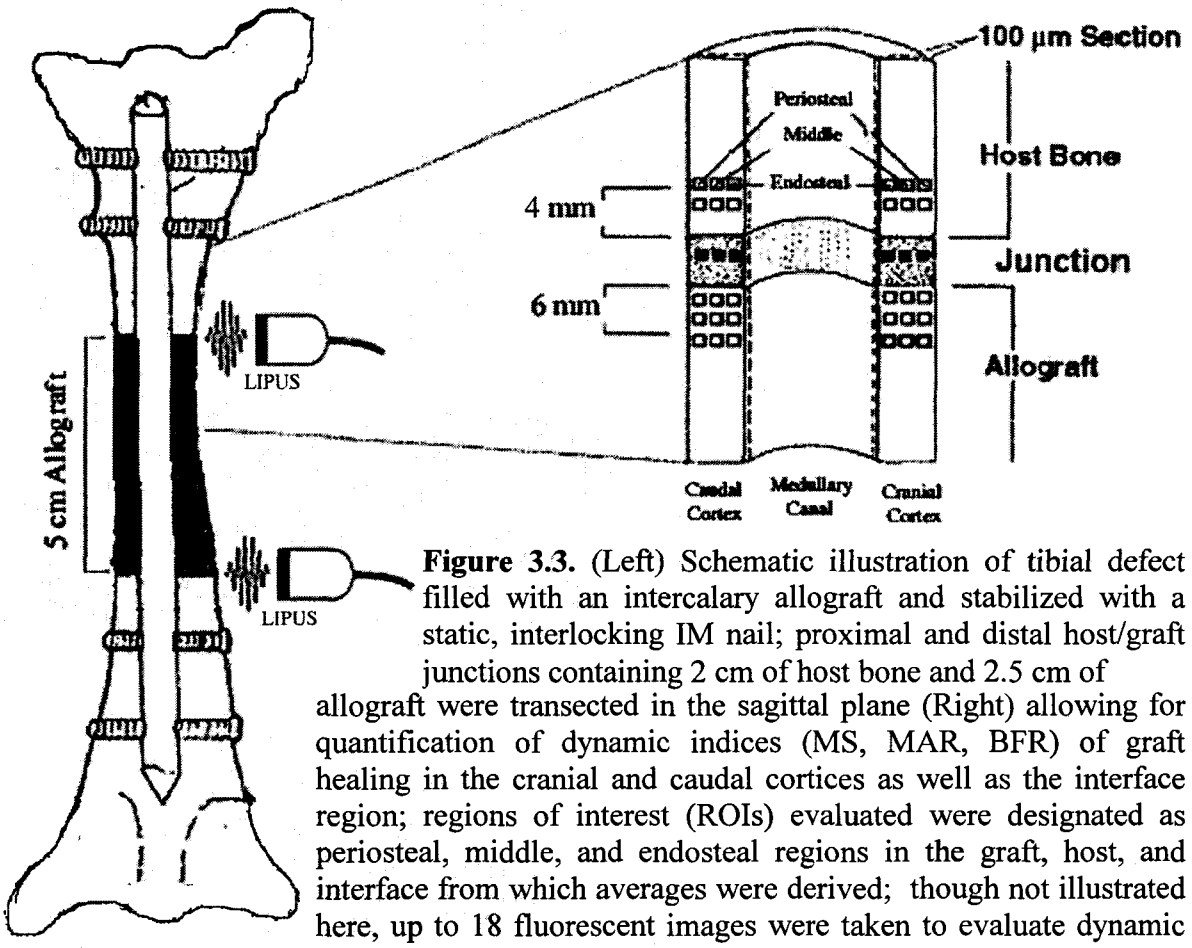

Figure 3.3. (Left) Schematic illustration of tibial defect filled with an intercalary allograft and stabilized with a static, interlocking IM nail; proximal and distal host/graft junctions containing 2 cm of host bone and 2.5 cm of allograft were transected in the sagittal plane (Right) allowing for quantification of dynamic indices (MS, MAR, BFR) of graft healing in the cranial and caudal cortices as well as the interface region; regions of interest (ROIs) evaluated were designated as periosteal, middle, and endosteal regions in the graft, host, and interface from which averages were derived; though not illustrated here, up to 18 fluorescent images were taken to evaluate dynamic parameters in the cranial and caudal callus regions; figure adapted from Zabka at al. [70].

are described according to the standardized system proposed by the ASBMR nomenclature committee[48]. The fluorescent images were used to measure or calculate mineralizing surface (MS), mineral apposition rate (MAR), bone formation rate (BFR), and penetration depth of new bone into allograft tissue (distance into allograft where active remodeling was identified). The specific definitions of each term as well as the nature in which each is calculated are presented for reference in Appendix III.

Images from stained sections were acquired, compiled and the following parameters were measured: osteoclast perimeter, allograft porosity (bone volume relative to total tissue volume), and callus area. Percent of new bone incorporation into allograft was quantified if detectable.

3.2.5. Statistical Analysis.

Decalcified histological parameters (Figure 3.3, Appendix III) were compared with a non-parametric Kruskal-Wallis test with a significance level of α=0.05. Mineralizing surface, mineral apposition rate, and bone formation rate within the host, graft, callus, and interface regions were compared using a 1-way ANOVA followed by a Dunnett's post hoc multiple comparison procedure with the allograft only treatment group serving as the control. Quantified static histomorphometric parameters were compared in a similar fashion. In a final analysis, structural parameters of the reconstructed limbs were correlated to the histologic findings. All statistical analyses were conducted using SAS statistical software (SAS Institute, Cary, NC).

3.3. Results

3.3.1 Decalcified Histology. Connectivity.

Connectivity scores presented in Figure 3.5 quantified the degree of osseous bridging between the host and allograft as well as the tissue composition of the periosteal callus. Although significant differences were not detected between groups for any of the connectivity parameters, the +CTL exhibited the greatest periosteal bridging and direct cortico-cortical bridging between the host and graft. Conversely, the negative control (-)CTL had poor osseous bridging. The LIPUS treatment appeared to improve the periosteal bridging with greater composition of bone in the callus mass. Surprisingly the LAP treatment group had callus thickness comparable to the LIPUS treated groups yet the composition of the callus contained less osseous tissue. Cortical-cortical bridging was most advanced in the positive control yet combination therapy seemed to improve direct healing over the other experimental treatment groups.

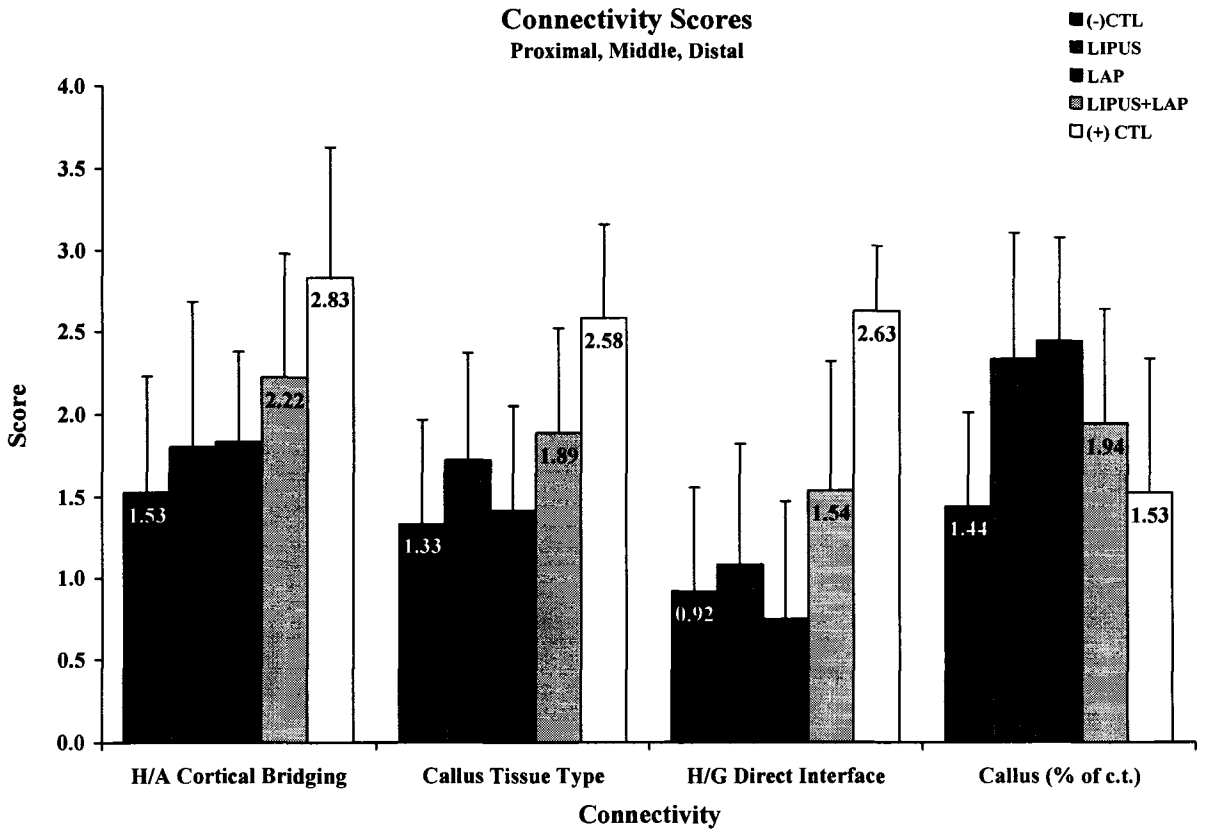

Figure 3.5. Decalcified connectivity scores. Results presented as Mean ± SEM where the mean was compiled by averaging scores from the proximal, middle and distal slides; connectivity scores were on average higher in the (+)CTL group relative to all other experimental treatments and the (-)CTL, which, at four months, elicited a minimal level of osseous bridging; LIPUS treatment appeared to improved osseous bridging and the degree of ossified tissue in the callus; a similar observation was made with the LAP treatment, though the degree of ossified tissue within the callus was smaller; combination treatment seemed to improve direct healing relative to all other treatment groups excluding the (+)CTL; LEGEND: H=host; A=allograft; G=graft; callus formation is expressed as percentage of cortical thickness.

3.3.3. Decalcified Histology - Ob/Oc Continuum & Graft Revitalization.

Host/graft continuum scores as well as graft revitalization scores are presented below in Figure 3.6. Graft revitalization in the experimental treatment groups proceeded periosteally from the highly vascularized and active periosteal callus as quantified by stained osteocytes residing in this general area (Figure 3.8). Osteocytes were also evident in grafts adjacent to interface regions that had progressed to a higher level of osseous bridging (LIPUS, LIPUS+LAP, (+)CTL, Figure 3.5). Host tissue adjacent to bone allograft was highly active as evidenced by high levels of osteoclastic resorption with extensive new bone development while grafted tissues exhibited more osteoclastic resorption with less new bone development. This trend was reversed for the (+)CTL group. No inflammatory cells were observed adjacent to the grafts in any treatment group. Grossly, remnants of the LAP treatment were empty with no evidence of creeping substitution of reparative tissue (Figure 3.7).

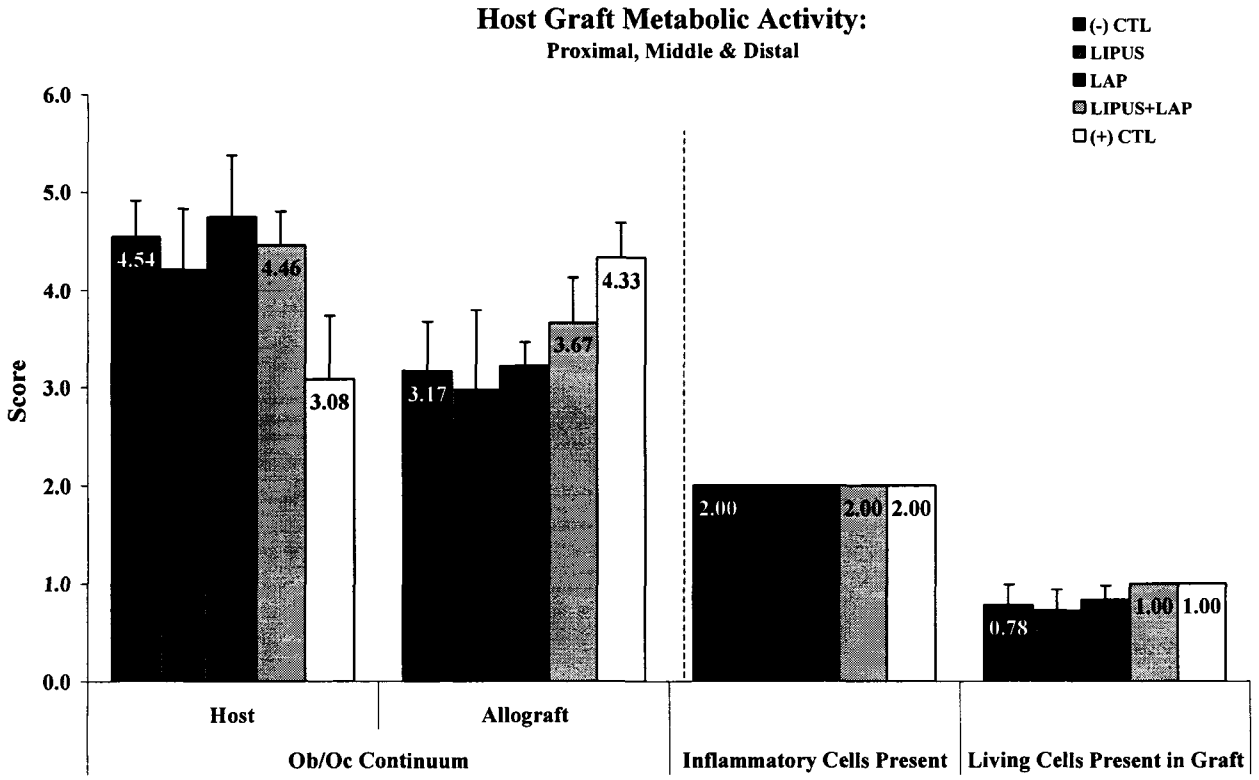

Figure 3.6. Decalcified Ob/Oc continuum scores and graft revitalization scores;host metabolic activity was upregulated adjacent to allografted tissue while it was down-regulated when limbs were reconstructed with autologous tissue; the reverse trend was quantified in grafted tissue (i.e. allografted tissue was characterized by extensive resorption with some osteoblastic activity while autologous grafts indicated demonstrated more osteoblastic activity concomitant with less graft resorption); no inflammatory cells were documented in any of the histopathological slides and osteocytes were documented in periosteally in the allografted and autografted tissues; Results presented as Mean ± SEM where the mean was compiled by averaging scores from the proximal, middle and distal slides.

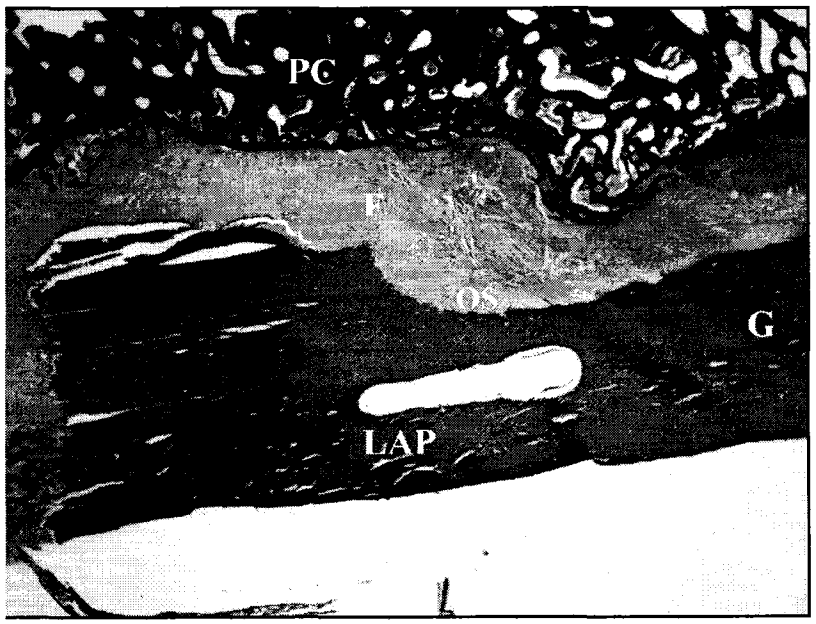

Figure 3.7. Decalcified image (2x) of a longitudinal perforation (LAP) that appears void on any new bone formation; general findings consistent among all treatment groups excluding the +CTL include a high degree of osteoclastic surface (OS) as well a proximal fibrovascular tissue (F) encapsulement of the allograft (G); also illustrated here is the highly porous periosteal callus (PC).

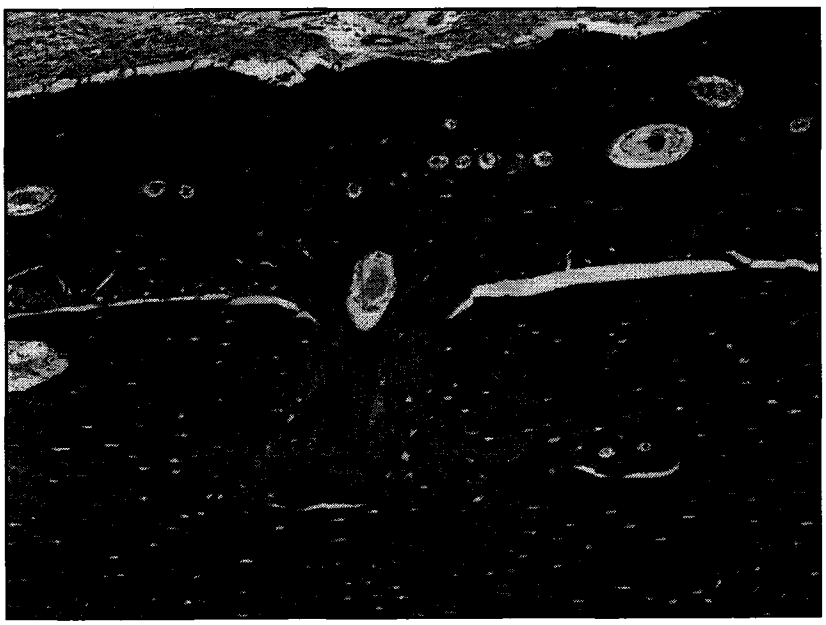

Figure 3.8. Decalcified image (10x) of the highly vascularized (V) periosteal callus (PC) infilatrating the allograft (G) resulting in periosteal graft revitalization (NB); arrow indicates osteocyte residing within a lacunae; image is of the –CTL group.

3.3.4. Undecalcified Histology - Static Histomorphometry

Perforations present in the LAP and LIPUS+LAP undecalcified slides filled to varying degrees with immature woven bone after 4 months of healing *in vivo*. Individual animals within both groups exhibited perforations that were entirely filled with new immature tissue while some animals within those same groups elicited osteogenesis that appeared isolated to the inner surface of the longitudinal perforation rather than the full width. Furthermore, the appositional bone extended the entire length of the 10 mm perforation (Figure 3.10).

Callus area measurements quantified using static histomorphometry correlated grossly with previously reported findings quantified from post-operative radiographs. Specifically, the largest area of periosteal callus was quantified in the LAP group, followed by the LIPUS+LAP group and the +CTL. Periosteal callus development was the least in the –CTL. Furthermore, within an individual animal, periosteal callus area was greater in the caudal aspect of the reconstructed limb relative to the cranial aspect and the general area of direct ultrasound stimulation (Table 3.2). Trabecular thickness within the measured callus was also greater caudally than cranially though the differences were small (-CTL, $p=0.760$; LIPUS, $p=0.387$; LAP, $p=0.200$; LIPUS+LAP, $p=0.617$; +CTL, $p=0.728$).

Qualitatively, both the cranial and caudal interfaces of the distal host/graft junctions progressed to a higher degree of cortical union relative to the proximal junctions within the same animal. This finding appeared to be independent of treatment group. Distal periosteal callus development was more uniform and continuous with callus extending

Table 3.2. Cranial vs. Caudal Callus Formation: Comparison by Treatment.

Treatment	Location	Callus Area (mm^2) Average	±	SEM	% Difference	p-value
(-)CTL	Cranial	36.134	±	20.412	53.25	0.208
	Caudal	77.294	±	31.245		
LIPUS	Cranial	60.516	±	32.049	29.66	0.369
	Caudal	86.035	±	26.704		
LAP	Cranial	66.948	±	30.933	58.44	0.0824
	Caudal	161.085	±	61.652		
LIPUS+LAP	Cranial	56.535	±	17.360	42.21	0.174
	Caudal	97.835	±	25.014		
(+)CTL	Cranial	91.473	±	13.895	(22.31)	0.454
	Caudal	74.790	±	26.912		

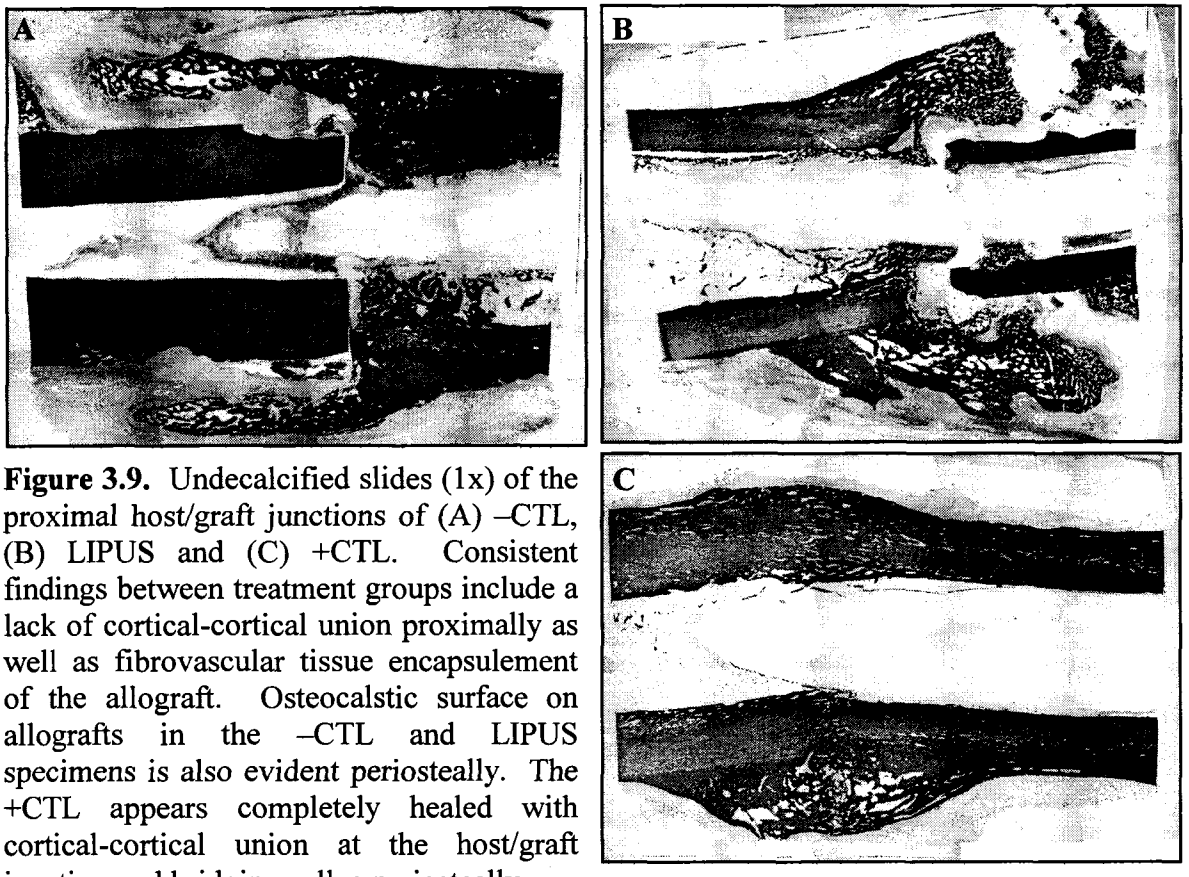

Figure 3.9. Undecalcified slides (1x) of the proximal host/graft junctions of (A) –CTL, (B) LIPUS and (C) +CTL. Consistent findings between treatment groups include a lack of cortical-cortical union proximally as well as fibrovascular tissue encapsulement of the allograft. Osteocalstic surface on allografts in the –CTL and LIPUS specimens is also evident periosteally. The +CTL appears completely healed with cortical-cortical union at the host/graft junction and bridging callus periosteally

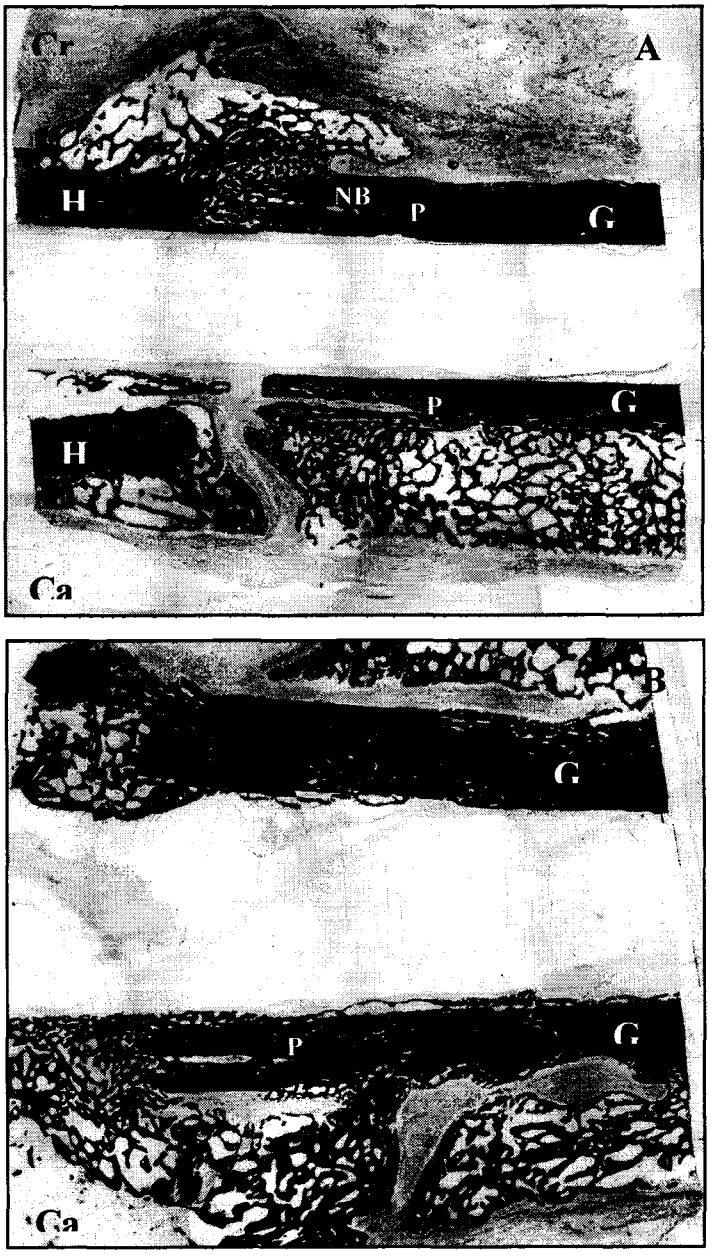

Figure 3.10. Undecalcified static image (2x) of two distal host /graft (G) junctions in the LAP (A) and LIPUS+LAP (B) treatment groups; Illustrated are two perforations (P) extending parallel to the long axis of the graft (G) filled to varying degrees with new, immature bone (NB); Cranially (Cr) in (a), the perforation is almost entirely filled with NB and extends the entire length of the LAP; Caudally (Ca) in (a) and (b), new bone deposition appears isolated to the interior surface of the LAP.

from the host, across the interface, and apposing onto the graft. Proximal host/graft junctions were characterized by fibrovascular tissue development that impeded cortical union in nearly all specimens and furthermore tended to isolate the graft from apposing callus (Figure 3.9). The presence of fibrovascular tissue was identified in all treatment groups excluding the +CTL. Proximally, graft revitalization appeared isolated to the periosteal surface extending no more than 1 mm into the surface of the graft.

Osteoclastic activity was observed on both the cranial and caudal surfaces of all grafts in each treatment group, though there was a trend towards decreased activity in the LIPUS treated allografts relative to the –CTL ($p=0.290$). Furthermore, the trend of decreased osteoclastic resorption was more pronounced on the cranial aspect of the graft on those limbs exposed to the low-intensity ultrasonic signal ($p=0.203$, % graft resorbed = 12.5% LIPUS; % graft resorbed = 19.2% -CTL). Proximally, osteoclastic activity appeared to have occurred without concomitant new bone deposition.

3.3.5. Dynamic Histomorphometry.

Extensive mineralizing tissue was observed to extend the length of the longitudinal conduits in the LAP and LIPUS+LAP treatment groups (Figure 3.11) resulting in MS, MAR and BFR that were significantly increased relative to the –CTL. LIPUS therapy increased dynamic indices of bone remodeling to an even larger degree in the graft, though these parameters were maximized at the periphery of the graft rather than mid-cortex (BFR: $p=0.0025$ proximally and $p=0.0042$ distally).

BFR in the callus were always larger than in the host and the graft for all treatment groups. Limbs treated with LIPUS only indicated 3 times greater BFR proximally and distally than the –CTL limbs ($p=0.0135$ & $p=0.0223$, respectively), while callus adjacent to perforated grafts and treated with LIPUS indicated BFR nearly 6 times greater than the –CTL ($p=0.0016$ & $p<0.001$, respectively). Callus adjacent to grafts with increased cortical porosity only also indicated higher BFR proximally and distally than the –CTL ($p=0.0063$ & $p<0.001$, respectively).

New, immature woven bone was identified both proximally and distally in the interface regions of the +CTL (Table 3.3, Figure 3.11). New bone formation was also identified in the interface regions both cranially and caudally in each of the remaining treatment groups distally including the –CTL (Table 3.2). Proximally, there was little evidence of cortical-cortical union in the –CTL, LIPUS, LAP, and LIPUS+LAP treatment groups, though mineralizing tissue was identified in the interface regions of the limbs treated with LAP and/or LIPUS (Table 3.3).

No dynamic differences in the contralateral intact control limbs were observed between experimental treatment groups. Fluorochrome label uptake was only observable on the endosteal and periosteal surfaces of the intact tibiae (Figure 3.13). In general, significant changes in histomorphometric parameters due to experimental treatment were positively and significantly correlated to increases in biomechanical integrity of the limb (Table 3.5).

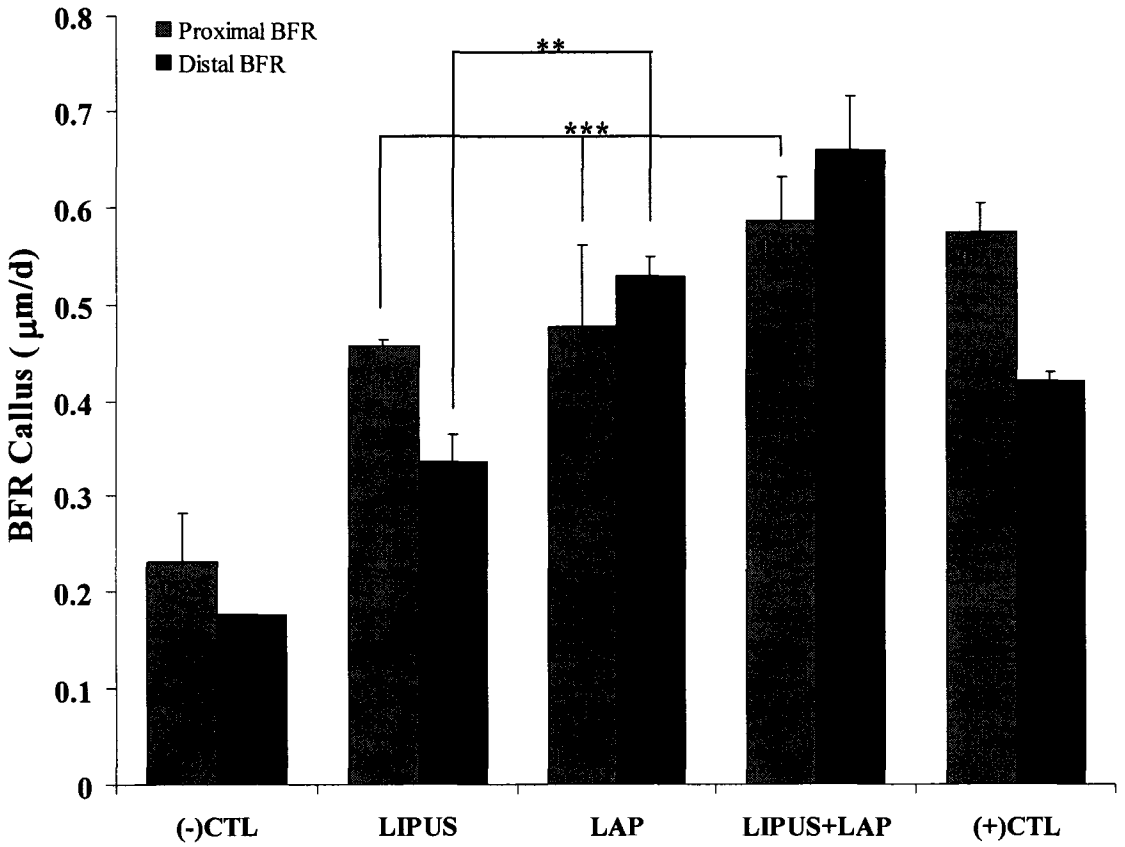

Figure 3.10. Bone formation rates (BFRs) quantified in the periosteal callus adjacent to the proximal and distal host/graft junctions; No significant treatment effects were quantified proximally (***, $p>0.05$), though treatment effects were significant relative to the negative control ($p<0.01$); Significant between treatment effects were quantified distally (**, $p<0.05$) as were effects relative to the negative control ($p<0.05$).

Table 3.3. Dynamic Parameters Quantified in Proximal and Distal Host/Graft Interface ROIs

Treatment		MS (MS/BP)	MAR (um/d)	BFR (MS*MAR)
(-) CTL	Proximal	0.0023 ± 0.0079	0.0000 ± 0.0000	0.0000 ± 0.0000
	Distal	0.2643 ± 0.2016	0.2198 ± 0.2881	0.0923 ± 0.1407
LIPUS	Proximal	0.0496 ± 0.0507	1.4643 ± 1.3329 *	0.0715 ± 0.1450
	Distal	0.1199 ± 0.0707	0.5148 ± 0.9512	0.0825 ± 0.1504
LAP	Proximal	0.1136 ± 0.1175 *	1.1164 ± 1.4915 *	0.2509 ± 0.3729 *
	Distal	0.3290 ± 0.1783	0.7058 ± 0.9435	0.1293 ± 0.2577
LIPUS+LAP	Proximal	0.2188 ± 0.1373 **	0.7401 ± 0.9730 *	0.2166 ± 0.2985
	Distal	0.3218 ± 0.1701	0.5764 ± 0.8777	0.1626 ± 0.2696
(+) CTL	Proximal	0.2662 ± 0.2503 **	1.2820 ± 1.2670 *	0.5694 ± 0.5700 **
	Distal	0.3389 ± 0.1119	1.6099 ± 0.7971 **	0.5317 ± 0.3434 **

* indicates $p<0.05$ relative to (-) CTL

** indicates $p<0.001$ relative to (-) CTL

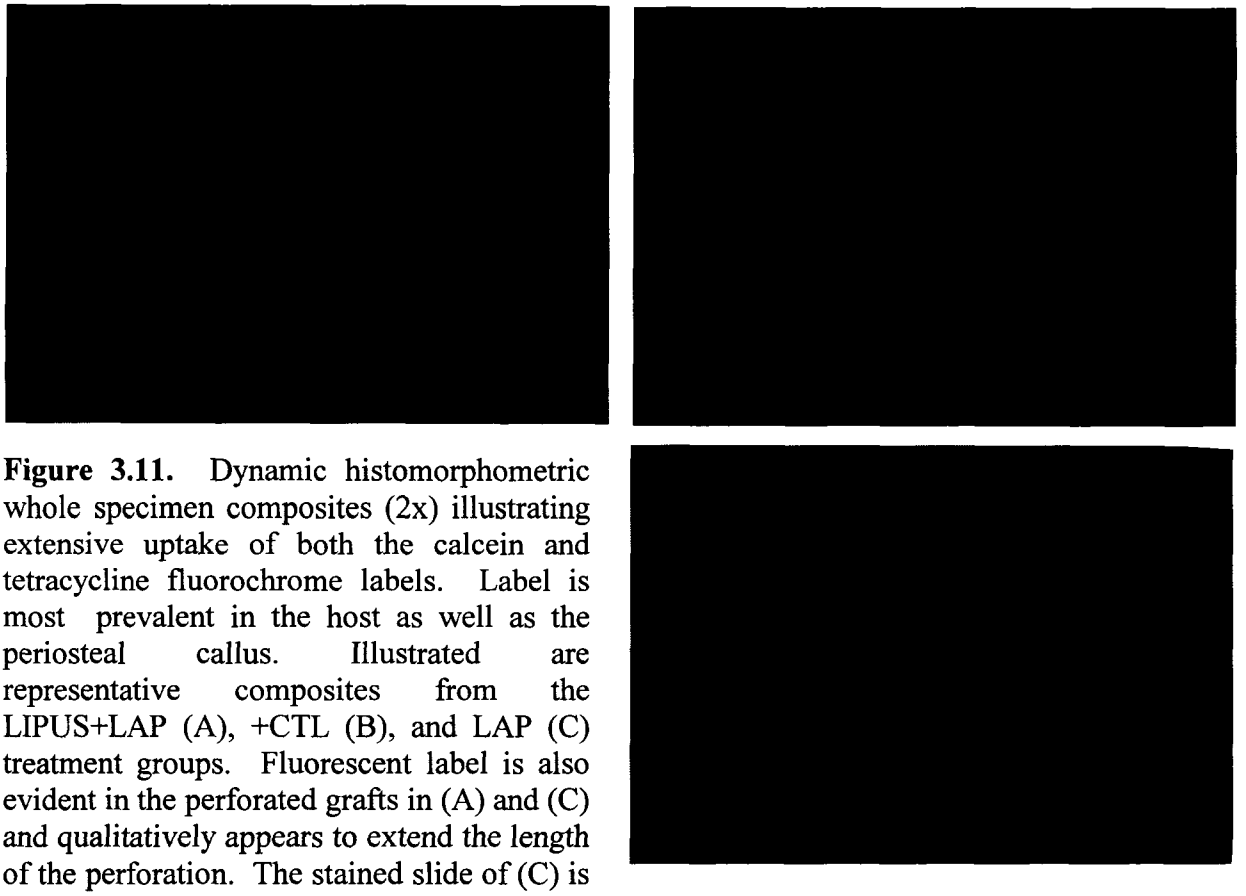

Figure 3.11. Dynamic histomorphometric whole specimen composites (2x) illustrating extensive uptake of both the calcein and tetracycline fluorochrome labels. Label is most prevalent in the host as well as the periosteal callus. Illustrated are representative composites from the LIPUS+LAP (A), +CTL (B), and LAP (C) treatment groups. Fluorescent label is also evident in the perforated grafts in (A) and (C) and qualitatively appears to extend the length of the perforation. The stained slide of (C) is presented above in Figure 18(A).

Table 3.4 Dynamic Histomorphometric Parameters in Graft Tissue

		MS (MS/BP)		MAR (mm/d)		BFR (MS*MAR)	
Region	Treatment	Mean ±	SEM	Mean ±	SEM	Mean ±	SEM
Proximal Graft	(-)CTL	0.004	0.01	0.000	0.00	0.000	0.00
	LIPUS	0.155	0.05 [A]	0.883	0.21 [A]	0.315	0.10 [A]
	LAP	0.088 ±	0.06	0.303 ±	0.18	0.116 ±	0.09
	LIPUS+LAP	0.136	0.04 [A]	0.696	0.29	0.257	0.13 [A]
	(+)CTL	0.173	0.05 [A]	0.358	0.20 [A]	0.169	0.10
Distal Graft	(-)CTL	0.123	0.03	0.046	0.04	0.018	0.02
	LIPUS	0.174	0.03	0.557	0.13 [A]	0.178	0.06 [A]
	LAP	0.185 ±	0.04	0.375 ±	0.15 [A]	0.107 ±	0.04
	LIPUS+LAP	0.285	0.03 [A]	0.404	0.10 [A]	0.102	0.03
	(+)CTL	0.329	0.07 [A]	0.913	0.255 [A]	0.333	0.08 [A]

[A] $p<0.01$

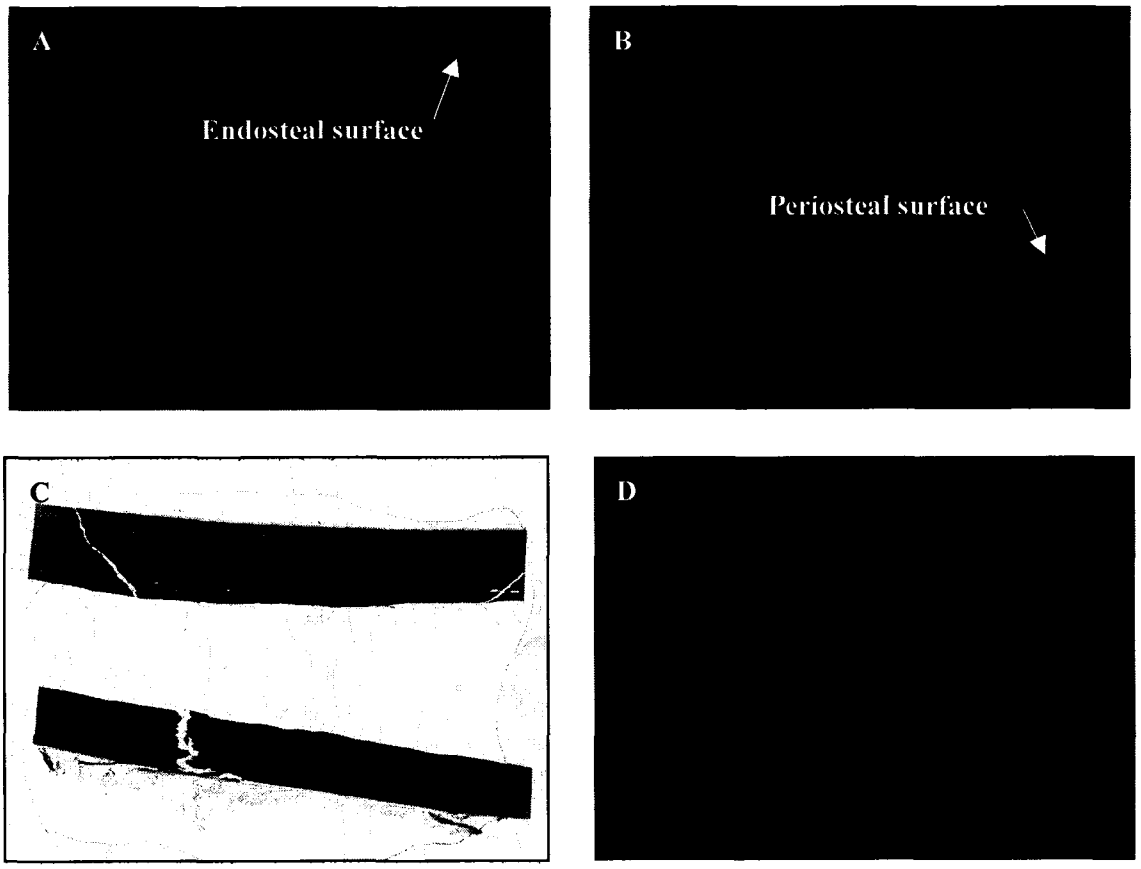

Figure 3.13. Comparison of dynamic (A&B) and static (C) iCTL images (4x) versus label uptake in experimental treatment limb (10x) (D). Dynamic histomorphometric images of the iCTL illustrate lack of fluorochrome label uptake in the mid-cortex of the allograft; tetracycline label is evident on the endosteal surface in (A) and the periosteal surface of (B); active remodeling in the contralateral limbs was isolated to one or both of these surfaces and may be the result of a lack of full weight-bearing in the reconstructed limbs; no qualitative differences were noted in fluorochrome uptake in the iCTL limbs between experimental treatment groups.

Table 3.5. Results of Final Correlation Analysis Relating Mechanics to Biology.

BIOLOGY			MECHANICS & RADIOGRAPHY: Ultimate Torque	Stiffness	Callus Area (Proximal/Distal)	Callus w/ Equivalent Cortical Density
PROXIMAL	MS	H	0.482, p=0.069	0.526, p=0.044	0.178, p=0525	0.178, p=0.526
		G	0.731, p=0.002	0.624, p=0.013	0.397, p=0.142	0.383, p=0.159
		C	0.646, p=0.009	0.749, p=0.001	0.391, p=0.150	0.365, p=0.181
	MAR	H	0.1449, p=0.597	0.210, p=0.459	0.245, p=0.379	0.085, p=0.763
		G	0.480, p=0.071	0.425, p=0.115	0.553, p=0.033	0.556, p=0.031
		C	0.413, p=0.126	0.442, p=0.099	0.672, p=0.006	0.589, p=0.023
	BFR	H	0.412, p=0.127	0.490, p=0.063	0.266, p=0.338	0.076, p=0.702
		G	0.505, p=0.055	0.441, p=0.099	0.509, p=0.054	0.402, p=0.137
		C	0.544, p=0.036	0.551, p=0.033	0.523, p=0.046	0.384, p=0.158
DISTAL	MS	H	0.091, p=0.748	0.210, p=0.458	0.047, p=0.867	0.132, p=0.640
		G	0.643, p=0.009	0.799, p<0.001	0.354, p=0.195	0.341, p=0.214
		C	0.067, p=0.812	0.019, p=0.944	0.034, p=0.903	0.194, p=0.489
	MAR	H	0.344, p=0.210	0.375, p=0.167	0.166, p=0.555	0.111, p=0.695
		G	0.771, p<0.001	0.802, p<0.001	0.352, p=0.197	0.636, p=0.011
		C	0.692, p=0.012	0.509, p=0.053	0.410, p=0.129	0.323, p=0.240
	BFR	H	0.116, p=0.681	0.196, p=0.484	0.065, p=0.816	0.0489, p=0.862
		G	0.784, p<0.001	0.854, p<0.001	0.312, p=0.256	0.571, p=0.023
		C	0.353, p=0.197	0.310, p=0.263	0.300, p=0.276	0.138, p=0.622

Legend: MS=mineralizing surface; MAR=mineral apposition rate; BFR=bone formation rate: H=host, G=graft; C=callus

the first number presented in each cell is the Pearson's correlation coefficient (r) and is a measure how well a linear equation describes the relation between two variables X and Y; r is followed by the p-value for that comparison;

Shaded regions represent the most significant correlations between mechanics & radiography and biology.

3.4. Dicussion and Conclusions.

The goal of the current study was to quantify the effects of low-intensity pulsed ultrasound (LIPUS) and/or longitudinal allograft perforation (LAP) on the incorporation and revitalization of 5 cm intercalary allografts in an ovine model compared to the natural course of allograft and autograft healing in the same model. Although the results are not always predictable, the role of bone allograft has a place in the operative treatment of failed total joint replacements[2, 13], bone tumors[21, 24, 42], and joint diseases[21] such as osteonecrosis since they provide adequate structural support, display mechanical properties similar to the diseased or damaged tissue, and act as an osteoconductor for neovascularization and osteogenic host cells[26]. Although there is considerable controversy among orthopaedists as to whether metal implants or osteoarticular allografts are best suited for the treatment of lesions when a joint must be resected[7, 18, 31], there is far less doubt about the use of intercalary segmental allografts in which the joint plays no role. Intercalary allografts have a good reputation since they are easy to insert and stabilize, they are associated with relatively low complication rates and they have been shown to survive for relatively long periods of time *in vivo*[25, 41, 42].

Stevenson and Horowitz[62] defined successful cortical bone allograft incorporation as concurrent revascularization following osteoclastic resorption and substitution with host bone without the loss of strength. In human patients, the initial resorptive phase has been reported to last as long as six months during which graft density decreases by as much as

40%[10]. Therefore, it seems absolutely necessary that the form of therapeutic intervention employed to promote long-term graft healing not involve the transplantation of a graft that has been modified in such a way that its structural and mechanical properties are already significantly reduced. Such has been the case with transversely perforated allografts as this modification has been reported to reduce the flexural properties of the graft by 40%[35, 37]. Premature failure of these grafts *in vivo* has led orthopaedists to abandon this method of graft modification[52]. Perforations extending parallel to the long axis of the graft provide an attractive alternative and concomitant mechanical investigations have revealed minimal effects on the tensile and compressive properties of these modified grafts (Chapter 4: 11.14 and 13.69%, respectively).

The current histologic investigation illustrated extensive new bone formation within the 500 μm conduits, 10 mm in depth, as evidenced with fluorescence microscopy after four months *in vivo*. It is hypothesized that the lack of bone development within the conduits as evidenced histopathologically (Figure 3.7) was a result of the extensive and aggressive processing that accompanies the decalcification process and is not representative of the appositional bone formation that occurred *in vivo*. As demonstrated via undecalcified histology, the filling of the conduits translated into near significant increases in graft revitalization as quantified by measuring MS, MAR, and BFR within the graft regions of interest (ROIs). The lack of statistical significance can most likely be explained by the fact that diffuse fluorochrome label was not measured in any of the dynamic ROIs. The lack of clearly identifiable bone surfaces within the new bone forming within the conduits resulted in large amounts of diffuse fluorescent label extending the length of the conduit. Had these areas been measured, the statistical results would have correlated to

the gross observation of extensive graft revitalization with the LAP procedure as illustrated in Figure 3.11C.

To the author's knowledge, this is the first study to demonstrate the positive effects of simple graft modification as a means to improve allograft healing and revitalization, and the only study to date to qualitatively and quantitatively illustrate extensive bone development within perforated allografts. The results presented here are in contrast to those reported by Lewandrowski et al.[36, 37] whom reported increased resorption of transversely perforated intercalary grafts with little histological evidence of graft healing after nine months in an ovine model. Since a higher rate of periosteal bone resorption than bone formation occurs after implantation of frozen allografts[16, 26, 27, 40, 65], it is likely that conduits extending from the periosteal surface to the endosteal surface provided for increased surface area on which the osteoclasts could act and may explain the negative results reported by Lewandrowski et al. with regard to allograft healing. The results from this study and those of Lewandrowski emphasize perforation orientation has a profound effect on both the structural properties of the transplanted tissue as well as graft revitalization. Transverse perforations favor osteoclastic resorption whereas perforations extending longitudinally promote osteoblastic bone formation and revitalization of the allograft. However, though the nature in which the conduits were created in this study was very repeatable, care should be taken to minimize creating conduits that deviate from running parallel to the long axis of the graft and perforate the periosteal surface. Such conduits may accelerate osteoclastic resorption of the graft resulting in histologic findings similar to those reported by Lewandrowski et al[36, 37].

Daily LIPUS stimulation accelerated maturation of the periosteal callus as demonstrated both through decalcified and undecalcified histology. Specifically, BFR in both the proximal and distal callus increased by at least three fold relative to the –CTL. Significant increases in callus maturity were paralleled by increases in periosteal callus area, though the greatest degree of callus formation was quantified in the LAP group. The findings that callus area not only increased following daily ultrasound stimulation but also exhibited accelerated maturation is consistent with a number of *in vitro*[32, 46, 71] and animal studies[4, 30] as well as human clinical studies[34, 66]. In fact, the evidence that low-intensity pulsed ultrasound not only has a positive influence on the quantity of callus but also significantly increases the mechanical strength and stiffness of the callus was first demonstrated by Pilla et al.[50] in a rabbit femoral fracture model. *In vitro* studies confirmed the mechanical findings at the biologic level and demonstrated that increases in mechanical integrity of fractured limbs exposed to LIPUS is in part the result of accelerated endochondral ossification[46] and neoangiogenesis[54, 67] within the callus. The significant increases in the dynamic parameters consistent with bone healing reported here following daily LIPUS stimulation of the proximal and distal host/graft junctions translated into 30% increases in ultimate torque to failure and stiffness after four months *in vivo*.

The finding that simple graft modification (LAP) resulted in a maximum amount of callus formation and slight increases in MS, MAR, and BFR relative to daily LIPUS stimulation is confounding but may be explained by the following limitations inherent to this study. The potent anabolic stimulus inherent to LIPUS has been well documented in a number of small animal studies as well as a number of human clinical cases with regard

to fresh fracture and non-union healing. The SAFHS device used in this study (as well as many of the small animal and human clinical studies) employs a single PZT transducer that delivers the ultrasonic signal to a 3.88 cm^2 area (approximately the size of a quarter). Given the dimensions of an average sheep tibia, only a small area of the healing host/graft junctions would be exposed to the potent stimulus. In addition, the human and small animal studies referred to earlier exposed fresh-fractures or non-unions to LIPUS to skeletal locations that were surrounded by minimal amounts of soft-tissue (i.e. mouse femora, rabbit tibiae, human tibiae, radii, and scaphoid bones). Ovine tibiae are surrounded by a small cuff of circumferential musculature. Given that ultrasonic energy is absorbed at a rate proportional to the density of the tissue in its path, it is possible that the ultrasonic signal may have been attenuated by the musculature between the PZT transducer and the host/graft junctions and therefore not delivered the full amount of energy to the healing tissues. These conjectures, either alone or in combination, may account for the discrepancy between the histological parameters quantified using LAP or LIPUS therapy. However, it should be noted that daily LIPUS stimulation appeared to have a more pronounced biomechanical effect than simple graft modification alone, illustrating that even though the signal may have not been used to its full potential, even in an attenuated or limited form it may still have application following massive tumor resection followed by replacement with bone allograft.

Contrary to our initial hypothesis, combination LIPUS+LAP therapy was not synergistic after four months of healing *in vivo*, though trends towards synergy did exist. Dynamic indices of bone formation in the host, graft, interface, and callus regions were elevated as

a result of both adjuvant therapies relative to individual therapies alone. The lack of statistical significance could be attributed to the low power of this study.

In conclusion, this study has demonstrated the clinical relevance of both LIPUS and LAP therapy at improving the degree of allograft incorporation and healing in a large animal model. This was the first study of its kind to demonstrate the potential of LIPUS therapy as a stand-alone intervention to promote allograft healing. In addition, this was the first study to demonstrate that the orientation of perforation within an intercalary allograft has profound effects on allograft revitalization. Future more robust studies are warranted to confirm the positive statistical findings reported here. In addition, to elucidate the effects of LIPUS at the biological level, immunohiostochemical staining of various molecules consistent with bone development and ossification should be undertaken. Proteins of interest may include VEGF (vascular endothelial growth factor) osteopontin, osteonectin and bone sialoprotein. Additional studies that evaluate multiple time points to elucidate the temporal sequence of events that accompany these adjuvant therapies are also warranted.

3.5 References.

1. NIH Consensus Statement on total knee replacement December 8-10, 2003. J Bone Joint Surg Am. 86-A:1328-1335, 2004.

2. Allan DG, Lavoie GJ, McDonald S, et al.: Proximal femoral allografts in revision hip arthroplasty. J Bone Joint Surg Br. 73:235-240, 1991.

3. Anglen J, University of Missouri H: The clinical use of bone stimulators. J South Orthop Assoc. 12(2):46-54, 2003.

4. Azuma Y, Ito M, Harada Y, et al.: Low-intensity pulsed ultrasound accelerates rat femoral fracture healing by acting on the various cellular reactions in the fracture callus. J Bone Miner Res. 16(4):671-680, 2001.

5. Bassett CA, Schink-Ascani M, Lewis SM: Effects of pulsed electromagnetic fields on Steinberg ratings of femoral head osteonecrosis. Clin Orthop. 1989.

6. Beck BR, Qin YX, McLeod KJ, et al.: On the relationship between streaming potential and strain in an *in vivo* bone preparation. Calcif Tissue Int. 71(4):335-343, 2002.

7. Brien EW, Terek RM, Healey JH, Lane JM: Allograft reconstruction after proximal tibial resection for bone tumors. An analysis of function and outcome comparing allograft and prosthetic reconstructions Clin Orthop Relat Res. 116-127, 1994.

8. Brostrèom LA, Nilsonne U, Nilsson OS: Survival of frozen bone allograft. Ann Chir Gynaecol. 77(2):1988.

9. Burchardt H: The biology of bone graft repair. Clin Orthop. 174:28-42, 1983.

10. Burchardt H: The biology of bone graft repair. Clin Orthop. 1983.

11. Burchardt H, Busbee GA, 3rd, Enneking WF: Repair of experimental autologous grafts of cortical bone. J Bone Joint Surg Am. 57(6):814-819, 1975.

12. Capanna R, Donati D, Masetti C, et al.: Effect of electromagnetic fields on patients undergoing massive bone graft following bone tumor resection. A double blind study. Clin Orthop. 213-221, 1994.

13. Chandler H, Clark J, Murphy S, et al.: Reconstruction of major segmental loss of the proximal femur in revision total hip arthroplasty. Clin Orthop Relat Res. 67-74, 1994.

14. Cook SD, Salkeld SL, Popich-Patron LS, et al.: Improved cartilage repair after treatment with low-intensity pulsed ultrasound. Clin Orthop Relat Res. S231-243, 2001.

15. Cullinane DM, Lietman SA, Inoue N, et al.: The effect of recombinant human osteogenic protein-1 (bone morphogenetic protein-7) impregnation on allografts in a canine intercalary bone defect. J Orthop Res. 20(6):1240-1245, 2002.

16. Delloye C, de Nayer P, Allington N, et al.: Massive bone allografts in large skeletal defects after tumor surgery: a clinical and microradiographic evaluation. Arch Orthop Trauma Surg. 107:31-41, 1988.

17. Duarte LR: The stimulation of bone growth by ultrasound. Arch Orthop Trauma Surg. 101(3):1983.

18. Eckardt JJ, Matthews JG, 2nd, Eilber FR: Endoprosthetic reconstruction after bone tumor resections of the proximal tibia. Orthop Clin North Am. 22:149-160, 1991.

19. Enneking WF, Campanacci DA: Retrieved human allografts: a clinicopathological study. J Bone Joint Surg Am. 83-A(7):971-986, 2001.

20. Fini M, Giavaresi G, Setti S, et al.: Current trends in the enhancement of biomaterial osteointegration: biophysical stimulation. Int J Artif Organs. 27(8):681-690, 2004.

21. Flynn JM, Springfield DS, Mankin HJ: Osteoarticular allografts to treat distal femoral osteonecrosis. Clin Orthop Relat Res. 303:38-43, 1994.

22. Friedenberg ZB, Harlow MC, Brighton CT: Healing of nonunion of the medial malleolus by means of direct current: a case report. J Trauma. 11(10):883-885, 1971.

23. Frykman GK, Taleisnik J, Peters G, et al.: Treatment of nonunited scaphoid fractures by pulsed electromagnetic field and cast. J Hand Surg [Am]. 11(3):344-349, 1986.

24. Gebhardt MC, Flugstad DI, Springfield DS, Mankin HJ: The use of bone allografts for limb salvage in high-grade extremity osteosarcoma. Clin Orthop. 1991.

25. Gebhardt MC, Lord FC, Rosenberg AE, Mankin HJ: The treatment of adamantinoma of the tibia by wide resection and allograft bone transplantation. J Bone Joint Surg Am. 69:1177-1188, 1987.

26. Goldberg VM, Stevenson S: Natural history of autografts and allografts. Clin Orthop. 225:7-16, 1987.

27. Griffiths HJ, Anderson JR, Thompson RC, et al.: Radiographic evaluation of the complications of long bone allografts. Skeletal Radiol. 24:283-286, 1995.

28. Gross TS, Edwards JL, McLeod KJ, et al.: Strain gradients correlate with sites of periosteal bone formation. J Bone Miner Res. 12(6):982-988, 1997.

29. Hadjiargyrou M, McLeod K, Ryaby JP, et al.: Enhancement of fracture healing by low intensity ultrasound. Clin Orthop. 1998.

30. Hantes ME, Mavrodontidis AN, Zalavras CG, et al.: Low-intensity transosseous ultrasound accelerates osteotomy healing in a sheep fracture model. J Bone Joint Surg Am. 86-A:2275-2282, 2004.

31. Horowitz SM, Glasser DB, Lane JM, Healey JH: Prosthetic and extremity survivorship after limb salvage for sarcoma. How long do the reconstructions last? Clin Orthop Relat Res. 293:280-286, 1993.

32. Korstjens CM, Nolte PA, Burger EH, et al.: Stimulation of bone cell differentiation by low-intensity ultrasound--a histomorphometric *in vitro* study. J Orthop Res. 22(3):495-500, 2004.

33. Kristiansen TK, Ryaby JP, McCabe J, et al.: Accelerated healing of distal radial fractures with the use of specific, low-intensity ultrasound. A multicenter, prospective, randomized, double-blind, placebo-controlled study. J Bone Joint Surg Am. 79(7):961-973, 1997.

34. Leung KS, Lee WS, Tsui HF, et al.: Complex tibial fracture outcomes following treatment with low-intensity pulsed ultrasound. Ultrasound Med Biol. 30(3):389-395, 2004.

35. Lewandrowski KU, Hornicek FJ, Pedlow FX, et al.: Clinical and Biomechanical Design Considerations for Engineered Cortical Bone Allografts. In Lewandrowski KU, Wise D, Trantolo D, Gresser JD, Yaszemski MJ, Altobelli DEChow SC (eds). Tissue Engineering and Biodegradable Equivalents: Scientific and Clinical Applications. New York, Maarcel Dekker 179-194, 2002.

36. Lewandrowski KU, Schollmeier G, Ekkemkamp A, et al.: Incorporation of perforated and demineralized cortical bone allografts. Part I: radiographic and histologic evaluation. Biomed Mater Eng. 11(3):2001.

37. Lewandrowski KU, Schollmeier G, Ekkemkamp A, et al.: Incorporation of perforated and demineralized cortical bone allografts. Part II: A mechanical and histologic evaluation. Biomed Mater Eng. 11(3):2001.

38. Lewandrowski KU, Schollmeier G, Ekkemkamp A, et al.: Incorporation of perforated and demineralized cortical bone allografts. Part I: radiographic and histologic evaluation. Biomed Mater Eng. 11(3):197-207, 2001.

39. Lewandrowski KU, Schollmeier G, Ekkemkamp A, et al.: Incorporation of perforated and demineralized cortical bone allografts. Part II: A mechanical and histologic evaluation. Biomed Mater Eng. 11(3):209-219, 2001.

40. Li XQ, Stevenson S, Klein L, et al.: Differential patterns of incorporation and remodeling among various types of bone grafts. Acta Anat (Basel) 140:236-244, 1991.

41. Makley JT: The use of allografts to reconstruct intercalary defects of long bones. Clin Orthop Relat Res. 197:58-75, 1985.

42. Mankin HJ, Springfield DS, Gebhardt MC, Tomford WW: Current status of allografting for bone tumors. Orthopedics. 15(10):1147-1154, 1992.

43. Mayr E, Frankel V, Rèuter A, Klinik fèur Unfall- und Wiederherstellungschirurgie ZAG: Ultrasound--an alternative healing method for nonunions? Arch Orthop Trauma Surg. 120(1-2):2000.

44. Meril AJ, Garland Orthopedic Clinic T: Direct current stimulation of allograft in anterior and posterior lumbar interbody fusions. Spine. 19(21):2393-2398, 1994.

45. Nelson FR, Brighton CT, Ryaby J, et al.: Use of physical forces in bone healing. J Am Acad Orthop Surg. 11(5):344-354, 2003.

46. Nolte PA, Klein-Nulend J, Albers GH, et al.: Low-intensity ultrasound stimulates endochondral ossification *in vitro*. J Orthop Res. 19(2):301-307, 2001.

47. Nolte PA, van der Krans A, Patka P, et al.: Low-intensity pulsed ultrasound in the treatment of nonunions. J Trauma. 51(4):693-702, 2001.

48. Parfitt AM, Drezner MK, Glorieux FH, et al.: Bone histomorphometry: standardization of nomenclature, symbols, and units. Report of the ASBMR Histomorphometry Nomenclature Committee. J Bone Miner Res. 2(6):595-610, 1987.

49. Parrish FF: Allograft replacement of all or part of the end of a long bone following excision of a tumor. J Bone Joint Surg Am. 55(1):1-22, 1973.

50. Pilla AA, Mont MA, Nasser PR, et al.: Non-invasive low-intensity pulsed ultrasound accelerates bone healing in the rabbit. J Orthop Trauma. 4(3):1990.

51. Pluhar GE, Manley PA, Heiner JP, et al.: The effect of recombinant human bone morphogenetic protein-2 on femoral reconstruction with an intercalary allograft in a dog model. J Orthop Res . 19:308-317, 2001.

52. Rees DC, Haddad FS: Bone transplantation. 64:205-209, 2003.

53. Rees DC, Haddad FS, Royal National Orthopaedic Hospital SM: Bone transplantation. Hosp Med. 64(4):205-209, 2003.

54. Reher P, Doan N, Bradnock B, et al.: Effect of ultrasound on the production of IL-8, basic FGF and VEGF. Cytokine. 11:416-423, 1999.

55. Rubin C: Peak microstrains induced by LIPUS. Personal Communication. 2004.

56. Rubin C, Bolander M, Ryaby JP, Hadjiargyrou M: The use of low-intensity ultrasound to accelerate the healing of fractures. J Bone Joint Surg Am. 83-A(2):259-270, 2001.

57. Rubin C, Pope M, Fritton JC, et al.: Transmissibility of 15-hertz to 35-hertz vibrations to the human hip and lumbar spine: determining the physiologic feasibility of delivering low-level anabolic mechanical stimuli to skeletal regions at greatest risk of fracture because of osteoporosis. Spine. 28(23):2621-2627, 2003.

58. Rubin C, Recker R, Cullen D, et al.: Prevention of postmenopausal bone loss by a low-magnitude, high-frequency mechanical stimuli: a clinical trial assessing compliance, efficacy, and safety. J Bone Miner Res. 19(3):343-351, 2004.

59. Rubin C, Turner AS, Mallinckrodt C, et al.: Mechanical strain, induced noninvasively in the high-frequency domain, is anabolic to cancellous bone, but not cortical bone. Bone. 30(3):445-452, 2002.

60. Sena K, Leven RM, Mazhar K, et al.: Early gene response to low-intensity pulsed ultrasound in rat osteoblastic cells. Ultrasound Med Biol. 31:703-708, 2005.

61. Sparrow KJ, Finucane SD, Owen JR, Wayne JS: The effects of low-intensity ultrasound on medial collateral ligament healing in the rabbit model. Am J Sport Med. 33:1048-1056, 2005.

62. Stevenson S, Horowitz M: The response to bone allografts. J Bone Joint Surg Am. 74(6):939-950, 1992.

63. Sun JS, Hong RC, Chang WH, et al.: *In vitro* effects of low-intensity ultrasound stimulation on the bone cells. J Biomed Mater Res. 57(3):449-456, 2001.

64. Tarsoly E, Ostrowski K, Moskalewski S, et al.: Incorporation of lyophilized and radiosterilized perforated and unperforated bone grafts in dogs. Acta Chir Acad Sci Hung. 10(1):55-63, 1969.

65. Thompson RC, Jr., Pickvance EA, Garry D: Fractures in large-segment allografts. J Bone Joint Surg Am. 75:1663-1673, 1993.

66. Tsumaki N, Kakiuchi M, Sasaki J, et al.: Low-intensity pulsed ultrasound accelerates maturation of callus in patients treated with opening-wedge high tibial osteotomy by hemicallotasis. J Bone Joint Surg Am. 86-A(11):2399-2405, 2004.

67. Wang FS, Kuo YR, Wang CJ, et al.: Nitric oxide mediates ultrasound-induced hypoxia-inducible factor-1alpha activation and vascular endothelial growth factor-A expression in human osteoblasts. Bone. 35:114-123, 2004.

68. Wang SJ, Lewallen DG, Bolander ME, et al.: Low intensity ultrasound treatment increases strength in a rat femoral fracture model. J Orthop Res. 12(1):40-47, 1994.

69. Warden SJ, Bennell KL, Matthews B, et al.: Efficacy of low-intensity pulsed ultrasound in the prevention of osteoporosis following spinal cord injury. Bone. 29:431-436, 2001.

70. Zabka AG, Pluhar GE, Edwards RB, 3rd, et al.: Histomorphometric description of allograft bone remodeling and union in a canine segmental femoral defect model: a comparison of rhBMP-2, cancellous bone graft, and absorbable collagen sponge. J Orthop Res. 19:318-327, 2001.

71. Zhang ZJ, Huckle J, Francomano CA, et al.: The effects of pulsed low-intensity ultrasound on chondrocyte viability, proliferation, gene expression and matrix production. Ultrasound Med Biol. 29(11):1645-1651, 2003.

CHAPTER 4. A MECHANICAL INVESTIGATION ON THE EFFECTS OF LONGITUDINAL ALLOGRAFT PERFORATIONS.

INCREASED CORTICAL POROSITY AND ALTERATION OF THE LOCAL MECHANICAL ENVIRONMENT MEASURED THROUGH UNIAXIAL COMPRESSION AND THE DIAMETRAL COMPRESSION TEST

4.1 Introduction.

4.1.1. Background.

Bone allografts are commonly used to reconstruct massive skeletal defects as a consequence of some form of skeletal trauma. Although initially advocated for the treatment of bone tumors and joint disease in the late 1800s[18], the allograft procedure is now commonly employed to add bone stock to the defective femoral shaft and acetabulum or knee after failed total joint replacement[1, 5] and more recently as a means to augment spinal fusion[14, 35]. Of particular importance to the orthopaedist using allografts are the associated difficulties and complications including allograft-related infection[19], graft fracture[32], and non-union at the host-allograft interface[7], all of which have a detrimental and unpredictable effect on the clinical prognosis. In addition to biologic factors that may impact graft healing, sterilizing donor tissue to prevent disease transmission by way of ethylene oxide, autoclaving, and irradiation is associated with deleterious changes in the mechanical properties of the bone graft[11, 23]. Clearly this has implication for the utility of such bone grafts, as augmenting lost bone stock following tumor resection or failed total joint replacement requires normal structural integrity for a successful outcome at both a mechanical and biological level. Though the field of bone

transplantation has been around for over a century, novel measures that aim to improve graft incorporation and decrease the biological unpredictability associated with massive allografts are lacking.

Increasing graft porosity via perforating the bony cortex *perpendicular* to the long axis of the graft has received considerable attention as a means to improve graft incorporation by the host, though these graft modifications have been reported to have mixed results[3, 8, 12, 15, 16, 30]. Lewandrowski et al.[15, 16] reported increased resorption and little evidence of incorporation of 3 cm intercalary sheep allografts containing multiple 300 μm perforations after 9 months *in vivo*. Conversely, Tarsoly et al.[30] reported considerable histological enhancement of cortical allograft incorporation after drilling numerous 1 mm diameter holes perpendicular to the longitudinal axis of 20 cm canine femoral allografts. Though the debate continues as to the biological effects of perforations perpendicular to the graft's long axis, the effects of such a graft modification on mechanical integrity have been previously documented. Lewandrowski et al. reported insignificant changes in compressive properties of the perforated graft, though the flexural properties, as measured via 4-point bending, of the tissue were reduced by 40%[13, 16]. The biological ambiguity combined with the severely deteriorated mechanical integrity has lead orthopaedists to abandon this particular form of graft modification in favor of expensive recombinant growth factors such as bone morphogenic proteins to improve the clinical prognosis[27].

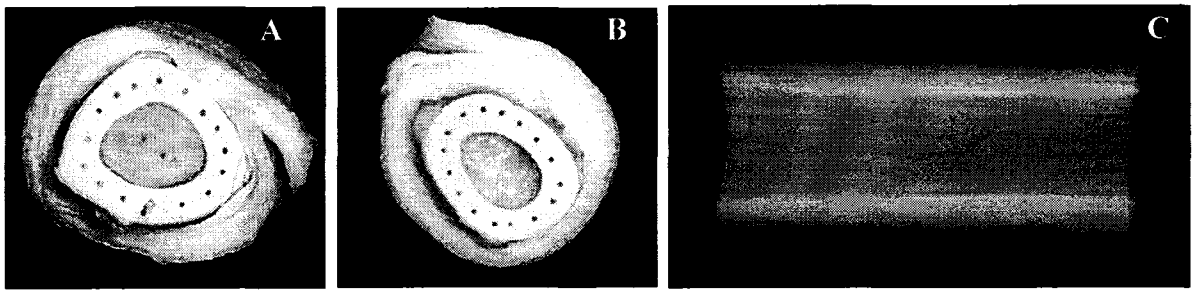

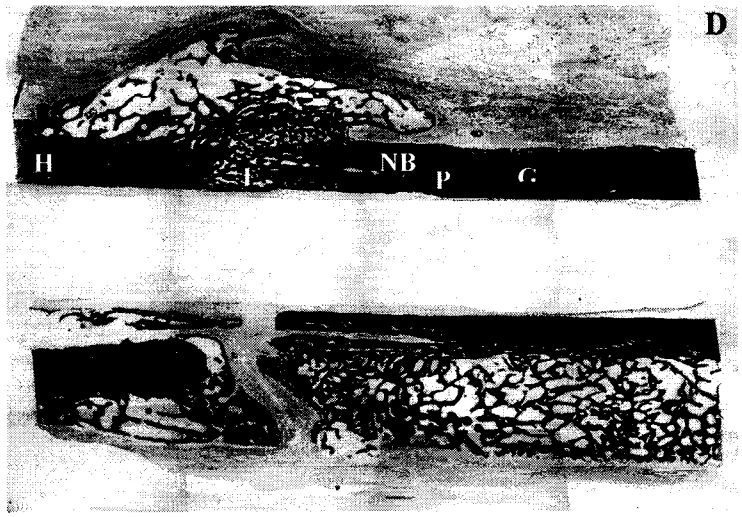

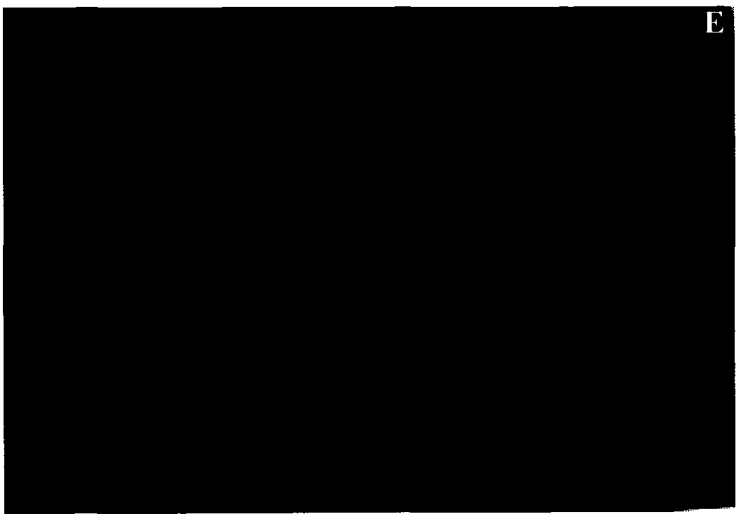

Figure 4.1. (A&B) Proximal and distal cortical end plates of 5 cm perforated allografts; (C) contact radiograph illustrating the consistency of cortical end plate penetration; (D) Undecalcified static image (2x) of two distal host(H) /graft(G) junctions in the LAP treatment group; illustrated are two perforations (P) extending parallel to the long axis of the graft (G) filled to varying degrees with new, immature bone (NB); cranially in (D), the perforation is almost entirely filled with NB and extends the entire length of the conduit; caudally new bone deposition appears isolated to the interior surface of the LAP; (E) dynamic histomorphometric whole specimen composites (2x) of (D) illustrating extensive uptake of both the calcein and tetracycline fluorochrome ; ossifying tissue qualitatively appears to extend the length of the perforation.

The current study utilized a novel method to increase cortical porosity by creating numerous 500 μm diameter holes perpendicular to the long axis of a 5 cm intercalary allograft. Static and dynamic histomorphometric analyses indicated improved graft revitalization with the 10 mm perforations filling with new osseous tissue after 4 months *in vivo* (Figure 4.1). Despite a favorable biological outcome and a lack of *in vivo* failure, the alteration of the graft's structural and mechanical properties following such a treatment are as yet un-characterized.

4.1.2. Biomechanics Background.

Prior mechanical investigations of modified grafts have traditionally utilized four-point bending tests to acquire a flexural rigidity profile as a measure of altered mechanical integrity[13, 15]. This testing method has been deemed appropriate since a constant bending moment is generated along a predetermined length of the modified graft. Such investigations, however, require securing the proximal- and distal-most regions of the tissue in high strength resin to couple the test specimen to the materials testing machine. Because graft porosity is only increased at the extremes of the allograft in the current study, four-point bending does not lend itself as a feasible testing regimen. It is hypothesized that the longitudinal 500 μm perforations serve as stress concentrations within the brittle allograft and may predispose the graft to premature failure under shear or tensile loads. Elementary mechanics predicts that the presence of a small full thickness hole with a diameter 10% of that of the rectangular specimen's width will result in a

three-fold increase in the local stress field*. The presence of such a stress concentration may thus predispose the material to failure at lower than expected loads. Theoretical computational investigations notwithstanding, the diametral compression test has been proven to be a promising experimental alternative for determining the tensile properties of various brittle biomaterials including brittle calcium phosphate ceramics[9, 10, 22, 25, 28, 31, 33], orthopaedic casting materials[4], and cortical bone allograft[29]. Tensile stresses grow perpendicularly to the loading direction and are proportional to the applied load (Figure 4.2). The diametral compression test is thus an indirect method for measuring the tensile strength of brittle materials. One generally considers only the vertical diametral plane of the tested specimen, because stresses are highest on this plane[26]. The stress distribution within the cylinder depends on the width of the insets; the wider the inset, the lower the compressive stress near the contact points, and the shorter the portion of the diametral plane in tension.

It has been reported that fracture type is dependent on inset width (Figure 4.4). In general, insets are used to lower the compressive stresses near the contact points between specimen and platens. It is generally acknowledged that the pad's width should not exceed one-tenth (1/10) of the cylinder's diameter to avoid producing a stress distribution that differs greatly from theory and to avoid fracture patterns other than pure tension. However, Peltier et al.[24] suggested a ratio of 0.2 (pad width/cylinder diameter) for a material whose compressive strength is nine times higher than its tensile strength. Published studies, however, have used ratios that vary from 0.05-0.3 (Table 4.1). Some

*It should be noted that this 3-fold increase in stress due to the presence of a full-thickness hole is valid for a linear, isotropic, and homogenous solid; bone tissue is viscoelastic, anistotropic, and non-homogeneous.

studies employing diametral compression to quantify the tensile properties of concrete have shown that the measured value of ultimate stress can be statistically different depending on the mechanical properties of the inset material[24]. The ideal inset must be deformable enough to match the shape of possible irregularities on the cylinder surface. In addition it must not break before specimen fracture occurs. Soft cardboard has been shown to conform to both conditions[26], though 1 mm thick medium-soft copper has been employed as well[31]. Cylinder diameter to thickness ratio seems to vary in the published reports employing diametral compression to quantify tensile properties of brittle test specimens (Table 4.1). Ratios of cylinder diameter to thickness range from 0.43 to 3.92 while loading rates range from 0.5 mm/min to 25 mm/min.

4.1.3. Objectives.

The aim of the current study was to compare the failure loads and stresses of longitudinally and transversely perforated and non-perforated grafts using diametral compression. It is hypothesized that the transversely perforated grafts will fail under smaller loads than non-perforated contralateral control specimens due to the presence of the 500 μm conduit. Longitudinally perforated grafts are also expected to fail under smaller compressive loads than the intact controls, though the orientation of these conduits is expected to have less of an effect on structural properties than the transversely perforated graft. These hypotheses are based not only on principles previously presented with regard to diametral compression but also on advanced solid mechanics principles with regard to bending of curved members. Curved beam theory suggests that the circumferential stresses (σ_θ) generated in a closed ring exposed to point loading along its

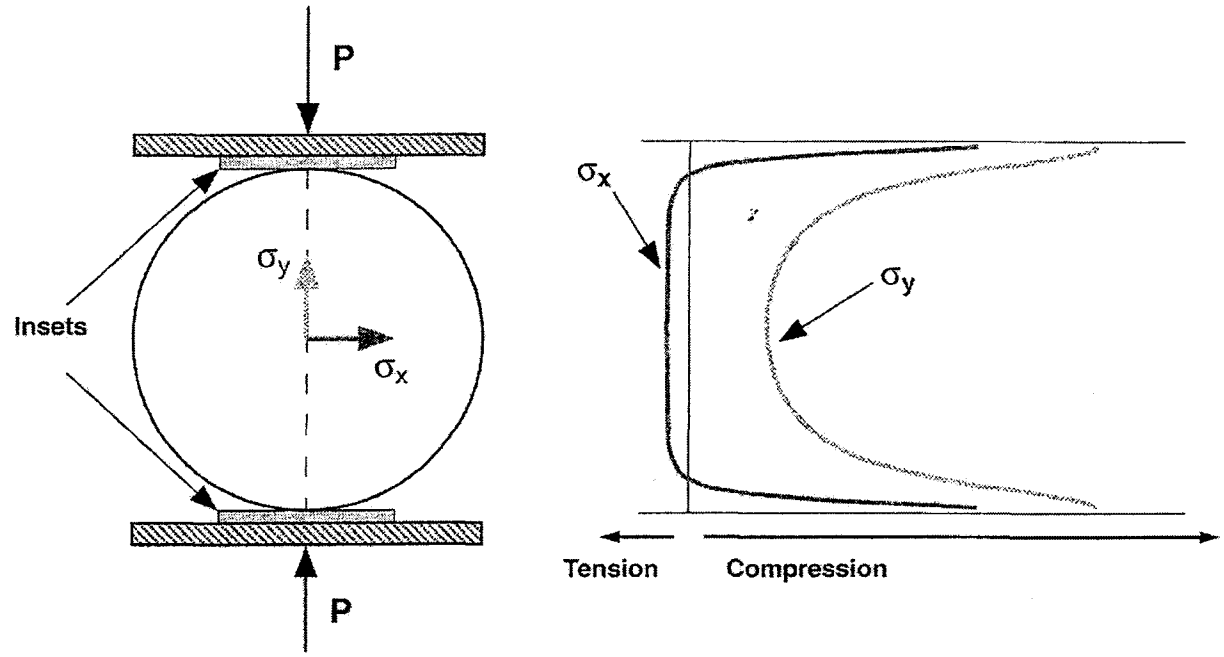

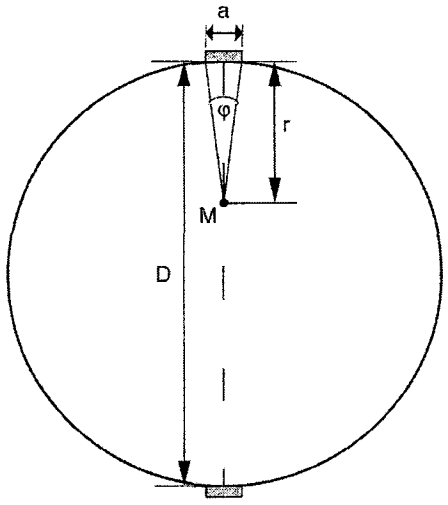

Figure 4.2. (top left) Illustration of the diametral compression testing set-up and (top right) the stresses induced in the material along the vertical, diametral plane (y-direction), as well as the horizontal plane (x-direction); tensile stress at failure is calculated with the following equation (Eqn. 4.1) $\sigma_x = -\frac{2P}{\pi DL}$; principal stresses acting on the loaded diametral plane at point M are expressed in the following manner with the assumption that $a \leq 0.1D$:

$$\sigma_x = -\frac{2P}{\pi DL}\left[1 - \frac{D}{2a}(\varphi - \sin\varphi)\right] \text{ and}$$

$$\sigma_y = -\frac{2P}{\pi DL}\left[1 - \frac{D}{2a}\left(\varphi + \sin\varphi - \frac{1}{1-\frac{r}{D}}\right)\right]$$ where P is the applied force, D is the cylinder diameter, L is the cylinder length and r is the distance between the considered point and the closest platen.

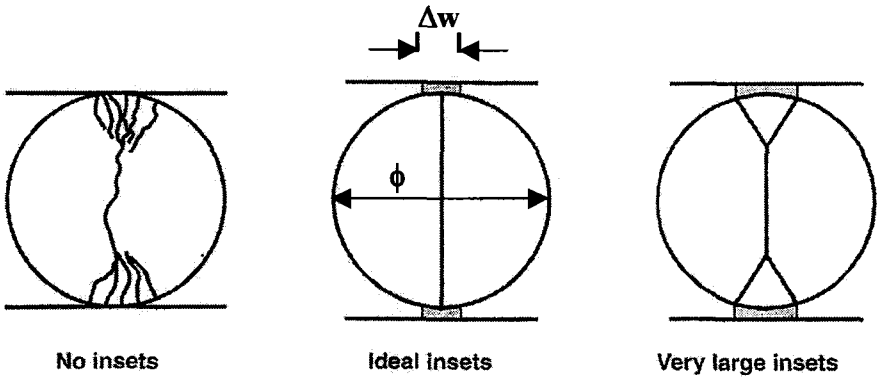

Figure 4.4. Typical modes of rupture obtained with different inset widths; inset width (Δw) in the literature has been reported to vary from 5% to 30% the cylinder diameter (ϕ); appropriate inset width promotes failure along the vertical, diametral axis; figure adapted from Pittet et al.[26]

Table 4.1. Diametral Compression Parameters.

Study	Test Material	Inset Material (pw/cd)	Cylinder Dimensions			Loading Rate
			Diameter	Thickness	Ratio	
Pittet et al.	Brushite cements	Cardboard (NA)	8.7 mm	6 mm	1.45	1 mm/min.
Callahan et al.	Plaster cast	NA	51 mm	13 mm	3.92	NA
Greish et al.	HA-Ca Poly(vinly phosphonate)	Fabric pad (NA)	NA	NA	NA	0.05 cm/min.
Thomas et al.	HA	1 mm thick soft-Cu	NA	NA	NA	0.05 cm/min.
Touny et al.	HAp protein composite	NA	NA	NA	NA	0.05 cm/min.
Pilliar et al.	CaP scaffolds	NA	4 mm	2 mm	2.00	0.5 mm/min.
Tay et al.	Glass/dental cements	NA	7.14-7.7 mm	16.7-30.5 mm	0.43	0.2 mm/min.
Summitt et al.	Femur/tibia bone allograft	NA	3-6 mm	5-7 mm	0.60	25 mm/min.

NA = not available; pw = insert pad width; cd = cylinder diameter

diameter vary in a non-linear fashion along the width of the ring (Figure 4.5, bottom left). More importantly, the neutral axis (i.e. the internal axis of a member in bending along which the strain is zero) shifts towards the center of rotation away from the centroidal surface. Therefore, the longitudinal perforations, which are oriented along the centroidal surface of the graft, would be exposed to tensile loading. On the other hand, the transverse perforations, which extend from the perioseal surface to the endosteal surface, would be exposed to a larger degree of tensile loading at the endosteal surface. It is therefore hypothesized that the transversely perforated grafts would fail at significantly lower compressive loads than the longitudinally perforated grafts. Though the very nature of the diametral compression test has limited direct biomechanical application, it may prove to be a viable means of quantifying changes in mechanical integrity that accompany graft modification.

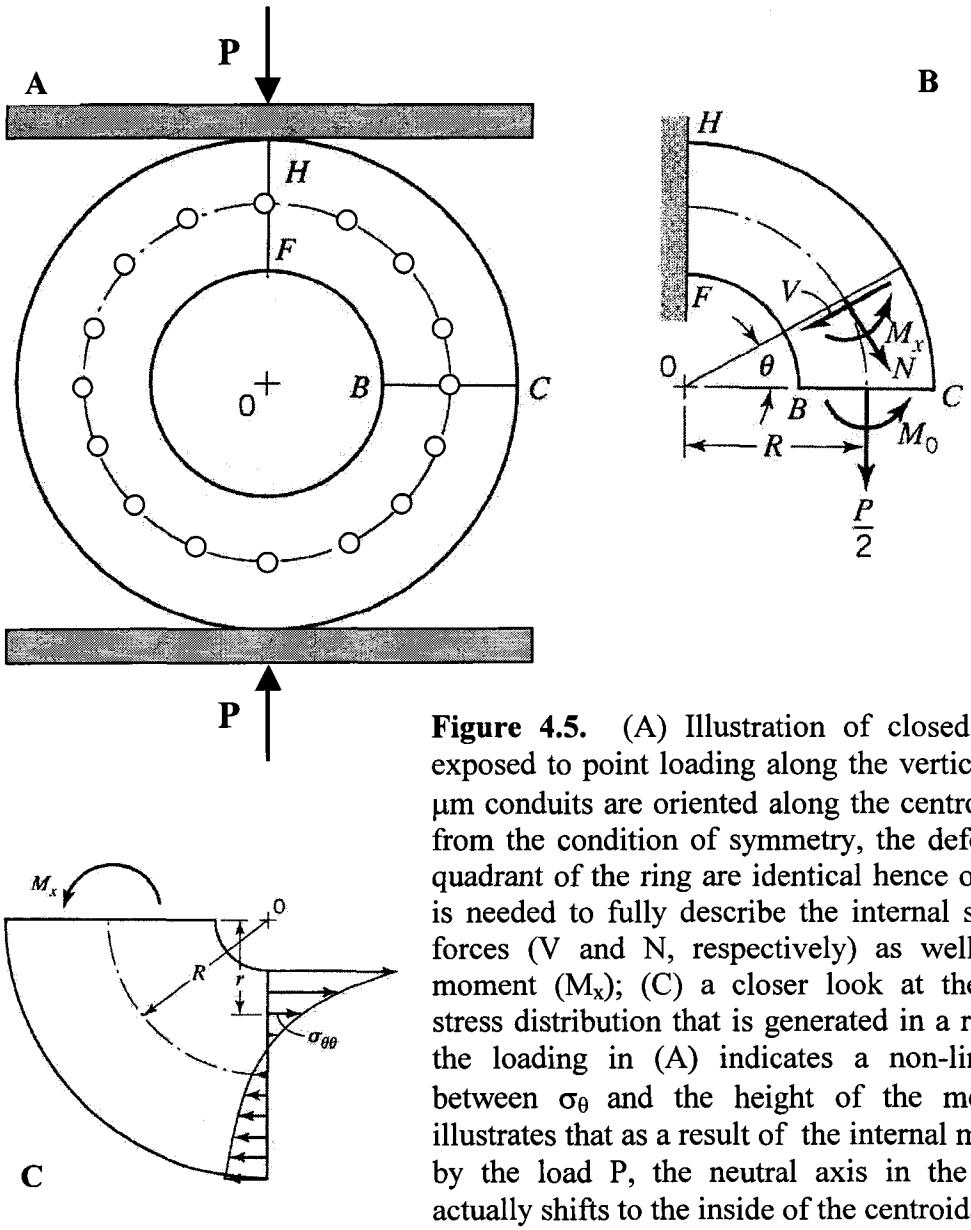

Figure 4.5. (A) Illustration of closed cylindrical ring exposed to point loading along the vertical plane; the 500 μm conduits are oriented along the centroidal surface; (B) from the condition of symmetry, the deformation of each quadrant of the ring are identical hence only one quadrant is needed to fully describe the internal shear and normal forces (V and N, respectively) as well as the internal moment (M_x); (C) a closer look at the circumferential stress distribution that is generated in a ring as a result of the loading in (A) indicates a non-linear relationship between σ_θ and the height of the member; (C) also illustrates that as a result of the internal moment generated by the load P, the neutral axis in the curved member actually shifts to the inside of the centroidal surface.

4.2 Materials and Methods.

4.2.1. Uniaxial Compression Test.

In a preliminary effort to quantify the effects of longitudinal perforation on allograft mechanical properties, uniaxial compression tests of 5 cm specimens of allograft bone harvested from 14 matched pairs of cadaveric sheep tibiae was performed (power > 0.80). Specifically, a repeatable pattern of 16, 500 μm diameter holes was drilled to a 10 mm depth in the proximal and distal cortex parallel to the long axis of the allograft. The centers of each perforation were approximately 5 mm apart and spanned the circumference of the cortex. Bone specimens from control allograft (non-perforated) and longitudinally perforated allografts were tested to failure by applying an axial load with a servohydraulic materials testing machine (MTS, Edan Prarie, MN) at a loading rate of 0.5 mm/min (Figure 4.6), similar to those conditions proposed by Lewandrowski et al.[13] who performed identical tests on transversely perforated and cortically demineralized allograft. Data on the failure loads and displacements of the longitudinally perforated bone allograft specimens were compared to the allograft control as well as to those values previously reported by Lewandrowski et al.[13] with regard to transverse perforations. Strain in the specimens under the applied axial load was determined by dividing the recorded displacement values by the length of the original specimen. Differences in structural parameters will be evaluated with a one-way ANOVA at a significance level of α=0.05 with SAS statistical software (SAS Institute, Cary, NC).

Figure 4.6. Uniaxial compression testing set-up. (Left) Illustration of 5 cm specimen in MTS machine prior to loading; (Top Right) Pre-test specimen; (Bottom Right) Pre-test graft in LAP treatment group depicting the pattern of 16, 500 μm conduits created in the proximal end plate; LAP was accomplished with a 500 μm steel drill bit (Cleveland Tools, Cleveland, OH) and a rotary tool affixed to a drilling press (Dremel, Racine, WI); conduits in the proximal and distal end plates extended to a depth of approximately 10 mm (Figure 2.2G, Chapter 2).

4.2.2. Diametral Compression Test.

Six pairs of skeletally mature, ovine femora were harvested for inclusion in the diametral compression study. These animals were humanely euthanized for inclusion in separate, non-related studies. Sheep femora exhibit considerably greater geometric homogeneity than sheep tibiae (Figure 4.1 A&B) and were considered more appropriate test specimens given their more circular dimensions.

Under constant irrigation, matching 12 cm sections of cortical bone were initially cut from the mid-diaphysis of the right and left femora using a diamond exact saw (Exakt Technologies, Oklahoma City, OK). The ostectomized intercalary sections were further cut transversely into eight, 5 mm thick cylindrical specimens for testing in diametral compression (Figure 4.7). In four of the six matched pairs, the cylindrical specimens taken from the right limbs were designated to the either the LAP (longitudinal allograft perforation) or TAP (transverse allograft perforation) experimental treatment group and received 16, 500 μm diameter cortical perforations along the cortical endplate and either parallel (LAP) or perpendicular (TAP) to the original long axis of the bone. A pattern of points was marked on the end plate with the first four marks placed at approximately the 12, 3, 6, and 9 o'clock positions and the remaining 90-degree increments filled with an additional three marks for a total of 16 points identified for drilled perforations. The remaining matched cylinders from the contralateral limbs of these four animals served as internal controls to compare the effects of LAP and TAP versus intact specimens.

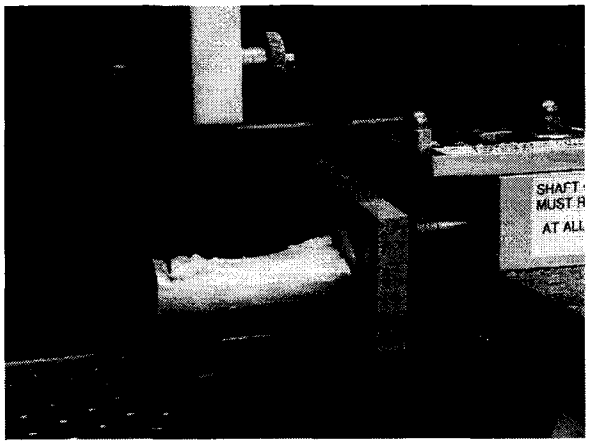

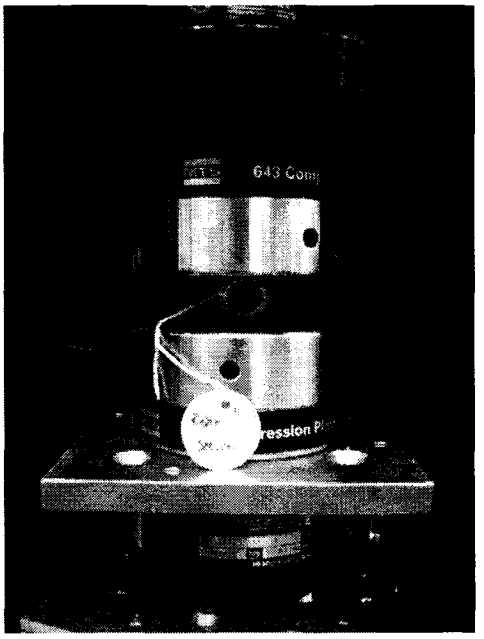

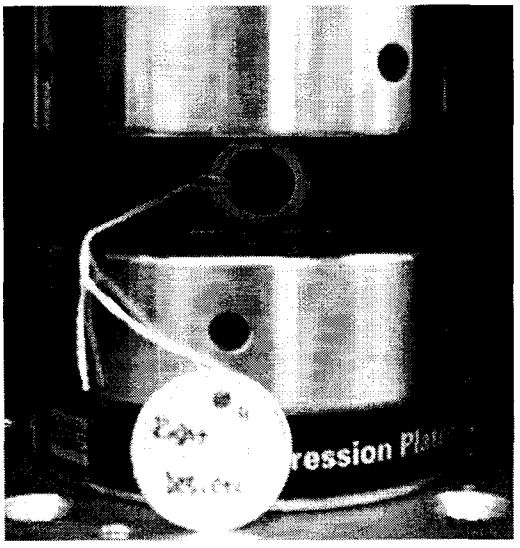

Figure 4.7. Diametral compression specimen preparation and testing. (Top Left) Specimen preparation included cutting 8, 5 mm thick sections from the mid-diaphysis of 6 pairs of ovine tibiae; specimens were identified DC1 (most proximal) through DC8 (most distal); (Top Right) Allograft sections were positioned between two compression platens in the MTS machine and loaded in the cranial/caudal direction; (Bottom Left) Sectioned specimens were secured between the patens with sand paper and the axial load was transmitted through two, 5 mm wide cardboard insets.

The two remaining matched pairs of sheep tibiae were cut and sectioned in an identical fashion to that just described. Cylindrical specimens cut from the right limbs were designated to the LAP treatment while the matched specimens from the contralateral left limbs received TAP treatment (Figure 4.8). This experiment allowed for direct comparison of the deleterious effects (if any) of perforation orientation within the bony cortex.

A total of n=96 sections (n=8/limb/animal, 6 animals: power > 0.80) were tested in diametral compression using a materials testing machine (MTS. Edan Prarie, MN) at a loading rate of 0.5 mm/min.[9, 10, 31, 33]. Force and displacement data was collected at 10 Hz. Soft cardboard insets[26] measuring approximately 5 mm in width were employed to ensure contact between the stainless steel compression platens and test specimens as well as to distribute the applied force so as to promote a mechanism of failure expected in the diametral compression test[6, 26]. Tissue hydration prior to and during the testing procedure was maintained with 0.9% NaCl. A laser alignment tool (Z-laser Optoelekctronik, Freiburg, Germany) was employed to ensure the perforations were aligned directly under the axis of loading thus ensuring that two of the perforations were exposed to tensile loading.

Failure loads for the perforated specimens and the non-perforated controls as well as the intraexperimental comprasion of LAP versus TAP were compared with a one-way ANOVA at a significance level of α=0.05 using SAS statistical software (SAS, Cary, NC).

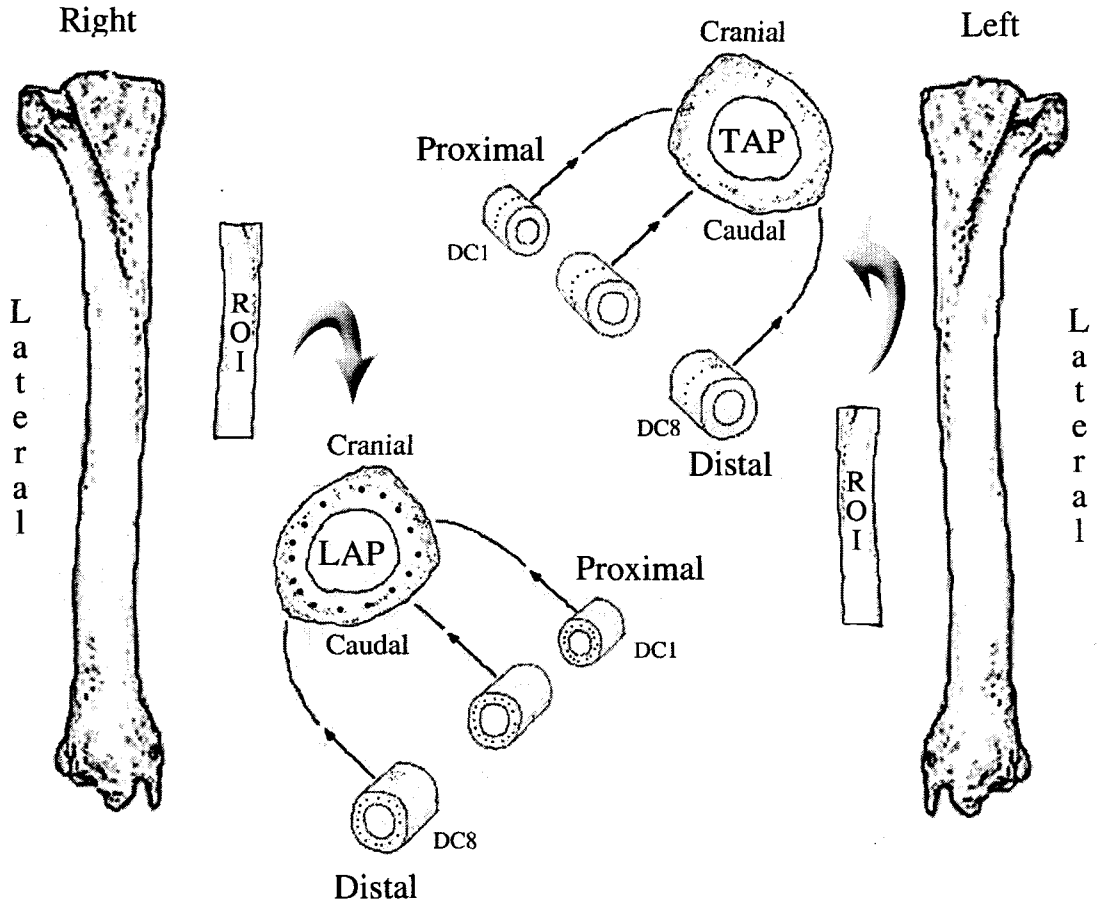

Figure 4.8. Illustration of experimental design for diametral compression testing; 40 mm intercalary sections (ROIs) were resected from the mid-diaphysis of matched sheep tibiae; from each ROI, 8, 5 mm specimens labeled DC1 (most proximal) through DC8 (most distal) were cut and identified for either longitudinal perforation (LAP) or transverse perforation (TAP); LAP modification consisted of creating 16, 500 μm diameter drill holes parallel to the long axis of the original ROI specimen; each LAP conduit extended the entire length of the 5 mm cortical cylinder thickness; TAP consisted of creating 16, 500 μm diameter conduits extending from the periosteal surface and perforating the endosteal surface adjacent to the medullary canal; during testing, perforations aligned with the cranial and caudal aspects of the modified grafts were aligned directly along the diametral plane and exposed to tension to quantify the effects of either LAP or TAP on graft mechanical integrity.

4.3. Results

Uniaxial compression tests of longitudinally perforated grafts resulted in a 6.70% decrease in compressive force to failure relative to non-perforated control limbs (Figure 4.7, p=0.140). Displacement at failure and failure strain were not significantly affected by the presence of the longitudinal conduits (Table 4.2). Failure typically occurred at the proximal or distal end plate in both the treatment and intact control groups. In some perforated grafts, fracture propagated between the 500 μm conduits and along the periosteal surface of the graft (Figure 4.9, top right). Fracture of the intact controls also occurred along the circumference of the cortical endplate and extended along the periosteal surface (Figure 4.9, bottom right).

Results from the diametral compression test are presented below in Figure 4.10. The presence of the longitudinal conduits resulted in an 11.14% decrease in ultimate force to failure that bordered on statistical significance (p=0.052). Within the same experimental set-up, transversely perforated grafts exhibited a significant 14.5% decrease in failure load relative the matched, non-perforated controls (p=0.018). No significant differences in stiffness were noted between longitudinally or transversely perforated specimens and their matched intact controls (LAP: p=0.473, TAP: p=0.956). Intra-animal comparisons of the effects of LAP versus TAP revealed no significant differences in ultimate force at failure, graft stiffness and displacement at failure (Figure 4.11). Failure in all diametral compression tests consistently occurred in the vertical, diametral plane (Figure 4.7, right), and through the longitudinal or transverse perforations when present.

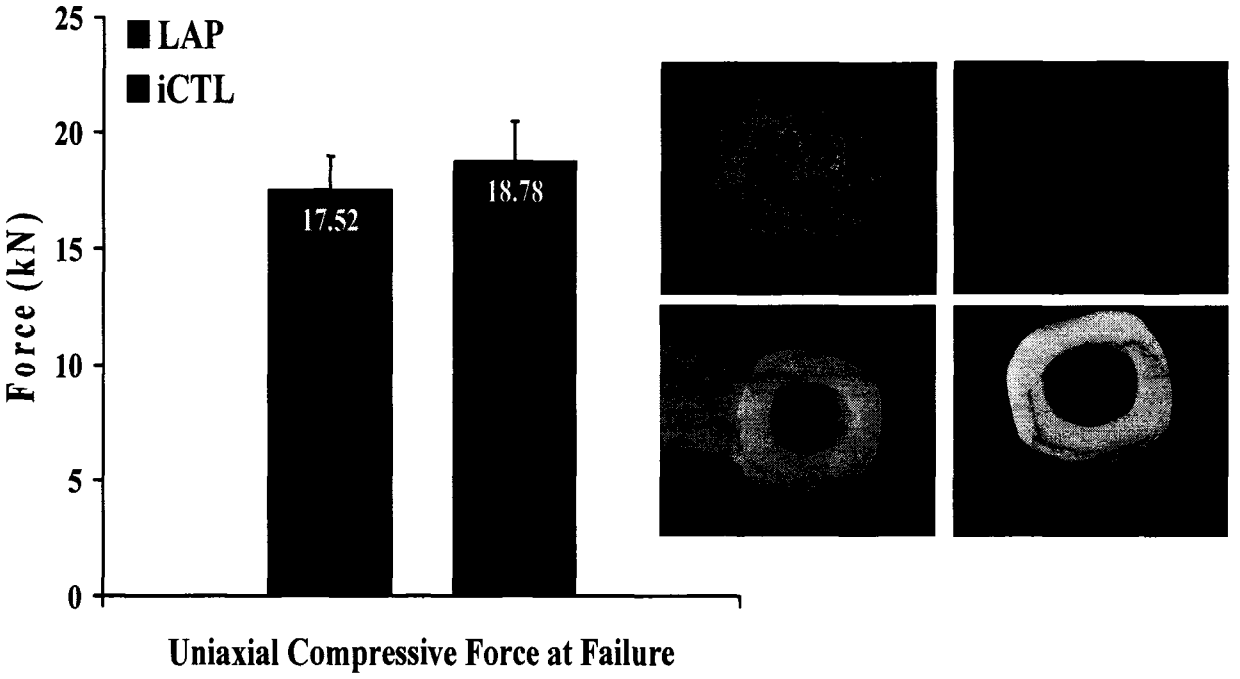

Figure 4.9. Uniaxial compression testing results; (Left) destructive compression tests resulted in a 6.70% decrease in ultimate force to failure; longitudinally perforated specimens failed at an average of 17.5 kN while non-perforated controls failed at an average of 18.8 kN (p=0.399); (Right) failure typically occurred at the proximal or distal endplate in both the perforated and non-perforated specimens; (Top Right) LAP specimen failure through perforations with fracture extending the length of the 10 mm conduits; (Bottom Right) iCTL specimen illustrating compressive failure of the proximal endplate with fracture extending along the periosteal surface of the graft.

Table 4.2. Uniaxial Compression Tests Results. Comparison of LAP vs. iCTL.

Group	Number of Specimens	Mean failure load (kN)	% diff p-value	Maximum displacement (mm)	% diff p-value
iCTL	14	18.77 ± 1.71	6.70%, p=0.399	0.484 ± 0.014	8.29%, p=0.319
LAP	14	17.52 ± 1.45		0.522 ± 0.026	

iCTL = internal, contralateral control; LAP = longitudinal allograft perforation.

Results presented as Mean ± SEM

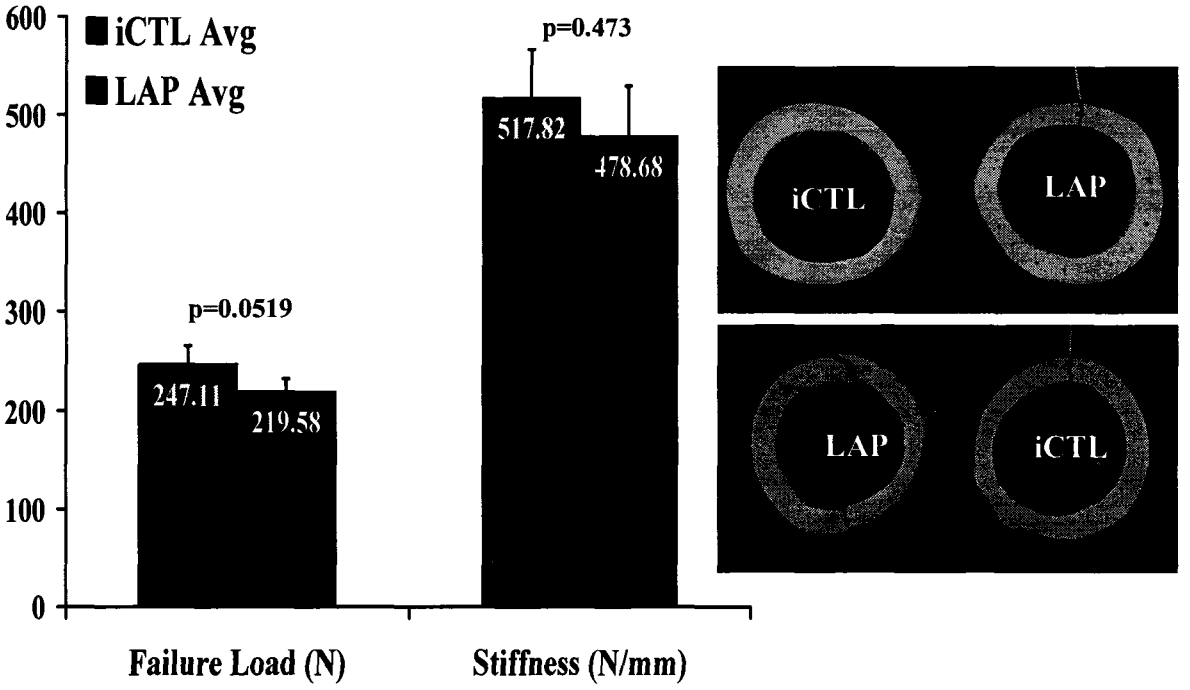

Figure 4.10. Diametral compression results. (Left) destructive diametral tests resulted in an 11.14% (p=0.0519) and 7.56% (p=0.473) decrease in failure load and stiffness, respectively; (Right) failure consistently occurred parallel to the axis of diametral loading in all tested samples (Figure 4.4, middle); (Top Right) matched DC4 pair illustrating failure through a longitudinal perforation in the cranial cortex; (Bottom Right) matched DC6 pair illustrating failure through a longitudinal perforation cranially and the identical cortex in the iCTL specimen.

Table 4.3. Diametral Compression Results Relative to Intact Controls. LAP & TAP vs iCTL

Group	Number of Specimens	Loss of Compressive Strength (% of iCTL)	p-value	Loss of Stiffness (% of iCTL)	p-value
LAP	16	11.14	p=0.051	7.56	p=0.473
TAP	16	14.50	p=0.018	0.33	p=0.956

iCTL = internal, contralateral control; LAP = longitudinal allograft perforation;
TAP= transverse allograft perforation; Results presented as Mean ± SEM

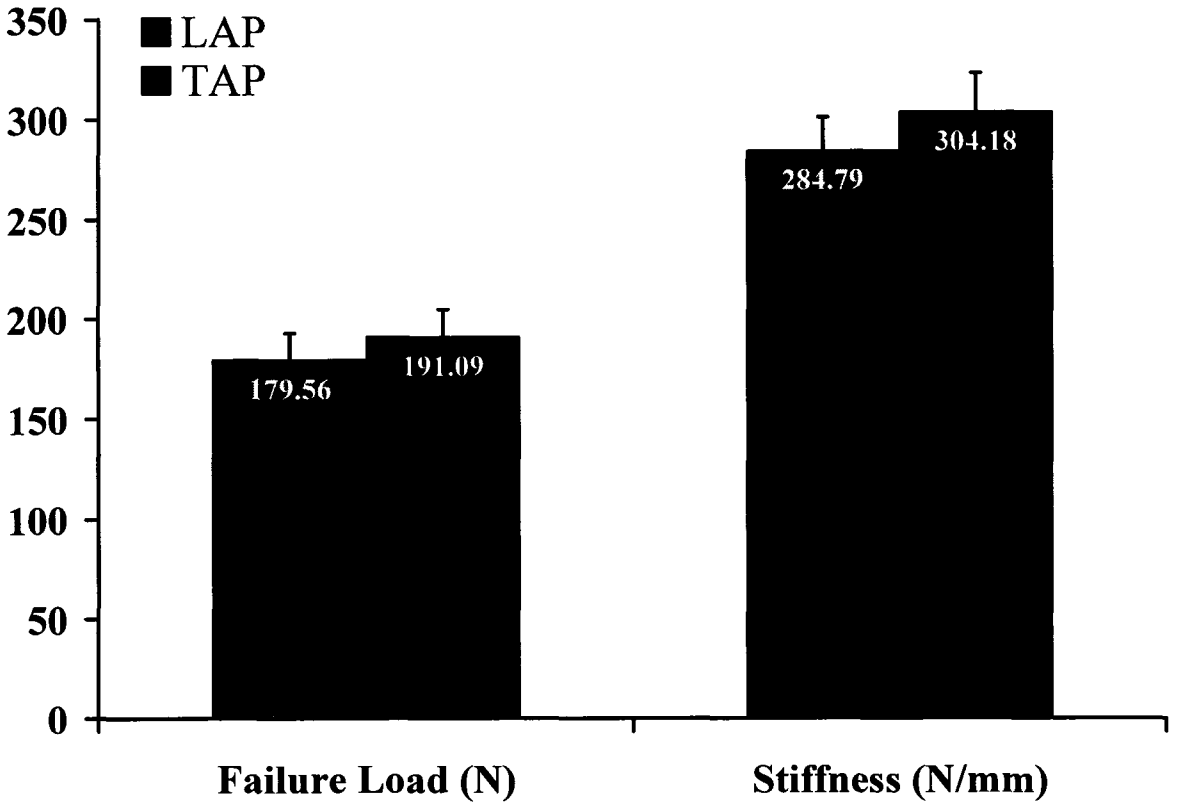

Figure 4.11. Intra-experimental diametral compression results comparing LAP versus TAP within the same animal; no significant differences in ultimate force to failure ($p=0.549$) or stiffness ($p=0.212$) were noted between 5 mm specimens receiving the longitudinal conduits or the transverse conduits; additionally, no difference in displacement at failure was noted between the LAP and TAP specimens ($p=0.114$); failure consistently occurred along the diametral plane with fracture extending through the conduits.

4.4. Discussion.

Concurrent histological studies concluded that 500 μm by 10 mm conduits created in 5 cm intercalary ovine allografts promoted improved graft revitalization, as demonstrated via fluorescence microscopy, relative to non-perforated grafts (Figure 4.1). Despite any evidence of *in vivo* failure, it is imperative to quantify the effects of such a form of graft modification prior to transplantation. The current study demonstrated that perforations extending 10 mm into the proximal and distal cortices of a 5 cm intercalary allograft (LAP) have minimal effects on graft structural integrity. Specifically, uniaxial compression tests of perforated 5 cm grafts resulted in a 6.70% ($p=0.399$) decrease in force to failure relative to non-perforated controls. Diametral compression tests of 5 mm thick cylindrical rings resulted in an 11.14% ($p=0.052$) decrease in ultimate force to failure relative to non-perforated grafts ($p=0.052$) while transversely perforated grafts (TAP), within the same experimental setup, exhibited a significant 14.5% decrease in compressive force to failure ($p=0.018$). These findings indicate that LAP and TAP graft modification may have deleterious effects under tensile loading as the 500 μm diameter conduits served as stress concentrations in the brittle mineral matrix. The effect of conduit orientation within the matrix appeared to have no significant effect on force to failure in diametral compression when compared directly within the same experiment ($p=0.549$). Despite near significant and significant differences in force to failure, no differences in stiffness or displacement to failure were noted between the perforated specimens and intact controls in either uniaxial compression or diametral compression.

The initial biologic response to massive cortical allografts is a transient period of accelerated bone resorption by osteoclasts that may last as long as six months in human patients[2]. The end result is to weaken the graft mechanically by as much as 40%. Given the documented course of healing, it seems absolutely necessary that the form of therapeutic intervention employed to promote long-term graft healing not involve the transplantation of a graft that has been modified in such a way that it's structural and mechanical properties are already significantly reduced. Destructive uniaxial compression tests of 5 cm intercalary allografts revealed a 6.7% decrease in ultimate force to failure (p=0.40) relative to non-perforated controls. These findings are in accordance with Lewandrowski et al.[13] whom reported a non-significant decrease in compressive force to failure of transversely perforated 3 cm allografts (Table 4.4). In addition, in the current study no significant differences were noted in stiffness or displacement (and strain) at failure.

Table 4.4. Uniaxial Compression Tests Results. Comparison of LAP vs. TAP

Study	Group	Number of Specimens	Mean failure load (kN)	Loss of Compression Strength (%)		Maximum displacement (mm)	
Santoni et al.							
	iCTL	14	18.77 ± 1.01			0.484 ± 0.014	
	LAP	14	17.52 ± 1.52	6.70	p=0.399	0.522 ± 0.026	p=0.132
Lewandrowski et al.[13]							
	iCTL	6	10.82 ± NR			0.450 ± NR	
	TAP	6	10.59 ± NR	2.7	p>0.05	0.473 ± NR	p>0.05

iCTL = internal, contralateral control; L/TAP = longitudinal/transverse allograft perforation; NR = not reported

Therefore, the mechanical and structural influences of the longitudinal perforations employing this particular form of mechanical testing are minimal in direct compression. However, the same favorable biologic response quantified *in vivo* utilizing LAP was not reported in those studies by O'Donnell et al.[21] and Lewandrowski et al.[15, 16] using transversely perforated grafts. Successful graft incorporation and revitalization in the aforementioned studies was only documented when graft perforation was combined with extensive cortical demineralization. In axial compression, these perforated and demineralized grafts failed at significantly lower ultimate loads and significantly higher failure strains than control grafts.

The diametral compression test has recently been utilized to evaluate the tensile strengths brittle biomaterials[9, 10, 22, 28, 33] including cortical allograft[20, 29]. In a recent study, Mroz et al.[20] employed diametral compression to quantify the effects of the BioCleanse sterilization process (Regeneration Technologies, Inc., Alachua, FL) on the tensile properties of cadaveric allograft cylinders. The application of a point force along the diameter of a full thickness cylinder results in the generation of a tensile stress perpendicular to this axis of loading (Figure 4.2). This form of testing results in an indirect measure of the tensile strength of various brittle materials. In the aforementioned study, Mroz et al.[20] reported no effect of the BioCleanse sterilization process on the ultimate tensile stress (and ultimate failure load) of the treated allograft specimens with a difference between treated and untreated grafts of less than 5%.

In the current study, 5 mm thick sections from sheep femora were compressed to failure along the cranial/caudal direction to evaluate the effect of the presence of the longitudinal perforations. It was hypothesized that the presence of the 500 μm conduits would result in failure loads that were significantly less than non-perforated controls since the conduit would act as a stress concentrator and alter the local circumferential stress field (Figure 4.8). Destructive compression tests resulted in a near significant 11.1% decrease in ultimate force to failure ($p=0.052$). The stiffness of the perforated grafts was not affected. These findings indicate that the circumferential stresses (σ_θ) were altered due to the presence of the conduit and thus affect the structural integrity of the graft in a negative way. Additionally, within the same experimental setup, transversely perforated cylindrical specimens failed on average at 85% of the intact, non-perforated controls ($p=0.018$). Direct, intra-animal comparisons of LAP versus TAP indicated no significant difference in structural properties between the two forms of graft modification, seemingly indicating a lack of any effect of conduit orientation in the brittle matrix on the tensile properties of the graft. This finding is in disagreement with our original hypothesis. The findings reported here may indicate that the non-linear circumferential stress distribution that develops in closed rings exposed to point loading is not as dramatic as described in Figure 4.8. Perhaps the discrepancy in σ_θ that the longitudinal and transverse conduits are exposed to is relatively small as a result of the small thickness of the ovine femoral cortex relative to the femoral diameter. In addition, radial stresses (σ_r) develop in cylindrical rings exposed to point loads and their effects were not considered here. In general their magnitudes are low relative to the circumferential stresses. However, for anisotropic materials, such as bone, they may be significant relative to the radial strength of the

material. Given that σ_r increases from zero at the endosteal surface to a maximum value adjacent to the periosteal surface, the multiaxial state of stress acting on the longitudinal conduits may explain the discrepancy between our initial hypothesis and the results reported here. These conjectures may be confirmed in the future by finite element computation models that take into account the inherent anisotropy of bone as well as its material properties.

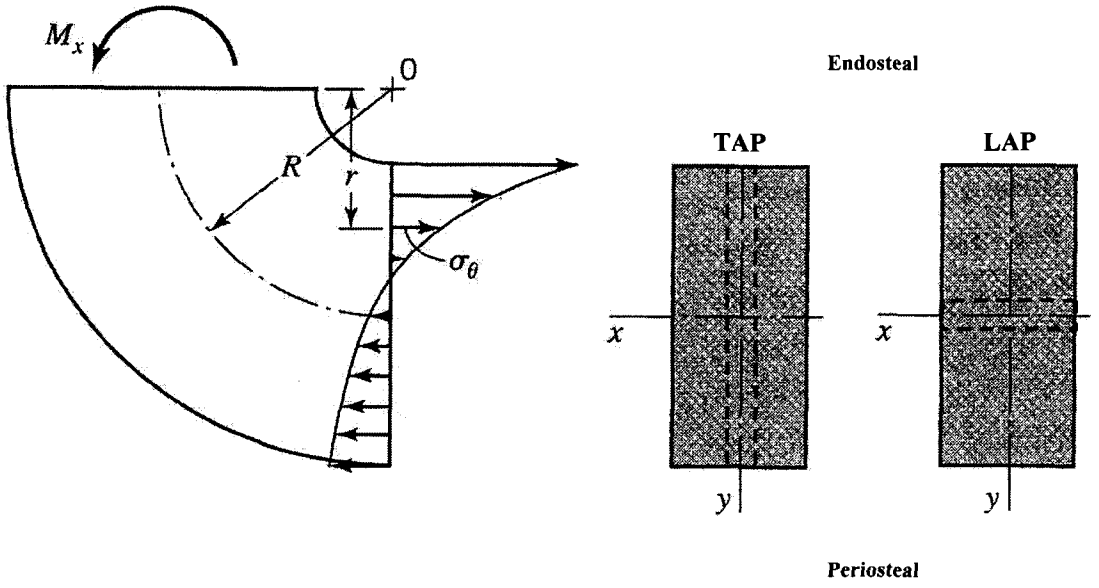

Figure 4.8. The discrepancy between the local circumferential stress magnitude that the transverse and longitudinal perforations are exposed to may be much smaller than hypothesized given the small thickness of the femoral cortical shell; this may explain the discrepancy between the results reported here and our initial hypothesis that TAP modification (given that the stress concentration is located on the endosteal surface and thus the area of highest circumferential stress) would lessen the structural properties of the graft to a higher degree than LAP; not depicted above are the radial stresses that are induced in the material as a result of point loading; though smaller in magnitude than σ_θ, they may be important in anisotropic materials with low radial strength and may also account for negligible differences between LAP and TAP modification.

Though the diametral compression test may have limited direct biomechanical application, it served as an adequate mechanical test to evaluate the changes in structural integrity that accompany LAP and TAP. Mechanical stresses were not quantified in the current study. The mechanical analysis presented as an accompaniment to Figure 4.2 is valid only for a full thickness cylindrical specimen and would therefore not be an appropriate method for analyzing the local stresses that develop following diametral compression of an allograft ring. In addition, though the cicumferential stresses that develop as a result of a ring exposed to point loading along one of it's two diametral axis may well be represented graphically in Figure 4.2 & Figure 4.8, it should be noted that the actual calculations presented in mechanics texts are derived from assumptions that follow from Euler-Bernoulli Beam Theory which are derived from a simplfication of the linear isotropic theory of elasticity. Given that the assumptions employed to derive stress equations are not entirely consistent with the mechanical properties of bone, calculations of circumferential stresses in bone may be grossly different from those that actually exitst. It seems unlikely then that the stress distribution present in cylindiral allograft specimens could be described by a simple equation derived from elasticity. Perhaps the only valid means to compute the stresses that arise in intact and perforated graft specimens would be to perform computational finite element analyses that take into account the viscoelastic, non-homogeneous, and anistropic properties of bone tissue.

Though the current study did demonstrate that longitudinal perforations have smaller relative effects on structural integrity compared to transversely perforated grafts, there are a few limitations that are inherent to this study. The first is the lack of direct

biomechanical relevance of the diametral compression test. Previous studies have successfully employed diametral compression to evaluate the tensile properties of bioceramics, however, prior investigations that have attempted to quantify the effects of allograft modification (i.e. perforating or demineralizeing the cortical matrix) on material properties have employed four-point bending. Given that the LAP alters the graft porosity only in the vicinity of the cortical endplates, it seems unlikely that such a form of modification would have significant effects on the flexural properties of the graft.

Secondly, though the current study did show that LAP has minimal effects on the compressive and tensile properties of the graft prior to insertion, this study did not quantify the structural changes in the graft that may result from cyclic, fatigue loading. It has been previously reported that cyclic loading of intact, healthy bone *in vivo* results in the accumulation of microdamage in the form of microcracks. Given that bone is a living tissue, it is able to repair itself and microdamage seems an important variable that stimulates the remodeling response in normal bone. In massive bone allograft, excessive cyclic loading also leads to the accumulation of microfracture density. Given that allograft bone is non-viable, these microcracks are unable to be repaired. Wheeler and Enneking[34] recently reported that it is partly the result of the accumulation of these microcracks that leads to the deterioration of the mechanical properties of bone allograft *in vivo* and leads to graft fracture and ultimate failure of the reconstructed limb. Contrary to those studies published by Lewandrowski et al.[13, 15-17] and O'Donnell et al.[21], the concurrent studies did illustrate that LAP promotes appositional bone formation *in vivo* within the conduits. Principles of fracture mechanics predict that under cyclic loading,

the perforations may serve as accelerators of crack formation and crack propagation within the allograft. Transversely perforated grafts then would appear to suffer from not only diminished structural properties prior to implantation but may also suffer from microfracture density accumulation that could not be repaired *in vivo* resulting in premature fatigue failure. In contrast, microfacture at the ends of the conduits within the longitudinally perofrated allograft that results from cyclic loading *in vivo* may potentiate improved graft revitalization given the newly viable tissue that has apposed onto the entire surface of the conduit.

In summary, modification of the cortical shell by introducing 500 μm diameter conduits parallel to the long axis of the graft has minimal effects on the compressive properties of the graft but does appear to affect the tensile properties of the graft in a negative way. Diametral compression of longitudinally perforated, 5 mm allograft cylinders resulted in a nearly statistically significant 11% decrease in ultimate load to failure relative to intact control specimens, presumably due to the presence of the stress concentration. From a clinical perspective, the small alteration of the tensile properties of the graft prior to transplantation may be of little clinical relevance given that after four months *in vivo* the conduits had filled with new appositional bone. It is hypothesized the the flexural properties of longitudinally perofrated grafts would be insignificantly altered given that the increase in matrix porosity occurs only at the extremities of the grafted tissue. Therfore, the mechanical and histological findings reported here merit LAP as a novel means to expedite graft revitlaization *in vivo* without significantly compromising the integrity of the graft prior to transplantation.

4.5. References.

1. Allan DG, Lavoie GJ, McDonald S, et al.: Proximal femoral allografts in revision hip arthroplasty. J Bone Joint Surg Br. 73:235-240, 1991.

2. Burchardt H: The biology of bone graft repair. Clin Orthop. 1983.

3. Burchardt H, Busbee GA, 3rd, Enneking WF: Repair of experimental autologous grafts of cortical bone. J Bone Joint Surg Am. 57(6):814-819, 1975.

4. Callahan DJ, Daddario N, Williams S, Walter NE: 3 Experimental-Designs Testing Orthopedic Casting Material Strength. Orthopedics. 9:673-675, 1986.

5. Chandler H, Clark J, Murphy S, et al.: Reconstruction of major segmental loss of the proximal femur in revision total hip arthroplasty. Clin Orthop Relat Res. 67-74, 1994.

6. Fahad MK: Stresses and failure in the diametral compression test. J Mater Sci. 31:3723-3729, 1996.

7. Gebhardt MC, Flugstad DI, Springfield DS, Mankin HJ: The use of bone allografts for limb salvage in high-grade extremity osteosarcoma. Clin Orthop. 1991.

8. Gendler E: Perforated demineralized bone matrix: a new form of osteoinductive biomaterial. J Biomed Mater Res. 20(6):687-697, 1986.

9. Greish YE, Brown PW: Formation and properties of hydroxyapatite-calcium poly(vinyl phosphonate) composites. J Am Ceram Soc. 85:1738-1744, 2002.

10. Greish YE, Brown PW: An evaluation of mechanical property and microstructural development in HAP-Ca polycarboxylate biocomposites prepared by hot pressing. J Biomed Mater Res. 53:421-429, 2000.

11. Kang JS, Kim NH: The biomechanical properties of deep freezing and freeze drying bones and their biomechanical changes after in-vivo allograft. 36:332-335, 1995.

12. Kondrai G, Tarsoly E: [On the increase of the incorporation ability of Kiel hard bone preparations]. 7:201-210, 1966.

13. Lewandrowski KU, Bonassar L, Uhthoff HK: Mechanical properties of perforated and partially demineralized bone grafts. Clin Orthop. 1998.

14. Lewandrowski KU, Hecht AC, DeLaney TF, et al.: Anterior spinal arthrodesis with structural cortical allografts and instrumentation for spine tumor surgery. 29:1150-1158; discussion 1159, 2004.

15. Lewandrowski KU, Schollmeier G, Ekkemkamp A, et al.: Incorporation of perforated and demineralized cortical bone allografts. Part I: radiographic and histologic evaluation. Biomed Mater Eng. 11(3):2001.

16. Lewandrowski KU, Schollmeier G, Ekkemkamp A, et al.: Incorporation of perforated and demineralized cortical bone allografts. Part II: A mechanical and histologic evaluation. Biomed Mater Eng. 11(3):2001.

17. Lewandrowski KU, Tomford WW, Schomacker KT, et al.: Improved osteoinduction of cortical bone allografts: a study of the effects of laser perforation and partial demineralization. J Orthop Res. 15(5):748-756, 1997.

18. Lexer E: Substitution of whole or half joints from freshly amputated extremities by free plastic operation. Surg Gynecol Obstet. 6:601-607, 1908.

19. Mankin HJ, Springfield DS, Gebhardt MC, Tomford WW: Current status of allografting for bone tumors. Orthopedics. 15(10):1147-1154, 1992.

20. Mroz TE, Lin EL, Summit MC, et al.: Biomechanical analysis of allograft bone treated with a novel tssue sterilization process. Spine. 6:34-39, 2006.

21. O'Donnell RJ, Deutsch TF, Flotte RJ, et al.: Effect of Er:YAG laser holes on osteoinduction in demineralized rat calvarial allografts. J Orthop Res. 14(1):108-113, 1996.

22. Osterstock F, Doltsinis IS, Vansse O: The Brazilian reliability test and micromechanical modelling for channelled cylinders of multiphased porous ceramics. Key Eng Mat. 280-283:1731-1737, 2005.

23. Pelker RR, Friedlaender GE, Markham TC, et al.: Effects of freezing and freeze-drying on the biomechanical properties of rat bone. 1:405-411, 1984.

24. Peltier R: Theoretical investigation of the Brazilian test. 13:29-69, 1954.

25. Pilliar RM, Filiaggi MJ, Wells JD, et al.: Porous calcium polyphosphate scaffolds for bone substitute applications - in vitro characterization. Biomaterials. 22:963-972, 2001.

26. Pittet C, Lemaitre J: Mechanical characterization of brushite cements: A Mohr circles' approach. J Biomed Mater Res. 53:769-780, 2000.

27. Rees DC, Haddad FS: Bone transplantation. Hosp Med. 64:205-209, 2003.

28. Sano H, Ciucchi B, Matthews WG, Pashley DH: Tensile Properties of Mineralized and Demineralized Human and Bovine Dentin. J Dent Res. 73:1205-1211, 1994.

29. Summit MC, Squillace DMK, Bianchi JR: Mechanical Evaluation of Allograft Bone. In Schutte E, Picciolo GLKaplan D (eds). Tissue engineered medical products (TEMPs). West Conshohocken, PA, ASTM [American Society for Testing and Materials] 47-58, 2004.

30. Tarsoly E, Ostrowski K, Moskalewski S, et al.: Incorporation of lyophilized and radiosterilized perforated and unperforated bone grafts in dogs. Acta Chir Acad Sci Hung. 10(1):1969.

31. Thomas MB, Doremus RH, Jarcho M, Salsbury RL: Dense Hydroxylapatite - Fatigue and Fracture Strength after Various Treatments, from Diametral Tests. J Mater Sci. 15:891-894, 1980.

32. Thompson RC, Jr., Pickvance EA, Garry D: Fractures in large-segment allografts. J Bone Joint Surg Am. 75:1663-1673, 1993.

33. Touny AH, Brown PW: HAp protein composites formed by hydrolysis of alpha-TCP. Key Eng Mat. 17:39-42, 2005.

34. Wheeler DL, Enneking WF: Allograft Bone Decreases in Strength In Vivo over Time. 435:36-42, 2005.

35. Yue WM, Brodner W, Highland TR: Long-term results after anterior cervical discectomy and fusion with allograft and plating: a 5- to 11-year radiologic and clinical follow-up study. 30:2138-2144, 2005.

CHAPTER 5. SUMMARY AND CONCLUSIONS TO THESIS

FINAL DISCUSSION CONCERNING THE EFFECTS OF AN EXOGENOUS, BIOPHYSICAL STIMULI AND INREASED CORTICAL POROSITY IN PROMOTING IMPROVED ALLOGRAFT INCORPORATION AND REVITALIZATION

5.1 General Conclusions.

Allograft tissue transplantation has become commonplace in clinical orthopaedics and massive allograft bone is the primary source of bone graft material for use in limb salvage procedures after oncological tumor resection. However, allograft bone has been found to incorporate slowly into host bone resulting in allograft susceptibility to non-union, fracture, infection and fatigue failure. Clinical studies have shown that massive allograft bone has a 50% to 75% success rate at 10 years[3, 10, 29], while other orthopaedic implants, such as total hip and knee replacements have a 10-year success rate of approximately 90%[1]. Tumor recurrence, non-union, infection, and immune reaction lead to mechanical failure of the allograft indicating the inherent biological variability and uncertain success of massive allograft bone transplantation[21]. Fracture rates of allograft limb-salvage reconstructions range from 10.4% to 16%[28] and usually occur within the first few years after implantation[21, 22]. Typically revitalization of the allograft proceeds slowly, superficially, and only a few millimeters in to the grafted tissue even after years *in vivo*. Improving incorporation of the allograft is key to a successful reconstruction and improving the long-term clinical outcome [9].

The overarching goal of this study was to determine if a low-intensity pulsed ultrasound signal (LIPUS), alone or in combination with increased cortical porosity, could improve the extent of healing of the proximal and distal host/graft junctions in sheep tibiae reconstructed with a 5 cm intercalary allograft. This exploratory study has established the potential of both ultrasound and longitudinal porosity to improve allograft incorporation when used to regenerate large bone defects (Table 5.1). Specifically this study elucidated the following:

(1) LAP transformed the solid cortical allograft to an osteoconductive scaffold promoting osseous apposition and graft revitalization without adversely affecting the structural integrity of the graft. To the author's knowledge, this is the first study to elucidate the structural and biological effects of perforation orientation within massive cortical allografts. Additionally, enhanced biologic incorporation of the graft can be achieved by perforations alone and is not dependant on cortical demineralization;

(2) LIPUS stimulates active bone/callus formation yet does not appear to influence an adverse cellular or immunological response within the host. This was the first *in vivo* study to confirm *in vitro* reports that LIPUS can attenuate an osteoclastic response. Attenuating excessive graft resorption, especially during the initial phase of allograft healing, while at the same time promoting the osteoblastic phenotype may have a dramatic, positive influence on bone allograft science;

(3) This was one of the first studies to include a positive control in addition to a negative control and mechanical, radiographical and histological data confirmed the healing differential between the two. Allografts transplanted without adjuvant LAP or LIPUS therapy did not heal after four months *in vivo* (even in the absence of an aggressive, chronic immune response) while 5 cm, intercalary autologous grafts fully healed as quantified biomechanically and histologically

Table 5.1. Summary of Findings. Mechanical, Radiographical, and Biological Effects of Longitudinal Porosity and LIPUS. Results Expressed as % Change from the -CTL.

	Mechanics		Radiography	
Experimental Group	Ultimate Torque (N-mm)	Stiffness (N-mm/deg)	Callus Area (mm^2)	Callus with Cortical Density
LIPUS	27.60	32.40	43.48	15.90
LAP	14.00	26.90	70.22	16.00
LIPUS+LAP	25.60	40.40	63.86	16.30
	Histopathology		Histomorphometry	
Experimental Group	Callus Tissue Type	Host Graft Interface	Callus BFR	Graft BFR
LIPUS	29.32	12.03	95.12	159.05
LAP	6.77	-12.78	146.43	114.96
LIPUS+LAP	42.11	46.62	204.87	231.49

Large animal models have been widely used to investigate various therapies and their effects on improving graft healing and incorporation[6, 18, 19, 31, 34, 46]. The sheep model was chosen for its size, a skeletal metabolism similar to humans, and the perceived conserved major histocompatibility complex (MHC) of genes within this species[17]. MHC genes are translated into proteins that are primarily responsible for eliciting transplantation immunogenicity and an ensuing immune response in a non-compatible MHC host[37, 38]. Conservation of the genes that produce the immunogenic proteins prevents the development of a chronic immune response that may serve as a confounding variable and mask any effect of the graft therapy. Histopathological analysis revealed the lack of any detectable immune response to the fresh, frozen grafts and re-affirms the sheep model as an appropriate model to investigate the effects of LIPUS and LAP as well as future therapies on graft healing.

In the present study, internal fixation of the graft was accomplished with a static, interlocking nail which is a less rigid form of internal stabilization than internal bone plating and may represent a limitation of this study. Intramedulary nailing, even if locked, does not provide for adequate torsional stability nor does it guarantee sufficient fixation and compression at the host graft junction sites. In addition, IM nailing prohibits endosteal callus formation due to the elimination of adjacent host marrow and cellularity. However, revitalization of the grafts within the 500 μm conduits was realized even in the presence of this relatively unstable form of fixation demonstrating the potential of such a therapy. Even without adjuvant therapy, given the more stable mechanical environment as well as direct compression across the host/graft interfaces and the accompanying

improvement in congruency, it is expected that graft revitalization may proceed to an even greater degree using rigid plate fixation. Furthermore, LIPUS and/or LAP may temporally expedite the healing progression resulting in an even quicker return to mechanical and biological integrity of the graft.

The great majority of basic science research and clinical data on the use of ultrasound relates to fresh fracture healing. In a pioneering article, Duarte[7] reported that low-intensity ultrasound accelerated cortical bridging across the site of a fibular osteotomy in rabbits. Work by Pilla et al.[30] demonstrated that brief periods of pulsed ultrasound accelerated the recovery of torsional strength and stiffness in rabbit mid-shaft tibial osteotomies. These early findings demonstrated that bone exposed to ultrasound achieves biomechanical stability in essentially half the time of untreated bones. Additional *in vivo* studies by Azuma et al.[2] and Wang et al.[42] confirmed the previous findings of Pilla et al. using rat femoral fracture models. Azuma et al.[2] reported that the beneficial effects of LIPUS were not dependent upon the timing of treatment during the healing progression, and suggested that LIPUS acts on the cellular reactions involved in each phase of the healing processes such as inflammation, angiogenesis, chondrogenesis, intramembranous ossification, endochondral ossification, and bone remodeling. Recent *in vitro* work has confirmed the early suggestions of Azuma et al. and reported direct osteogenic[13, 15, 24, 25, 35, 36, 39], angiogenic[32], chondrogenic[15, 27, 45], as well as anti-osteoclastogenic[39] capabilities. Thus, ultrasound acts as a non-invasive surrogate to the mechanical forces and underpinning biological responses at work in Wolff's law without high loads presenting a risk to the wound-healing process. In essence, ultrasound provides an optimal

environment, both biologically and biophysically, to promote skeletal maintenance and repair.

In the current study daily ultrasound stimulation of the proximal and distal host/allograft junctions resulted in increases in torque to failure (27%) and torsional stiffness (33%) of the reconstructed limbs relative to the –CTL, though these differences were not significant after four months of healing. This finding may be attributed to the low sample size per treatment group and low statistical power of the study (50%). The increased structural properties of the reconstructed limbs treated with LIPUS appears to be the direct result of three times greater bone formation rates in the periosteal callus. Though osseous tissue was reported in the interface regions of the host/graft junctions, improved torsional integrity was more likely the result of periosteal callus. LIPUS appeared to accelerate the endochondral ossification process maturing the callus to a dense osseous bridge between the graft and host bone. Radiographical analyses and histomorphometric findings indicated that daily LIPUS treatment increased the amount of periosteal callus area and increased the percentage of high-density callus within that area. These findings concur with documented evidence that ultrasound upregulates the biology of the healing callus, ultimately translating to a more biomechanically competent reconstruction[30,42]. While no evidence graft revitalization was observed the –CTL group, daily LIPUS stimulation promoted robust callus development across the host/graft junctions and histomorphometric evidence of periosteal revitalization of the graft. These findings indicate that even when used as a stand-alone therapy, daily LIPUS treatment of limbs reconstructed with massive allograft may promote more extensive graft revitalization and

incorporation as well as a quicker return to mechanical stability. It can be concluded that the biologic effects of LIPUS on skeletal defect healing are similar, albeit slower since graft revitalization requires significant time, to the course of healing using the same modality for the treatment of fresh fracture and non-unions.

Though daily LIPUS administration was tolerated well by the animals used in this study, one limitation may be the small area of host/graft interface exposure to the ultrasound signal (3.88 cm^2 or approximately the size of a quarter). Rather than a unidirectional approach, future studies may utilize multiple PZT transducers that deliver separate signals simultaneously to a larger area of the host/graft junctions. Additionally, the human and small animal studies employing LIPUS to stimulate fresh fracture and non-union healing stimulated skeletal sites that were void of extensive subcutaneous tissue such as musculature, tendons, and ligaments. Ovine tibiae are surrounded by a small cuff of circumferential musculature. Given that ultrasonic energy can be easily attenuated at such low intensities, it is possible that the LIPUS signal may have been absorbed by the musculature in its path and therefore not been delivered at its full intensity to the host/ graft junctions. Despite the possibly attenuated signal delivered in this study, trends towards increased torsional properties due to significant increases in callus development and maturation were still quantified. Increasing the stimulated area may result in even more profound mechanical integrity paralleled by enhanced graft revitalization and callus maturation. A new form of LIPUS administration employs an internal, intraosseous PZT transducer[12] that can deliver the signal transcutaneoulsy and minimize signal attenuation as it passes through soft tissues. Though more invasive, this form of administration may

hold potential for healing large segmental grafts even in the distal femora of human patients where LIPUS exposure may be severely diminished if not completely attenuated by large quadriceps and hamstring muscles.

To the author's knowledge this is the second study that has evaluated the effect of a biophysical stimulus on allograft healing, and the first study to employ LIPUS. Capanna et al.[5] evaluated the effect of pulsed electromagnetic field stimulus delivered for eight hours a day in 25 patients following tumor resection and limb reconstruction with either intercalary or osteochondral allograft. The clinical and radiographic findings were compared to individuals with similar reconstructions with no PEMF stimulation. The overall host/graft junction healing rate was the same in both control and actively stimulated patients at 67% yet a positive effect was identified for PEMF therapy for those host graft junctions with a cortico-cortical contact between allograft and host bone. In the subpopulation of patients without postoperative chemotherapy, a significant improvement in healing time was seen in the PEMF stimulated group, decreasing healing time by three months relative to the control group (healing time in the active group was 6.7 months). Though the LIPUS and PEMF signals are different in nature, their effects on skeletal biology following trauma are quite similar[8, 23, 26].

One potential documented advantage of the LIPUS signal is its reported anti-osteoclastic effects[36, 39], which may have important ramifications to allograft transplantation science and healing. Attenuating osteoclastic activity while upregulating the osteogenic phenotype, especially during the first few months of healing, may maintain graft density

and integrity and potentiate a better clinical prognosis even in the presence of an aggressive immune response. Though this is the first *in vivo* study to report decreased osteoclastic response following LIPUS therapy, this study did not examine the effects of LIPUS on malignant cell types that may remain in the skeletal site following tumor resection and allograft transplantation. Though Campana et al.[5] observed no difference with respect to local or distal tumor recurrence rates in patients receiving PEMF stimulation; future studies are warranted to demonstrate the same effect of LIPUS therapy.

Seeking a means of improving bone allograft incorporation, researchers first looked to increase the cortical porosity and exposed surface area of cortical allograft so as to provide increased access to surrounding vasculature and the host of cells responsible for inducing the reparative cascade. Tarsoly et al.[14, 40] first reported considerable histological enhancement of cortical allograft incorporation after drilling numerous 1mm diameter holes perpendicular to the longitudinal axis of 20 cm canine femoral allografts. At two weeks following transplantation the perforated grafts showed considerably more vascularized granulation tissue that had penetrated the graft via the drill holes compared to contralateral, non-perforated controls. By four weeks, the holes were filled with a network of thick bone trabeculae while non-perforated controls qualitatively exhibited increased cortical resporption. At the eight-week end point of this study, the perforated grafts had nearly been completely substituted with new bone.

Additional *in vivo* animal studies performed by Lewandrowski et al.[18-20] and Gendler et al.[11] have shown that laser perforation perpendicular to the long axis of the allograft combined with partial cortical demineralization has beneficial effects with regard to allograft incorporation and remodeling, presumably by further increasing the cortical porosity relative to perforations alone. However, such surface modifications render the allograft less mechanically stable as such treatments reduce the flexural rigidity to 60% of the rigidity of original tissue[16]. In contrast, laser perforation was shown to have only minimal effects in terms of mechanical performance, but the beneficial biological response seen with partial cortical demineralization was not realized, a finding that may be attributed to the small diameter of the transverse perforations (~300 μm) as well as the method by which the perforations were created (Er:YAG laser). The actual mechanism through which partial demineralization combined with laser perforation enhanced the biologic response was not elucidated, but may be associated with an increased exposed surface area and increased porosity allowing access to surrounding vasculature.

In this study, increasing allograft porosity with longitudinal perforations extending 10mm into the graft cortex resulted in improved torsional properties relative to the negative control (ultimate torque, >15%; stiffness, >25%), though the effects of LAP alone do not appear to be as profound as daily LIPUS treatment using mechanical integrity at four months post surgery as a critical endpoint. The pattern of sixteen perforations spaced equally along the proximal and distal endplates of the intercalary graft increased the exposed surface area by approximately 20%. The mechanical findings were paralleled by significant increases in mineral apposition rates (MAR) and bone formation rates (BFR)

in the host, graft, callus and interface regions relative to the negative control. Increases in MAR and BFR in the host were attributed primarily to the perforations filling to varying degrees with new, immature bone at four months as evidenced by calcein and tetracycline uptake along the length of the perforation. Micro-CT analysis of two of the six perforated grafts revealed a lack of complete LAP filling but that perforation diameter had decreased by approximately 20% after four months *in vivo*. Extent of new bone development within the perforation appeared to be dependent on the quality of the host/graft interface and the extent of new bone development within that area of interest. The distal graft/host junction in this model was more stable and congruent than the proximal junction thus emphasized the effects of LAP treatment by clear evidence of new bone infiltration extending continuously from the host, across the interface and into the longitudinal conduit.

The proximal host/graft junctions adjacent to perforated grafts were characterized by extensive fibrovascular tissue development and lack of cortico-cortical union, a finding attributed to a lesser degree of direct cortico-cortical congruency (78%) relative to the distal junctions (90%). Nevertheless, new bone was identified on the inner surface of the proximal perforations despite a lack of cortical bridging. Therefore, increasing graft porosity with longitudinal perforations alone does not improve the degree of allograft incorporation but in combination with adequate stabilization and graft-host reduction/congruity improves graft revitalization. Future studies should examine the temporal degree of graft revitalization including perforation filling and associated allograft remodeling.

The mechanism by which LAP therapy improved graft revitalization is speculative and the results from this study are in contrast to those results employing transverse perforations reported by Lewandrowski et al. [18, 19] employing the same animal model. Following processing, cortical bone allograft loses its osteogenic capacity, but does maintain a small degree of osteoinductivity yet offers little osteoconductive advantages due to the dense cortical structure [33]. In the current study, intercalary bone allografts underwent a minimal extent of processing and no sterilization prior to implantation. It is possible a high level of graft osteoinductivity was maintained while graft osteoconductivity was improved by 20% due to the LAP treatment and may explain some of the differences between Lewandroski's studies and the present study. Given the orientation of the perforations, the exposed osteoinductive/conductive surface along the length of the LAP may have generated a small chemotactic gradient along its length that extended into the host/graft interface. This gradient may have attracted the cells and growth factors responsible for improving the osseous quality of the callus and interface relative to the negative control, ultimately translating into a more rigid construct after four months *in vivo*. A recent study has confirmed the existence of significant amounts of proteins including the BMPs in sterilized allograft matrix[44]. Combining the LAP procedure with a more rigid form of internal fixation as well as a surgical procedure that provides direct cortico-cortical contact may lead to a more favorable clinical outcome and provide a mechanical and biological environment that is most conductive to allograft incorporation and revitalization.

In the current study, longitudinal perforations were created manually along the area of the proximal and distal cortical endplates with a 500 μm drill bit. This size of perforation was chosen based on studies done by Tsuruga et al. [41]and Burchardt et al.[4] with the former quantifying the degree of bony ingrowth into porous hydroxyapaptie blocks with pore diameters ranging from 106-212 μm (smallest) to 300-400 μm (largest). These results indicated that the optimal pore size for attachment, differentiation, and growth of osteoblasts and vascularization was in the 300-400 micron range. In contrast to this study Lewandrowski et al.[18, 19] employed Er:YAG lasers to ablate the bone tissue rendering 300 μm perforations in the bony cortex. However, the first studies published implicating the effects of increased cortical porosity on allograft incorporation utilized strictly mechanical means (i.e. drill with drill bit) to produce the holes[4, 40]. Though there may be certain advantages to utilizing the Er:YAG lasers, including repeatability and precision, a purely mechanical approach offers potential advantages as well. Firstly, perforations created by drill bits may render the interior surfaces of longitudinal holes for amenable to cell adherence than those produced with laser ablation Secondly, the laser approach completely vaporizes the tissue in its path, mechanical drilling may leave deposits of morsellized bone in the tract of the bit that, when *in vivo*, may act as a stimulating conductive scaffold for bone development and revitalization of the allograft.

After four months *in vivo*, combined LIPUS and LAP therapy resulted in 25.7 and 40.4% increases in ultimate torque to failure and stiffness, respectively, relative to the negative control. These gross improvements in structural integrity were paralleled by increases in callus maturity, the extent of callus bridging and the quality of the host/graft interface as

measured histopathologically and histomorphometrically. However, the extent to which the perforations filled with new bone does not appear to be dependent upon exposure to the LIPUS signal. This finding may be attributed to the acoustic properties of bone. Relative to the acoustic properties of the surrounding soft tissues, bone has a high absorption coefficient, a high acoustic impedance and a capacity to propagate shear waves[43]. These inherent properties restrict LIPUS propagation into intact bone and therefore prevent the ultrasonic signal from interacting with the newly developing osseous tissue within the perforations. Given the high density of cortical bone and the parameters inherent to the LIPUS signal used in this study, it has been calculated that only 12% of the incident energy transmitted by the ultrasound transducers would remain after 1mm of propagation into the perforated tibiae, a distance that prevents interaction between LIPUS and LAP. Therefore, even if multiple transducers were used to stimulate an even larger area of the host/graft junctions, it seems unlikely that the combined therapies would improve the quality and extent of new bone development within the perforations. Combined therapy, instead, appears to have the most dramatic effect with regard to the maturity of the bridging callus. Though at four months LIPUS&LAP therapy shows only a small synergistic trend, future long-term studies employing both graft therapies while stimulating a larger area of the healing interface may potentiate a significant cumulative healing response.

In summary, this investigation has identified a potential new application of non-invasive LIPUS therapy as it pertains to bone allograft transplantation science and healing. Daily stimulation of the proximal and distal host/graft junctions of sheep tibiae reconstructed

with 5 cm intercalary bone allograft improved mechanical integrity of the limb by accelerating endochondral ossification within the apposing callus. Exposing only 3.88 cm^2 of the host graft interface resulted in a 27% increase in torque to failure and a 25% increase in reconstruction stiffness relative to no therapy after four months *in vivo*, and illustrates the potential role of LIPUS as a stand alone therapy for bone grafting, even in the presence of a mechanically unstable form of internal fixation. Increasing graft porosity via the introduction of longitudinal perforations 10 mm into the bony cortex also had advantageous effects in terms of mechanical stability and healing though the mechanism of such a graft therapy is unclear. The extent of reconstruction healing was not as prominent with LAP treatment as with LIPUS therapy, the perforations filled to limited degrees with new bone tissue at four months. The LAP therapy, therefore, serves as a conduit for new bone development and revitalization within the graft. Significant synergism of the two therapies in this study was not realized, though small trends were identified mechanically and histologically. Clearly, future studies are warranted to confirm the findings reported here and should include additional time points to clearly elucidate the temporal sequence of allograft healing events that result from LIPUS and/or LAP therapy.

5.2 References.

1. NIH Consensus Statement on total knee replacement December 8-10, 2003. J Bone Joint Surg Am. 86-A:1328-1335, 2004.

2. Azuma Y, Ito M, Harada Y, et al.: Low-intensity pulsed ultrasound accelerates rat femoral fracture healing by acting on the various cellular reactions in the fracture callus. J Bone Miner Res. 16(4):671-680, 2001.

3. Brostrèom LA, Nilsonne U, Nilsson OS: Survival of frozen bone allograft. Ann Chir Gynaecol. 77(2):1988.

4. Burchardt H, Busbee GA, 3rd, Enneking WF: Repair of experimental autologous grafts of cortical bone. J Bone Joint Surg Am. 57(6):814-819, 1975.

5. Capanna R, Donati D, Masetti C, et al.: Effect of electromagnetic fields on patients undergoing massive bone graft following bone tumor resection. A double blind study. Clin Orthop. 213-221, 1994.

6. Cullinane DM, Lietman SA, Inoue N, et al.: The effect of recombinant human osteogenic protein-1 (bone morphogenetic protein-7) impregnation on allografts in a canine intercalary bone defect. J Orthop Res. 20(6):1240-1245, 2002.

7. Duarte LR: The stimulation of bone growth by ultrasound. Arch Orthop Trauma Surg. 101(3):1983.

8. Eck JC, Hodges SD, Humphreys SC, University of Health Sciences CoOMKCMUSA: Techniques for stimulating spinal fusion: efficacy of electricity, ultrasound, and biologic factors in achieving fusion. Am J Orthop. 30(7):535-541, 2001.

9. Enneking WF, Campanacci DA: Retrieved human allografts: a clinicopathological study. J Bone Joint Surg Am. 83-A(7):971-986, 2001.

10. Gebhardt MC, Flugstad DI, Springfield DS, Mankin HJ: The use of bone allografts for limb salvage in high-grade extremity osteosarcoma. Clin Orthop. 1991.

11. Gendler E: Perforated demineralized bone matrix: a new form of osteoinductive biomaterial. J Biomed Mater Res. 20(6):687-697, 1986.

12. Hantes ME, Mavrodontidis AN, Zalavras CG, et al.: Low-intensity transosseous ultrasound accelerates osteotomy healing in a sheep fracture model. J Bone Joint Surg Am. 86-A:2275-2282, 2004.

13. Kokubu T, Matsui N, Fujioka H, et al.: Low intensity pulsed ultrasound exposure increases prostaglandin E2 production via the induction of cyclooxygenase-2 mRNA in mouse osteoblasts. Biochem Biophys Res Commun. 256(2):284-287, 1999.

14. Kondrai G, Tarsoly E: [On the increase of the incorporation ability of Kiel hard bone preparations]. Acta Chir Acad Sci Hung. 7:201-210, 1966.

15. Korstjens CM, Nolte PA, Burger EH, et al.: Stimulation of bone cell differentiation by low-intensity ultrasound--a histomorphometric in vitro study. J Orthop Res. 22(3):495-500, 2004.

16. Lewandrowski KU, Bonassar L, Uhthoff HK: Mechanical properties of perforated and partially demineralized bone grafts. Clin Orthop. 1998.

17. Lewandrowski KU, Rebmann V, Pèassler M, et al.: Immune response to perforated and partially demineralized bone allografts. J Orthop Sci. 6(6):2001.

18. Lewandrowski KU, Schollmeier G, Ekkemkamp A, et al.: Incorporation of perforated and demineralized cortical bone allografts. Part I: radiographic and histologic evaluation. Biomed Mater Eng. 11(3):2001.

19. Lewandrowski KU, Schollmeier G, Ekkemkamp A, et al.: Incorporation of perforated and demineralized cortical bone allografts. Part II: A mechanical and histologic evaluation. Biomed Mater Eng. 11(3):2001.

20. Lewandrowski KU, Tomford WW, Schomacker KT, et al.: Improved osteoinduction of cortical bone allografts: a study of the effects of laser perforation and partial demineralization. J Orthop Res. 15(5):748-756, 1997.

21. Mankin HJ, Gebhardt MC, Jennings LC, et al.: Long-term results of allograft replacement in the management of bone tumors. Clin Orthop. 1996.

22. Mankin HJ, Springfield DS, Gebhardt MC, Tomford WW: Current status of allografting for bone tumors. Orthopedics. 15(10):1147-1154, 1992.

23. Mooney V: A randomized double-blind prospective study of the efficacy of pulsed electromagnetic fields for interbody lumbar fusions. Spine. 21:708-712, 1990.

24. Naruse K, Mikuni-Takagaki Y, Azuma Y, et al.: Anabolic response of mouse bone-marrow-derived stromal cell clone ST2 cells to low-intensity pulsed ultrasound. Biochem Biophys Res Commun. 268(1):216-220, 2000.

25. Naruse K, Miyauchi A, Itoman M, et al.: Distinct anabolic response of osteoblast to low-intensity pulsed ultrasound. J Bone Miner Res. 18(2):360-369, 2003.

26. Nelson FR, Brighton CT, Ryaby J, et al.: Use of physical forces in bone healing. J Am Acad Orthop Surg. 11(5):344-354, 2003.

27. Nolte PA, Klein-Nulend J, Albers GH, et al.: Low-intensity ultrasound stimulates endochondral ossification in vitro. J Orthop Res. 19(2):301-307, 2001.

28. Ottolenghi CE: Massive osteo and osteo-articular bone grafts. Technic and results of 62 cases. Clin Orthop. 87:156-164, 1972.

29. Parrish FF: Allograft replacement of all or part of the end of a long bone following excision of a tumor. J Bone Joint Surg Am. 55(1):1-22, 1973.

30. Pilla AA, Mont MA, Nasser PR, et al.: Non-invasive low-intensity pulsed ultrasound accelerates bone healing in the rabbit. J Orthop Trauma. 4(3):1990.

31. Pluhar GE, Manley PA, Heiner JP, et al.: The effect of recombinant human bone morphogenetic protein-2 on femoral reconstruction with an intercalary allograft in a dog model. J Orthop Res. 19:308-317, 2001.

32. Rawool D, Goldberg B, Forsberg F, et al.: Power doppler assessment of vascular changes during fracture treatment with low -intensity ultrasound. 1998:1998.

33. Rees DC, Haddad FS, Royal National Orthopaedic Hospital SM: Bone transplantation. Hosp Med. 64(4):205-209, 2003.

34. Salkeld SL, Patron LP, Barrack RL, et al.: The effect of osteogenic protein-1 on the healing of segmental bone defects treated with autograft or allograft bone. J Bone Joint Surg Am. 83-A(6):803-816, 2001.

35. Sant'Anna EF, Leven RM, Virdi AS, Sumner DR: Effect of low intensity pulsed ultrasound and BMP-2 on rat bone marrow stromal cell gene expression. J Orthop Res. 23:646-652, 2005.

36. Sena K, Leven RM, Mazhar K, et al.: Early gene response to low-intensity pulsed ultrasound in rat osteoblastic cells. Ultrasound Med Biol. 31:703-708, 2005.

37. Stevenson S, Emery SE, Goldberg VM,: Factors affecting bone graft incorporation. Clin Orthop. 1996.

38. Stevenson S, Horowitz M: The response to bone allografts. J Bone Joint Surg Am. 74(6):939-950, 1992.

39. Sun JS, Hong RC, Chang WH, et al.: In vitro effects of low-intensity ultrasound stimulation on the bone cells. J Biomed Mater Res. 57(3):449-456, 2001.

40. Tarsoly E, Ostrowski K, Moskalewski S, et al.: Incorporation of lyophilized and radiosterilized perforated and unperforated bone grafts in dogs. Acta Chir Acad Sci Hung. 10(1):1969.

41. Tsuruga E, Takita H, Itoh H, et al.: Pore size of porous hydroxyapatite as the cell-substratum controls BMP-induced osteogenesis. J Biochem (Tokyo). 121(2):317-324, 1997.

42. Wang SJ, Lewallen DG, Bolander ME, et al.: Low intensity ultrasound treatment increases strength in a rat femoral fracture model. J Orthop Res. 12(1):40-47, 1994.

43. Warden SJ, Bennell KL, Matthews B, et al.: Efficacy of low-intensity pulsed ultrasound in the prevention of osteoporosis following spinal cord injury. Bone. 29:431-436, 2001.

44. Wildemann B, Kadow-Romacker A, Pruss A, et al.: Quantification of osteoinductive growth factors in allogenic bone grafts extracted with three different methods. Transaction of the Orthopaedic Research Society. 1736, 2006

45. Wu C, Lewallen DG, Bolander ME, et al.: Exposure to low intensity ultrasound stimulates aggrecan gene expression by cultured chondrocytes. Transaction of the Orthopaedic Research Society. 21:622, 1996.

46. Zabka AG, Pluhar GE, Edwards RB, 3rd, et al.: Histomorphometric description of allograft bone remodeling and union in a canine segmental femoral defect model: a comparison of rhBMP-2, cancellous bone graft, and absorbable collagen sponge. J Orthop Res. 19:318-327, 2001.

APPENDIX
APPENDIX I – RAW DATA

Appendix Table 1.1. Raw Structural and Mechanical Torsional Biomechanics Data.

			Structural Properties			
Sheep ID	Side	Treatment	Ultimate Torque (kN-mm)	Max. Angular Displ. (deg)	Stiffness (kN*mm/deg)	Energy Absorbed (kN*mm*deg)
L1	L	(-)CTL	19.879	40.933	0.594	406.839
L1	R	iCTL	87.466	30.389	3.103	1329.004
L2	L	(-)CTL	26.474	26.620	1.123	352.360
L2	R	iCTL	74.996	28.024	2.890	1050.839
L3	L	(-)CTL	20.675	34.049	0.679	351.973
L3	R	iCTL	81.515	20.668	4.285	842.378
*L4	L	LIPUS	12.828	17.530	0.658	112.440
*L4	R	iCTL	101.567	23.110	4.369	1173.603
L5	L	LIPUS	53.120	20.038	2.972	532.214
L5	R	iCTL	67.983	17.420	4.103	592.135
L6	L	LIPUS	30.075	35.450	0.887	533.073
L6	R	iCTL	92.356	31.270	3.372	1443.982
L7	L	LAP	33.979	15.010	2.480	255.011
L7	R	iCTL	90.726	22.760	4.224	1032.461
L8	L	LAP	19.386	45.400	0.469	440.057
L8	R	iCTL	80.476	41.900	1.795	1685.979
L9	L	LAP	39.854	25.020	1.849	498.574
L9	R	iCTL	62.525	22.060	2.656	689.653
L10	L	LIPUS+LAP	30.719	27.820	1.229	427.303
L10	R	iCTL	61.274	41.020	1.499	1256.737
L11	L	LIPUS+LAP	38.110	33.310	1.412	634.729
L11	R	iCTL	107.745	20.834	5.501	1122.378
L12	L	LIPUS+LAP	61.118	18.170	3.480	555.259
L12	R	iCTL	81.667	21.690	3.978	885.676
L13	L	(+)CTL	58.996	24.645	2.394	726.982
L13	R	iCTL	76.663	48.540	1.739	1860.621
L14	L	(+)CTL	63.241	18.170	4.465	574.544
L14	R	iCTL	56.271	15.960	3.460	449.042
L15	L	(+)CTL	69.723	18.550	3.898	646.676
L15	R	iCTL	48.311	14.110	3.268	340.835

*Animal euthanized 3 weeks prior to four-month euthanasia date due to metatarsal fracture

Appendix Table 1.1. Raw Structural and Mechanical Torsional Biomechanics Data (cont.).

			Mechanical Properties	
			Torsional	Shear Modulus
Sheep ID	Side	Treatment	Strength (N/mm^2)	(N*mm/deg)
L1	L	(-)CTL	4.123	1.059
L1	R	iCTL	60.927	23.570
L2	L	(-)CTL	5.246	1.941
L2	R	iCTL	58.369	27.399
L3	L	(-)CTL	4.227	1.289
L3	R	iCTL	57.528	32.733
*L4	L	LIPUS	3.225	1.504
*L4	R	iCTL	65.433	31.606
L5	L	LIPUS	4.730	3.256
L5	R	iCTL	47.002	30.896
L6	L	LIPUS	4.439	1.189
L6	R	iCTL	68.245	31.305
L7	L	LAP	2.167	1.139
L7	R	iCTL	71.472	43.006
L8	L	LAP	4.828	0.943
L8	R	iCTL	58.237	14.847
L9	L	LAP	2.578	0.668
L9	R	iCTL	44.233	19.538
L10	L	LIPUS+LAP	3.006	0.819
L10	R	iCTL	40.672	9.904
L11	L	LIPUS+LAP	4.226	1.291
L11	R	iCTL	61.368	30.352
L12	L	LIPUS+LAP	9.286	3.327
L12	R	iCTL	58.229	32.377
L13	L	(+)CTL	22.658	7.999
L13	R	iCTL	58.036	15.550
L14	L	(+)CTL	5.948	3.373
L14	R	iCTL	42.392	33.448
L15	L	(+)CTL	10.342	5.579
L15	R	iCTL	30.563	22.727

*Animal euthanized 3 weeks prior to four-month euthanasia date due to metatarsal fracture

Appendix Table 1.2. Raw Radiographical Callus Area as Quantified with Post-Operative Cranial/Caudal and Medial/Lateral Radiographs.

		Proximal (mm^2)				
Specimen	Treatment	Medial	Lateral	Cranial	Caudal	Total
L1	(-)CTL	101.13	220.95	84.01	184.79	590.87
L2	(-)CTL	190.63	150.84	85.09	119.80	546.36
L3	(-)CTL	97.39	261.12	84.41	186.04	628.96
*L4	LIPUS	142.64	211.22	37.38	372.05	763.28
L5	LIPUS	264.21	342.35	310.91	362.31	1279.78
L6	LIPUS	81.01	195.16	52.06	93.64	421.87
L7	LAP	137.80	629.79	235.17	343.93	1346.69
L8	LAP	34.87	155.85	65.44	123.74	379.90
L9	LAP	243.89	486.52	236.03	361.73	1328.17
L10	LIPUS+LAP	305.89	199.71	143.21	333.37	982.18
L11	LIPUS+LAP	227.71	254.68	198.13	272.34	952.86
L12	LIPUS+LAP	241.81	213.11	106.98	304.05	865.95
L13	(+)CTL	150.28	137.33	52.36	233.71	573.68
L14	(+)CTL	332.93	217.58	254.18	329.98	1134.67
L15	(+)CTL	26.57	249.51	125.73	73.63	475.44

		Distal (mm^2)				
Specimen	Treatment	Medial	Lateral	Cranial	Caudal	Total
L1	(-)CTL	42.95	252.74	61.93	172.40	530.03
L2	(-)CTL	33.58	41.09	33.71	86.14	194.52
L3	(-)CTL	101.27	321.07	74.05	263.59	759.97
*L4	LIPUS	62.34	338.05	119.76	262.65	782.80
L5	LIPUS	104.35	239.80	148.15	188.87	681.17
L6	LIPUS	120.32	361.07	137.90	115.81	735.11
L7	LAP	74.76	490.25	67.19	258.58	890.78
L8	LAP	43.36	277.58	112.68	201.06	634.67
L9	LAP	56.83	360.96	248.93	286.57	953.29
L10	LIPUS+LAP	81.19	57.91	42.15	310.36	491.60
L11	LIPUS+LAP	205.33	319.14	246.28	314.24	1084.99
L12	LIPUS+LAP	128.75	500.02	218.87	101.73	949.36
L13	(+)CTL	36.16	543.52	21.75	91.47	692.89
L14	(+)CTL	52.12	159.83	62.33	236.41	510.68
L15	(+)CTL	33.18	384.33	254.60	132.28	804.39

*Animal euthanized 3 weeks prior to four-month euthanasia date due to metatarsal fracture

Appendix Table 1.3. Raw Histopathological Data. Connectivity Scores.

			CONNECTIVITY			
Animal #	Treatment	Region	H/A Cortical Bridging	Callus Tissue Type	H/G Direct Interface	Callus (% of c.t.)
1	(-)CTL	Proximal	2.00	0.00	0.00	3.00
1	(-)CTL	Middle	1.00	2.25	0.00	1.75
1	(-)CTL	Distal	0.50	0.00	1.00	2.50
2	(-)CTL	Proximal	2.00	1.75	1.00	1.25
2	(-)CTL	Middle	0.50	1.50	0.00	0.25
2	(-)CTL	Distal	4.00	3.00	3.00	1.00
3	(-)CTL	Proximal	1.50	2.00	0.00	1.25
3	(-)CTL	Middle	0.00	0.00	0.00	0.00
3	(-)CTL	Distal	2.25	1.50	0.50	2.00
4	LIPUS	Proximal	0.00	0.75	0.00	1.50
4	LIPUS	Middle	1.00	3.00	0.00	2.25
4	LIPUS	Distal	4.00	2.25	2.00	2.50
5	LIPUS	Proximal	2.50	2.00	1.50	4.00
5	LIPUS	Middle	2.00	2.75	0.00	5.00
5	LIPUS	Distal	4.00	3.00	3.00	1.50
6	LIPUS	Proximal	0.75	0.75	0.00	1.25
6	LIPUS	Middle	0.00	1.00	0.00	1.00
6	LIPUS	Distal	2.00	0.00	0.00	2.00
7	LAP	Proximal	2.00	0.75	0.00	2.75
7	LAP	Middle	2.00	1.50	0.00	2.50
7	LAP	Distal	3.75	3.00	3.00	2.25
8	LAP	Proximal	0.50	0.00	0.00	1.25
8	LAP	Middle	1.00	1.25	0.00	1.75
8	LAP	Distal	2.00	0.00	0.00	1.50
9	LAP	Proximal	2.25	1.50	1.50	5.00
9	LAP	Middle	1.00	1.75	0.00	2.25
9	LAP	Distal	2.00	3.00	0.00	2.75
10	LIPUS+LAP	Proximal	1.25	2.25	0.00	1.50
10	LIPUS+LAP	Middle	1.00	3.00	0.00	0.50
10	LIPUS+LAP	Distal	4.00	3.00	3.00	1.25
11	LIPUS+LAP	Proximal	1.25	0.00	0.00	2.00
11	LIPUS+LAP	Middle	0.50	0.50	0.00	0.25
11	LIPUS+LAP	Distal	3.75	2.00	1.75	2.50
12	LIPUS+LAP	Proximal	2.75	1.75	1.50	2.50
12	LIPUS+LAP	Middle	2.00	3.00	0.00	3.00
12	LIPUS+LAP	Distal	3.50	1.50	3.00	4.00
13	(+)CTL	Proximal	4.00	3.00	2.50	1.25
13	(+)CTL	Middle	0.00	0.00	0.00	0.00
13	(+)CTL	Distal	4.00	3.00	3.00	0.50
14	(+)CTL	Proximal	2.25	2.25	1.25	4.75
14	(+)CTL	Middle	2.00	3.00	0.00	1.00
14	(+)CTL	Distal	4.00	3.00	3.00	1.75
15	(+)CTL	Proximal	3.75	3.00	3.00	1.00
15	(+)CTL	Middle	2.00	3.00	0.00	1.00
15	(+)CTL	Distal	3.50	3.00	3.00	2.50

Table Legend: H=host; G/A=graft

Appendix Table 1.4. Static Histomorphometry Results. Proximal and Distal Periosteal Callus Area Measurements, Callus Trabecular Thickness, and bone perimeter within specified region of interest (ROI).

Animal	Treatment	ROI		B.Area	B.Perim	PercBone	ROIarea	TrabTh
1		prox	caudal	126.028	577.036	0.627	200.986	0.218
1		prox	cranial	69.785	552.823	0.483	144.483	0.126
2		prox	caudal	26.433	393.666	0.340	77.673	0.067
2		prox	cranial	99.738	209.634	0.503	198.456	0.476
3		prox	caudal	21.826	139.778	0.646	33.784	0.156
3		prox	caudal	53.931	211.664	0.723	74.644	0.255
3		prox	cranial	7.990	111.375	0.665	12.021	0.072
3	(-)CTL	prox	cranial	13.038	63.981	0.774	16.845	0.204
1		distal	caudal	155.794	276.278	0.659	236.567	0.564
1		distal	cranial	7.360	64.776	0.458	16.083	0.114
2		distal	caudal	20.941	68.901	0.796	26.312	0.304
2		distal	cranial	24.029	52.891	0.853	28.168	0.454
3		distal	caudal	50.950	113.829	0.773	65.904	0.448
3		distal	caudal	7.859	16.556	0.919	8.554	0.475
3		distal	cranial	28.514	88.822	0.757	37.670	0.321
4		prox	caudal	76.136	215.826	0.745	102.164	0.353
4		prox	cranial	52.822	103.236	0.796	66.361	0.512
5		prox	caudal	87.106	341.797	0.684	127.264	0.255
5		prox	caudal	23.307	329.179	0.395	58.983	0.071
5		prox	cranial	161.733	387.448	0.684	236.425	0.417
5		prox	cranial	8.400	67.604	0.574	14.625	0.124
6		prox	caudal	48.574	191.635	0.676	71.815	0.253
6	LIPUS	prox	cranial	31.587	170.618	0.729	43.344	0.185
6		prox	caudal	33.399	389.693	0.461	72.404	0.086
6		prox	cranial	15.509	363.198	0.418	37.091	0.043
4		distal	caudal	167.575	199.615	0.661	253.545	0.839
4		distal	cranial	17.644	82.451	0.664	26.566	0.214
5		distal	caudal	108.605	203.267	0.669	162.343	0.534
5		distal	cranial	96.258	317.288	0.631	152.576	0.303
6		distal	caudal	57.547	191.884	0.525	109.673	0.300
6		distal	cranial	39.660	129.090	0.597	66.401	0.307

Table Legend: B.Area=bone area; B.Perim= bone perimeter; PerBone=percent bone; TrabTh=trabecular thickness

Appendix Table 1.4 (cont.). Static Histomorphometry Results. Proximal and Distal Periosteal Callus Area Measurements, Callus Trabecular Thickness, and bone perimeter within specified region of interest (ROI).

Animal	Treatment	ROI		B.Area	B.Perim	PercBone	ROIarea	TrabTh
7		prox	caudal	344.164	771.895	0.621	554.220	0.446
7		prox	cranial	54.592	540.351	0.484	112.778	0.101
8		prox	caudal	48.043	239.223	0.638	75.281	0.201
8		prox	caudal	1.656	21.434	0.494	3.351	0.077
8		prox	cranial	6.889	21.409	0.773	8.912	0.322
8		prox	cranial	11.380	172.573	0.548	20.753	0.066
9		prox	caudal	150.447	504.943	0.597	251.992	0.298
9	LAP	prox	cranial	128.737	601.608	0.438	294.109	0.214
7		distal	caudal	211.087	553.396	0.538	392.566	0.381
7		distal	cranial	45.868	257.598	0.682	67.281	0.178
8		distal	caudal	139.537	682.785	0.648	215.237	0.204
8		distal	cranial	16.445	160.890	0.679	24.209	0.102
9		distal	caudal	71.577	410.804	0.552	129.610	0.174
9		distal	cranial	33.897	86.497	0.655	51.763	0.392
9		distal	cranial	103.883	351.181	0.554	187.443	0.296
10		prox	caudal	2.259	29.026	0.503	4.489	0.078
10		prox	caudal	84.214	380.927	0.670	125.683	0.221
10		prox	cranial	36.576	233.397	0.491	74.477	0.157
10		prox	cranial	42.596	146.772	0.737	57.808	0.290
11		Prox	caudal	88.136	508.595	0.634	139.016	0.173
11		prox	cranial	55.789	320.029	0.671	83.085	0.174
12		prox	caudal	181.328	317.702	0.635	285.409	0.571
12	LIPUS+LAP	prox	cranial	67.313	286.336	0.651	103.387	0.235
10		distal	caudal	81.417	466.298	0.428	190.274	0.175
10		distal	cranial	42.379	112.388	0.759	55.820	0.377
11		distal	caudal	95.599	233.765	0.699	136.791	0.409
11		distal	cranial	27.265	223.688	0.651	41.896	0.122
11		distal	cranial	7.685	136.934	0.384	19.989	0.056
12		distal	caudal	48.979	195.201	0.577	84.826	0.251
12		distal	caudal	5.080	25.186	0.805	6.315	0.202
12		dista	cranial	118.148	337.418	0.583	202.801	0.350
13		prox	caudal	54.864	213.145	0.790	69.475	0.257
13		prox	cranial	71.587	158.905	0.787	90.981	0.450
14		prox	caudal	160.488	605.258	0.582	275.520	0.265
14		prox	cranial	124.077	265.467	0.812	152.798	0.467
15		prox	caudal	31.414	115.030	0.790	39.781	0.273
15	(+)CTL	prox	cranial	95.125	197.409	0.757	125.629	0.482
13		distal	caudal	74.882	71.137	0.883	84.777	1.053
13		distal	cranial	56.431	78.853	0.950	59.381	0.716
14		distal	caudal	41.315	157.482	0.858	48.155	0.262
14		distal	cranial	104.115	294.544	0.849	122.564	0.353
15		distal	caudal	85.777	290.279	0.608	141.179	0.295
15		distal	cranial	97.504	392.686	0.671	145.345	0.248

Table Legend: B.Area=bone area; B.Perim= bone perimeter; PerBone=percent bone; TrabTh=trabecular thickness

Appendix Table 1.5. Dynamic Histomprhometric Parameters Collected from Proximal ROIs.B31

Proximal		ROI		MS (MS/BP) AVG		SEM	MAR (um/d) AVG		SEM	BFR (MS*MAR) AVG		SEM
(-)CTL	Cranial	Host	E	0.061	±	0.041	0.000	±	0.000	0.000	±	0.042
			M	0.048		0.047	0.424		0.490	0.072		0.094
			P	0.232		0.097	0.751		0.867	0.163		0.000
			Overall	0.114		0.059	0.392		0.217	0.078		0.047
		Graft	E	0.000	±	0.000	0.000	±	0.000	0.000	±	0.000
			M	0.000		0.000	0.000		0.000	0.000		0.000
			P	0.000		0.000	0.000		0.000	0.000		0.000
			Overall	0.000		0.000	0.000		0.000	0.000		0.000
		Norm. Callus		0.048	±	0.035	0.197	±	0.334	0.038	±	0.045
		Non-Zero Only		0.102		0.027	1.770		0.248	0.169		0.105
	Caudal	Host	E	0.183	±	0.106	0.000	±	0.000	0.000	±	0.000
			M	0.259		0.055	0.578		0.392	0.107		0.074
			P	0.141		0.040	0.459		0.306	0.089		0.060
			Overall	0.194		0.035	0.345		0.176	0.065		0.033
		Graft	E	0.000	±	0.000	0.000	±	0.000	0.000	±	0.000
			M	0.000		0.000	0.000		0.000	0.000		0.000
			P	0.023		0.032	0.000		0.000	0.000		0.000
			Overall	0.008		0.008	0.000		0.000	0.000		0.000
		Norm. Callus		0.027	±	0.035	0.278	±	0.338	0.024	±	0.051
		Non-Zero Only		0.109		0.046	1.430		0.162	0.293		0.081
		Host TOTAL		0.154	±	0.050	0.369	±	0.178	0.072	±	0.037
		Graft TOTAL		0.004		0.005	0.000		0.000	0.000		0.000
		Callus TOTAL		0.105		0.003	1.600		0.139	0.231		0.051

Distal		ROI		MS (MS/BP) AVG		SEM	MAR (um/d) AVG		SEM	BFR (MS*MAR) AVG		SEM
(-)CTL	Cranial	Host	E	0.442	±	0.0915	0.3298	±	0.148	0.1524	±	0.0442
			M	0.4109		0.0883	0.1512		0.1166	0.0766		0.024
			P	0.2858		0.0916	0.0883		0.1019	0.0416		0.0754
			Overall	0.3796		0.0477	0.1898		0.0724	0.0902		0.0327
		Graft	E	0.1685	±	0.0973	0	±	0	0	±	0
			M	0.0231		0.0133	0		0	0		0
			P	0.1178		0.068	0.0223		0.0129	0.0038		0.0022
			Overall	0.1031		0.0426	0.0074		0.0074	0.0013		0.0013
		Norm. Callus		0.1605	±	0.0949	0.1921	±	0.176	0.0634	±	0.064
		Non-Zero Only		0.2465		0.0771	0.5321		0.1581	0.1756		0.0696
	Caudal	Host	E	0.3229	±	0.1283	0.1814	±	0.1244	0.046	±	0.0348
			M	0.295		0.0977	0.2029		0.167	0.0477		0.049
			P	0.1207		0.0391	0.2166		0.1453	0.0346		0.0244
			Overall	0.2462		0.0633	0.2003		0.0102	0.0428		0.0041
		Graft	E	0.1171	±	0.1309	0.1227	±	0.1735	0.0695	±	0.0983
			M	0.1757		0.1586	0		0	0		0
			P	0.1363		0.0874	0.1335		0.1217	0.0343		0.0307
			Overall	0.1431		0.0173	0.0854		0.0428	0.0346		0.0201
		Norm. Callus		0.2108	±	0.1064	0.1559	±	0.1538	0.054	±	0.0585
		Non-Zero Only		0.3036		0.082	0.5103		0.1285	0.1768		0.0634
		Host TOTAL		0.3129	±	0.0655	0.195	±	0.0463	0.0665	±	0.0257
		Graft TOTAL		0.1231		0.0317	0.0464		0.0369	0.0179		0.0165
		Callus TOTAL		0.2751		0.0233	0.5212		0.0089	0.1762		0.0005

Appendix Table 1.5 (cont.). Dynamic Histomprhometric Parameters Collected from Proximal ROIs.

Proximal		ROI		MS (MS/BP) AVG		MS (MS/BP) SEM	MAR (um/d) AVG		MAR (um/d) SEM	BFR (MS*MAR) AVG		BFR (MS*MAR) SEM
LIPUS	Cranial	Host	E	0.184		0.088	0.442		0.510	0.147		0.245
			M	0.165	±	0.111	1.241	±	0.955	0.424	±	0.292
			P	0.210		0.092	1.563		1.062	0.505		0.143
			Overall	0.186		0.013	1.082		0.333	0.359		0.108
		Graft	E	0.177		0.102	1.552		0.896	0.416		0.240
			M	0.244	±	0.141	0.813	±	0.469	0.388	±	0.224
			P	0.010		0.006	0.430		0.248	0.013		0.007
			Overall	0.144		0.070	0.932		0.329	0.272		0.130
			Norm. Callus	0.143	±	0.064	1.571	±	0.790	0.299	±	0.202
			Non-Zero Only	0.163		0.061	2.408		0.471	0.449		0.196
	Caudal	Host	E	0.268		0.110	1.760		1.175	0.557		0.376
			M	0.379	±	0.111	0.347	±	0.400	0.059	±	0.069
			P	0.151		0.026	1.316		1.003	0.218		0.156
			Overall	0.266		0.066	1.141		0.417	0.278		0.147
		Graft	E	0.159		0.144	0.956		0.855	0.441		0.423
			M	0.251	±	0.247	0.729	±	0.658	0.409	±	0.489
			P	0.090		0.083	0.820		0.736	0.224		0.210
			Overall	0.167		0.047	0.835		0.066	0.358		0.068
			Norm. Callus	0.141	±	0.157	1.382	±	0.690	0.320	±	0.188
			Non-Zero Only	0.201		0.053	2.233		0.365	0.466		0.172
		Host TOTAL		0.226		0.049	1.111		0.338	0.318		0.118
		Graft TOTAL		0.155	±	0.054	0.883	±	0.215	0.315	±	0.097
		Callus TOTAL		0.182		0.015	2.321		0.071	0.457		0.007

Distal		ROI		MS (MS/BP) AVG		MS (MS/BP) SEM	MAR (um/d) AVG		MAR (um/d) SEM	BFR (MS*MAR) AVG		BFR (MS*MAR) SEM
LIPUS	Cranial	Host	E	0.1866		0.047	1.1848		0.7967	0.1572		0.0435
			M	0.4238	±	0.0643	0.2483	±	0.2867	0.0754	±	0.0841
			P	0.4151		0.0835	0.4327		0.4996	0.1456		0.0652
			Overall	0.3418		0.0777	0.6219		0.2864	0.1261		0.0256
		Graft	E	0.1942		0.1121	0.4385		0.2532	0.1348		0.0778
			M	0.1954	±	0.1128	0.3814	±	0.2202	0.1599	±	0.0923
			P	0.2415		0.1395	0.7248		0.4184	0.345		0.1992
			Overall	0.2104		0.0156	0.5149		0.1062	0.2132		0.0663
			Norm. Callus	0.0934	±	0.047	0.6687	±	0.5834	0.1004	±	0.0928
			Non-Zero Only	0.1293		0	2.0501		0	0.3013		0
	Caudal	Host	E	0.1949		0.0462	0.3585		0.4139	0.0959		0.1107
			M	0.429	±	0.0767	0.5181	±	0.5983	0.2689	±	0.3105
			P	0.2669		0.0365	0.3774		0.4358	0.1318		0.1521
			Overall	0.2969		0.0692	0.418		0.0504	0.1655		0.0527
		Graft	E	0.1765		0.0584	0.6394		0.7154	0.0905		0.0853
			M	0.0783	±	0.0423	0.2952	±	0.4175	0.0567	±	0.0802
			P	0.1601		0.1013	0.8637		0.5651	0.2802		0.1987
			Overall	0.1383		0.0304	0.5994		0.1653	0.1425		0.0695
			Norm. Callus	0.1265	±	0.0557	0.9091	±	0.6142	0.1702	±	0.1337
			Non-Zero Only	0.1686		0.0414	1.9252		0.3638	0.3713		0.1164
		Host TOTAL		0.3194		0.0673	0.52		0.1949	0.1458		0.0391
		Graft TOTAL		0.1743	±	0.0314	0.5572	±	0.1271	0.1779	±	0.0648
		Callus TOTAL		0.1489		0.0161	1.9877		0.051	0.3363		0.0286

Appendix Table 1.5(cont.). Dynamic Histomprhometric Parameters Collected from Proximal ROIs.

Proximal		ROI		MS (MS/BP) AVG		MS (MS/BP) SEM	MAR (um/d) AVG		MAR (um/d) SEM	BFR (MS*MAR) AVG		BFR (MS*MAR) SEM
LAP	Cranial	Host	E	0.222		0.083	1.239		0.807	0.372		0.256
			M	0.115	±	0.074	0.729	±	0.557	0.149	±	0.137
			P	0.036		0.029	0.729		0.434	0.031		0.043
			Overall	0.124		0.054	0.899		0.170	0.173		0.100
		Graft	E	0.190		0.151	0.337		0.386	0.201		0.234
			M	0.232	±	0.198	0.586	±	0.531	0.385	±	0.348
			P	0.070		0.053	0.734		0.678	0.092		0.086
			Overall	0.164		0.049	0.552		0.116	0.226		0.085
		Norm. Callus		0.085	±	0.053	1.187	±	0.768	0.180	±	0.148
		Non-Zero Only		0.134		0.049	2.467		0.405	0.374		0.151
	Caudal	Host	E	0.350		0.169	1.197		0.758	0.697		0.448
			M	0.265	±	0.089	1.123	±	0.785	0.435	±	0.310
			P	0.224		0.087	1.696		0.770	0.534		0.264
			Overall	0.280		0.037	1.339		0.180	0.555		0.077
		Graft	E	0.000		0.000	0.000		0.000	0.000		0.000
			M	0.015	±	0.025	0.161	±	0.279	0.021	±	0.037
			P	0.020		0.020	0.000		0.000	0.000		0.000
			Overall	0.012		0.006	0.054		0.054	0.007		0.007
		Norm. Callus		0.164	±	0.062	1.714	±	0.879	0.355	±	0.202
		Non-Zero Only		0.204		0.045	2.723		0.545	0.580		0.149
		Host TOTAL		0.202		0.064	1.119		0.209	0.370		0.142
		Graft TOTAL		0.088	±	0.057	0.303	±	0.177	0.116	±	0.088
		Callus TOTAL		0.169		0.029	2.595		0.105	0.477		0.084

Distal		ROI		MS (MS/BP) AVG		MS (MS/BP) SEM	MAR (um/d) AVG		MAR (um/d) SEM	BFR (MS*MAR) AVG		BFR (MS*MAR) SEM
LAP	Cranial	Host	E	0.3547		0.1788	1.2511		0.6609	0.5299		0.5423
			M	0.4562	±	0.0719	1.2164	±	0.4905	0.5572	±	0.2632
			P	0.4167		0.0728	1.1515		0.3523	0.3093		0.1475
			Overall	0.4092		0.0295	1.2063		0.0292	0.4655		0.0785
		Graft	E	0.1053		0.0781	0		0	0		0
			M	0.1773	±	0.1025	0.6697	±	0.7673	0.1236	±	0.1416
			P	0.2722		0.0874	0.6477		0.5785	0.1753		0.1695
			Overall	0.1849		0.0484	0.4391		0.2196	0.0996		0.052
		Norm. Callus		0.1789	±	0.1119	0.8383	±	0.5692	0.2238	±	0.1838
		Non-Zero Only		0.276		0.1016	1.8862		0.2431	0.5035		0.1698
	Caudal	Host	E	0.3618		0.1588	0.3819		0.3465	0.1423		0.1276
			M	0.5351	±	0.0964	0.7001	±	0.4436	0.4356	±	0.285
			P	0.3765		0.0405	0.6914		0.4414	0.2662		0.1712
			Overall	0.4245		0.0555	0.5911		0.1047	0.2814		0.085
		Graft	E	0.2016		0.1377	0.2161		0.3743	0.0982		0.1701
			M	0.0927	±	0.0752	0.2329	±	0.4033	0.0452	±	0.0783
			P	0.2628		0.0911	0.4823		0.5834	0.1976		0.2318
			Overall	0.1857		0.0498	0.3104		0.0861	0.1137		0.0447
		Norm. Callus		0.2509	±	0.0766	1.2301	±	0.6637	0.3476	±	0.1903
		Non-Zero Only		0.2765		0.0638	2.2141		0.2318	0.5542		0.1301
		Host TOTAL		0.4168		0.0401	0.8987		0.2063	0.3734		0.0935
		Graft TOTAL		0.1853	±	0.0439	0.3748	±	0.1547	0.1066	±	0.0436
		Callus TOTAL		0.2763		0.0002	2.0502		0.1339	0.5288		0.0207

Appendix Table 1.5(cont.). Dynamic Histomprhometric Parameters Collected from Proximal ROIs.

Proximal		ROI		MS (MS/BP) AVG		SEM	MAR (um/d) AVG		SEM	BFR (MS*MAR) AVG		SEM
LIPUS+LAP	Cranial	Host	E	0.165	±	0.109	0.594	±	0.533	0.140	±	0.134
			M	0.305		0.178	0.678		0.637	0.375		0.292
			P	0.282		0.169	0.386		0.502	0.209		0.138
			Overall	0.251		0.043	0.553		0.087	0.241		0.070
		Graft	E	0.051	±	0.048	0.969	±	1.110	0.126	±	0.191
			M	0.165		0.137	0.742		0.850	0.383		0.445
			P	0.240		0.155	1.463		0.844	0.650		0.441
			Overall	0.152		0.055	1.058		0.213	0.386		0.151
			Norm. Callus	0.144	±	0.078	1.064	±	0.725	0.232	±	0.184
			Non-Zero Only	0.211		0.065	2.395		0.321	0.531		0.154
	Caudal	Host	E	0.296	±	0.171	0.767	±	0.702	0.490	±	0.449
			M	0.165		0.099	0.000		0.000	0.000		0.000
			P	0.199		0.184	0.909		0.583	0.330		0.279
			Overall	0.220		0.039	0.559		0.282	0.273		0.144
		Graft	E	0.090	±	0.107	0.000	±	0.000	0.000	±	0.000
			M	0.100		0.104	0.307		0.532	0.172		0.298
			P	0.171		0.100	0.692		0.805	0.212		0.252
			Overall	0.120		0.026	0.333		0.200	0.128		0.065
			Norm. Callus	0.218	±	0.103	1.521	±	0.637	0.442	±	0.294
			Non-Zero Only	0.268		0.093	2.249		0.265	0.642		0.291
		Host TOTAL		0.236		0.038	0.556		0.187	0.257		0.102
		Graft TOTAL		0.136	±	0.040	0.696	±	0.294	0.257	±	0.132
		Callus TOTAL		0.239		0.023	2.322		0.060	0.586		0.045

Distal		ROI		MS (MS/BP) AVG		SEM	MAR (um/d) AVG		SEM	BFR (MS*MAR) AVG		SEM
LIPUS+LAP	Cranial	Host	E	0.4541	±	0.1428	0	±	0	0	±	0
			M	0.3927		0.0709	0.45		0.4374	0.4133		0.2054
			P	0.3544		0.0932	0.5744		0.5596	0.3041		0.2973
			Overall	0.4004		0.029	0.3415		0.1745	0.2391		0.1236
		Graft	E	0.3637	±	0.1523	0.4236	±	0.504	0.1153	±	0.1476
			M	0.3086		0.1239	0.3817		0.4374	0.0956		0.1127
			P	0.3069		0.1387	0.6269		0.5437	0.1812		0.1619
			Overall	0.3264		0.0187	0.4774		0.0757	0.1307		0.0259
			Norm. Callus	0.2019	±	0.1293	0.5257	±	0.5302	0.1887	±	0.2206
			Non-Zero Only	0.3893		0.0871	2.0276		0.2301	0.7277		0.24
	Caudal	Host	E	0.4922	±	0.1439	0.3008	±	0.4254	0.0803	±	0.1135
			M	0.3845		0.0684	1.0794		0.5069	0.4554		0.2187
			P	0.3727		0.1162	0.2845		0.4024	0.1588		0.2246
			Overall	0.4165		0.038	0.5549		0.2623	0.2315		0.1142
		Graft	E	0.2418	±	0.1581	0.5714	±	0.5225	0.0919	±	0.1035
			M	0.2843		0.1221	0.2655		0.4598	0.0648		0.1122
			P	0.2024		0.0946	0.1553		0.269	0.0635		0.11
			Overall	0.2428		0.0237	0.3307		0.1245	0.0734		0.0093
			Norm. Callus	0.1645	±	0.1205	0.6014	±	0.5377	0.1865	±	0.2073
			Non-Zero Only	0.3101		0.1131	1.9104		0.2687	0.5925		0.239
		Host TOTAL		0.4084		0.0307	0.4482		0.2104	0.2353		0.1065
		Graft TOTAL		0.2846	±	0.0326	0.4041	±	0.1032	0.102	±	0.0251
		Callus TOTAL		0.3497		0.0323	1.969		0.0479	0.6601		0.0552

Appendix Table 1.5(cont.). Dynamic Histomprhometric Parameters Collected from Proximal ROIs.

Proximal		ROI		MS (MS/BP) AVG		SEM	MAR (um/d) AVG		SEM	BFR (MS*MAR) AVG		SEM
(+)CTL	Cranial	Host	E	0.350		0.135	1.374		0.726	0.698		0.408
			M	0.109	±	0.124	0.629	±	0.326	0.124	±	0.175
			P	0.160		0.157	0.399		0.000	0.000		0.000
		Overall		0.206		0.073	0.801		0.294	0.274		0.215
		Graft	E	0.129		0.066	0.000		0.000	0.000		0.000
			M	0.058	±	0.054	0.286	±	0.496	0.073	±	0.126
			P	0.255		0.144	0.990		0.765	0.417		0.297
		Overall		0.147		0.057	0.425		0.294	0.163		0.129
		Norm. Callus		0.239	±	0.085	1.229	±	0.601	0.374	±	0.209
		Non-Zero Only		0.264		0.076	2.034		0.229	0.613		0.148
	Caudal	Host	E	0.197		0.089	1.133		0.725	0.337		0.216
			M	0.300	±	0.167	1.201	±	0.768	0.675	±	0.451
			P	0.676		0.085	1.988		0.355	1.300		0.191
		Overall		0.391		0.146	1.441		0.274	0.771		0.282
		Graft	E	0.121		0.114	0.272		0.471	0.135		0.233
			M	0.275	±	0.208	0.414	±	0.477	0.330	±	0.387
			P	0.200		0.092	0.188		0.325	0.060		0.104
		Overall		0.199		0.044	0.291		0.066	0.175		0.081
		Norm. Callus		0.154	±	0.083	0.829	±	0.601	0.219	±	0.185
		Non-Zero Only		0.224		0.068	2.034		0.234	0.537		0.164
		Host TOTAL		0.299		0.119	1.121		0.325	0.522		0.274
		Graft TOTAL		0.173	±	0.049	0.358	±	0.195	0.169	±	0.096
		Callus TOTAL		0.244		0.016	2.034		0.000	0.575		0.031

Distal		ROI		MS (MS/BP) AVG		SEM	MAR (um/d) AVG		SEM	BFR (MS*MAR) AVG		SEM
(+)CTL	Cranial	Host	E	0.2413		0.0549	0.4967		0.497	0.1781		0.1897
			M	0.4195	±	0.1012	1.0746	±	0.483	0.3593	±	0.1898
			P	0.3316		0.1135	1.3894		0.2737	0.4549		0.2379
		Overall		0.3308		0.0514	0.9869		0.2614	0.3307		0.0812
		Graft	E	0.2763		0.0845	0.6182		0.5422	0.2155		0.2135
			M	0.4098	±	0.0989	0.9144	±	0.5292	0.3706	±	0.2285
			P	0.3521		0.0488	1.3645		0.3065	0.4705		0.1317
		Overall		0.3461		0.0387	0.9657		0.217	0.3522		0.0742
		Norm. Callus		0.1663	±	0.0674	0.9334	±	0.5481	0.2196	±	0.1421
		Non-Zero Only		0.2041		0.0545	1.8114		0.218	0.4089		0.1072
	Caudal	Host	E	0.3214		0.0799	0.5524		0.4942	0.2311		0.2134
			M	0.3511	±	0.0718	0.4093	±	0.3741	0.1837	±	0.1721
			P	0.2685		0.123	0.2693		0.3809	0.0286		0.0405
		Overall		0.3137		0.0241	0.4104		0.0817	0.1478		0.0611
		Graft	E	0.1223		0.106	0.3608		0.4158	0.1342		0.1553
			M	0.4693	±	0.0874	0.7214	±	0.5268	0.3462	±	0.2465
			P	0.3418		0.0611	1.4979		0.575	0.4581		0.1753
		Overall		0.3111		0.1013	0.86		0.3355	0.3128		0.095
		Norm. Callus		0.1561	±	0.0759	1.1478	±	0.6087	0.248	±	0.1492
		Non-Zero Only		0.2134		0.0624	1.9369		0.3279	0.4321		0.1092
		Host TOTAL		0.3222		0.0363	0.6986		0.2515	0.2393		0.0865
		Graft TOTAL		0.3286	±	0.0695	0.9129	±	0.2549	0.3325	±	0.0772
		Callus TOTAL		0.2088		0.0038	1.8742		0.0513	0.4205		0.0094

Appendix Table 1.6. Uniaxial Compression Data Evaluating the Effects of LAP on Graft Structural Properties.

ID	Compressive Force at Failure (kN)	Displacment At Failure (mm)	% Strain At Failure (%)	% Diff Failure Force (%)	% Diff Failure Strain (%)
1_iCTL	x	x	x	..	..
1_LAP	20.890	0.569	1.053		
2_iCTL	19.136	0.451	0.852	-26.66	1.64
2_LAP	24.236	0.427	0.838		
3_iCTL	22.348	0.445	0.889	49.09	-48.84
3_LAP	11.378	0.662	1.272		
4_iCTL	23.926	0.472	0.925	11.60	4.36
4_LAP	21.152	0.451	0.885		
5_iCTL	22.875	0.507	0.993	36.31	-4.69
5_LAP	14.569	0.530	1.061		
6_iCTL	23.640	0.534	1.068	16.34	1.95
6_LAP	19.777	0.524	1.027		
7_iCTL	21.538	0.582	1.142	-1.95	4.73
7_LAP	21.958	0.555	1.110		
8_iCTL	23.971	0.462	0.924	12.35	-16.42
8_LAP	21.010	0.538	1.075		
9_iCTL	17.299	0.472	0.891	41.34	-41.60
9_LAP	10.147	0.669	1.286		
10_iCTL	16.185	0.445	0.855	-23.29	-17.83
10_LAP	19.956	0.524	1.007		
11_iCTL	16.334	0.507	0.844	10.02	9.41
11_LAP	14.697	0.459	0.778		
13_iCTL	10.709	0.420	0.779	-47.47	-11.47
13_LAP	15.793	0.469	0.884		
14_iCTL	7.442	0.507	0.956	-64.47	19.73
14_LAP	12.239	0.407	0.767		

Appendix Table 1.7. Diametral Compression Summary: Ultimate Force to Failure, Stiffness, and Displacement at Failure

			Diameter (mm)		Failure		Stiffness		Max	
Specimen	Trt	Width	$\phi_{\perp}$	$\phi_{\parallel}$	Load (N)	%Diff	(N/mm)	%Diff	Displ. (mm)	%Diff
DC1	iCTL	5.34	22.87	22.15	299.201	22.63	676.976	3.08	0.434	22.12
DC1	LAP	5.79	22.07	21.73	231.479		656.149		0.338	
DC2	iCTL	4.73	22.25	21.96	257.671	10.83	677.888	11.48	0.386	5.44
DC2	LAP	4.68	21.93	21.5	229.755		600.047		0.365	
DC3	iCTL	4.8	22.25	21.18	274.903	3.20	643.878	-3.11	0.448	17.63
DC3	LAP	4.61	21.23	21.92	266.115		663.882		0.369	
DC4	iCTL	4.67	21.07	21.13	281.624	-1.84	697.307	26.91	0.365	-53.97
DC4	LAP	4.71	20.78	20.96	286.794		509.655		0.562	
DC5	iCTL	5.14	21.03	21.06	265.77	3.63	601.801	2.48	0.414	0.56
DC5	LAP	4.64	20.88	20.56	256.12		586.888		0.4117	
DC6	iCTL	4.74	22.07	21.01	299.028	18.84	731.636	-3.18	0.403	33.25
DC6	LAP	5.55	21.77	21.09	242.679		754.92		0.269	
DC7	iCTL	4.67	21.64	21.29	254.914	1.82	682.311	22.44	0.358	-57.82
DC7	LAP	4.73	22.01	21.07	250.263		529.207		0.565	
DC8	iCTL	4.65	22	20.99	227.343	15.61	432.592	-19.16	0.5824	40.93
DC8	LAP	4.66	22.7	21.16	191.845		515.472		0.344	
DC1	iCTL	4.82	22.25	21.99	203.39	10.00	355.889	4.56	0.589	27.50
DC1	LAP	5.2	22.38	22.25	183.056		339.661		0.427	
DC2	iCTL	5.52	22.16	21.62	307.472	13.67	642.792	43.15	0.465	-16.34
DC2	LAP	4.84	21.57	21.08	265.45		365.445		0.541	
DC3	iCTL	5.32	21.06	22.33	322.464	14.10	498.327	-15.40	0.424	-26.89
DC3	LAP	5.18	21.08	21.56	277.012		575.045		0.538	
DC4	iCTL	5.27	21.39	22.5	275.076	10.02	527.969	-6.50	0.431	-32.02
DC4	LAP	5.01	21.73	21.35	247.504		562.278		0.569	
DC5	iCTL	5.59	21.39	22.9	286.104	20.22	462.735	-12.44	0.42	-39.52
DC5	LAP	4.59	21.75	21.37	228.256		520.279		0.586	
DC6	iCTL	5.25	22.45	21.6	231.651	17.78	462.846	21.89	0.534	15.54
DC6	LAP	5.45	21.65	21.49	190.466		361.522		0.451	
DC7	iCTL	5.23	22.22	21.56	281.969	23.41	494.48		0.524	100.00
DC7	LAP	4.78	22.42	21.51	215.97					
DC8	iCTL	4.84	23.31	21.87	175.891	-25.14	183.674	-135.27	0.431	-99.07
DC8	LAP	5.27	22.37	21.64	220.105		432.123		0.858	
DC1	iCTL	5.15	24.62	24.44	283.175	28.60	366.925	-32.48	0.469	23.67
DC1	LAP	4.99	23.86	23.73	202.184		486.108		0.358	
DC2	iCTL	5.1	24.35	23.7	261.635	14.29	484.804	-5.61	0.476	17.44
DC2	LAP	5.38	23.31	23.34	224.241		511.997		0.393	
DC3	iCTL	5.66	22.98	23.78	250.089	18.26	489.802	21.43	0.479	-1.46
DC3	LAP	4.71	23.83	22.73	204.424		384.813		0.486	
DC4	iCTL	4.58	23.97	22.94	243.196	11.00	460.036	13.59	0.551	28.68
DC4	LAP	4.86	23.8	22.75	216.435		397.531		0.393	
DC5	iCTL	5.17	23.29	22.6	167.548	-7.92	474.743	59.63	0.324	-74.38
DC5	LAP	5.34	23.5	22.33	180.816		191.637		0.565	
DC6	iCTL	5.1	23.32	22.5	167.375	-10.81	323.938	4.10	0.376	-33.78
DC6	LAP	5.19	24.4	22.27	185.469		310.663		0.503	
DC7	iCTL	4.87	23.52	22.02	146.524	-25.76	417.121	-24.18	0.283	1.41
DC7	LAP	5.69	23.7	21.91	184.263		517.989		0.279	
DC8	iCTL	5.03	24.53	21.78	166.514	13.04	344.981	52.85	0.42	-11.67
DC8	LAP	5.57	24.91	21.87	144.801		162.644		0.469	

Appendix Table 1.8. Diametral Compression Summary Data. TAP vs. iCTL

Trt	Ring Width	Diameter (mm) $\phi_{\perp}$	Diameter (mm) ϕ_{II}	Failure Load (N)	%Diff	Stiffness (N/mm)	%Diff	Max Displ. (mm)	%Diff
iCTL	4.96	24.2	22.78	137.391	18.31	202.79	-23.29	0.572	30.77
TAP	4.85	23.68	22.27	112.233		250.02		0.396	
iCTL	4.6	23.94	22.59	138.598	28.99	192.37	.	0.669	.
TAP	4.98	23.94	22.97	98.423		.		.	
iCTL	4.62	23.24	22.63	136.702	12.23	251.96	9.45	0.489	6.34
TAP	4.79	23.24	22.35	119.987		228.14		0.458	
iCTL	4.75	23.25	22.13	124.812	7.59	219.70	-12.54	0.438	10.27
TAP	4.48	23.25	22.3	115.334		247.24		0.393	
iCTL	4.8	23.35	22.05	118.436	8.79	232.04	-0.74	0.451	-6.21
TAP	4.94	23.25	22.15	108.029		233.76		0.479	
iCTL	5.26	23.68	22.14	156.174	47.00	263.66	39.00	0.527	13.09
TAP	4.22	23.68	22.17	82.766		160.82		0.458	
iCTL	3.96	24.31	21.85	112.405	10.58	201.52	10.90	0.499	4.01
TAP	4.55	24.31	22.15	100.515		179.56		0.479	
iCTL	5.42	24.83	21.83	109.993	13.00	195.78	19.64	0.499	-8.42
TAP	4.56	24.83	22.24	95.689		157.33		0.541	
iCTL	5	23.8	21.8	150.143	22.84	240.10	15.81	0.510	-6.09
TAP	5	24	22.1	115.851		202.13		0.541	
iCTL	4.83	22.8	20.9	115.679	2.23	212.52	-9.33	0.527	20.26
TAP	5	23.2	22.2	113.094		232.34		0.420	
iCTL	4.94	22.4	21.1	106.546	-27.50	227.20	-13.85	0.434	-8.73
TAP	5.15	23.4	21.4	135.841		258.67		0.472	
iCTL	4.66	23	20.6	112.06	0.92	215.23	-6.44	0.407	-15.25
TAP	4.91	22.9	20.9	111.026		229.10		0.469	
iCTL	4.88	23.4	20.9	145.146	0.71	237.33	-28.92	0.572	22.89
TAP	5.8	22.9	20.8	144.112		305.96		0.441	
iCTL	5.81	23.2	20.8	186.503	34.00	292.20	23.30	0.531	-0.01
TAP	4.96	22.8	21.1	123.089		224.11		0.531	
iCTL	5.8	24	21	189.777	27.51	309.02	14.86	0.559	6.96
TAP	5.05	23.8	21.1	137.564		263.12		0.520	
iCTL	5.15	25	21.1	147.731	-6.18	207.29	-37.84	0.571	4.64
TAP	5.55	25.1	21.2	156.864		285.74		0.544	

Appendix Table 1.9. Diametral Compression Summary Data. LAP vs.TAP

Trt	Ring Width (mm)	Diameter (mm) $\phi_{\perp}$	Diameter (mm) $\phi_{\parallel}$	Failure Load (N)	%Diff	Stiffness (N/mm)	%Diff	Max Displ. (mm)	%Diff
LAP	5	24.6	24	259.739	-3.91	369.735	-8.67	0.706	0.98
TAP	5.8	25	23.6	269.906		401.786		0.700	
LAP	4.98	25	24	186.848	-10.61	370.647	29.65	0.462	-63.43
TAP	4.7	22.9	21.9	206.664		260.735		0.755	
LAP	4.98	25.2	23.2	253.019	15.94	365.085	2.33	0.713	15.94
TAP	4.8	24.8	23.9	212.696		356.585		0.600	
LAP	4.89	25.1	23	249.400	12.71	306.765	17.72	0.806	16.67
TAP	5	24.6	23.7	217.693		252.420		0.672	
LAP	4.865	25.1	23	221.829	-12.51	304.569	-18.79	0.665	-5.18
TAP	4.9	26	22.9	249.572		361.793		0.700	
LAP	5	25	23.3	228.549	-11.84	330.383	2.11	0.662	-16.67
TAP	4.9	25.8	24.75	255.603		323.398		0.772	
LAP	4.75	26	23	198.221	-32.77	292.931	-31.51	0.665	-6.74
TAP	5	25.9	23.8	263.186		385.237		0.710	
LAP	4.89	23.6	25.9	182.884	-25.82	263.938	1.49	0.837	6.96
TAP	4.96	22.8	22.7	230.100		260.000		0.779	
LAP	5	24.2	22.7	111.026	-56.34	184.836	-43.75	0.779	12.39
TAP	5	23	21	173.579		265.701		0.682	
LAP	5.2	24.6	22	136.875	-35.38	286.128	-59.56	0.603	37.14
TAP	5.1	23.4	20.5	185.297		456.557		0.379	
LAP	4.89	23.4	21.6	164.274	16.05	232.777	-25.46	0.689	34.00
TAP	5	23	21	137.908		292.044		0.455	
LAP	5.05	23.8	21.2	147.214	-7.96	291.035	-18.59	0.689	39.50
TAP	4.95	22.9	20.9	158.932		345.136		0.417	
LAP	5	24	20.8	176.863	17.74	323.961	-22.49	0.841	55.33
TAP	5	24.3	20.5	145.491		396.826		0.376	
LAP	5.1	24.1	20.7	154.968	18.13	229.661	-22.15	0.600	15.52
TAP	5	24.6	20.2	126.880		280.530		0.507	
LAP	4.9	23.5	20.8	94.139	-12.45	154.642	-14.47	0.520	-19.21
TAP	5	23.8	20.4	105.857		177.014		0.620	
LAP	5.2	24.9	20.8	107.063	-10.30	190.337	-6.94	0.555	9.32
TAP	4.8	23.3	21.3	118.092		203.556		0.503	

APPENDIX II - 1 SCORING SYSTEM FOR DECALCIFIED HISTOLOGICAL ANALYSIS: Semi-quantitative decalcified histological scoring of the proximal host/graft junctions and the distal host/graft junctions was divided into three primary categories: Connectivity, which included parameters such as the degree of osseous host to graft bridging and the quality and quantity (measured as a % relative to the cortical thickness) of the callus that bridged the two, as well as the osseous quality (or lack thereof) of the interface at the host/allograft junction; Osteoblast/Osteoclast continuum to quantify the degree of osteoclastic resorption, if any, followed by new bone deposition by osteoblasts, if any, in both the host and the graft. This allowed quantification of treatment effects on local metabolic activity in the host and allograft tissue; and a final graft revitalization category that quantified the degree of graft neovascularization as well as any indication of an inflammatory response elicited against the graft. The latter was evaluated by the graduate student in charge of this project and also independently by two board certified pathologists: Dr. E.J. Ehrhart, an oncological pathologist, and Dr. Robert Norrdin, a bone pathologist. The detailed scoring system is provided below for reference.

SCORE	CONNECTIVITY			
	Host - Allograft Cortical Bridging	Callus Tissue Type	Host/Graft Direct Interface	Callus (% of c.t.)
0	No Bridging	Fibrous/pseudoarthrosis	Fibrous/pseudoarthrosis	None
1	Bridging callus on 1 side	Cartilage	Cartilage	50%
2	Bridging callus on 2 sides	Endochondral ossification	Endochondral ossification	100%
3	Bridging callus and cortex on 1 side	Bone	Bone	150%
4	Bridging callus and cortex on 2 sides			200%
5				>200%
6				

SCORE	Ob/Oc CONTINUUM	
	Host	Allograft
0	No Oc Resporption	No Oc Resporption
1	Extensive Oc Resorption / No Ob	Extensive Oc Resorption / No Ob
2	Some Oc Resorption / No Ob	Some Oc Resorption / No Ob
3	Extensive Oc Resorption / Some Ob	Extensive Oc Resorption / Some Ob
4	Some Oc Resorption/Some Oc	Some Oc Resorption/Some Oc
5	Some Oc Resorption / Extensive Ob	Some Oc Resorption / Extensive Ob
6	Extensive Oc Resorption / Extensive Ob	Extensive Oc Resorption / Extensive Ob

SCORE	GRAFT REVITALIZATION	
	Allograft Vascularity	Live Cells Present In Allograft
0	None	NO
1	Some	YES
2	Moderate	
3	Prolific	
4		
5		
6		

APPENDIX III – CALCULATING DYNAMIC HISTOMORPHOMETRIC PARAMETERS FROM STATIC MEASUREMENTS: Fluorochrome labels were intravenously administered to all sheep three days (tetracycline at 30 mg/kg IV) and 14 days (calcein green at 20 mg/kg IV) prior to euthanasia. Fluorochrome labels are taken up into actively mineralizing bone matrix and allow for easy detection of allograft turnover and active bone remodeling. Dynamic histomorphometry provides a means to compare the rates and progression of bone healing between groups. This labeling protocol has been used previously by the investigators and has provided excellent sequential information in longitudinal studies of bone healing and remodeling. The American Society of Bone and Mineral Research developed the following definitions of the relevant dynamic parameters pertinent to this research. Figure A3.1 below describes the measurement of these parameters.

Mineralized Surface (MS) – defined as the sum of lengths of single calcein and tetracycline labels as well as the sum of the length of double label normalized to the bone surface perimeter in that particular region of interest; the latter is quantified in stained histomorphometric images this parameter is unitless.

Mineral Apposition Rate (MAR) – calculated as the average distance between the 1st and second fluorescent markers divided by the time between label administration (in this research, Δt=11 days); results are expressed in μm/day.

Bone Formation Rate (BFR) – calculated as the product of MS and MAR; results are expressed in μm/day.

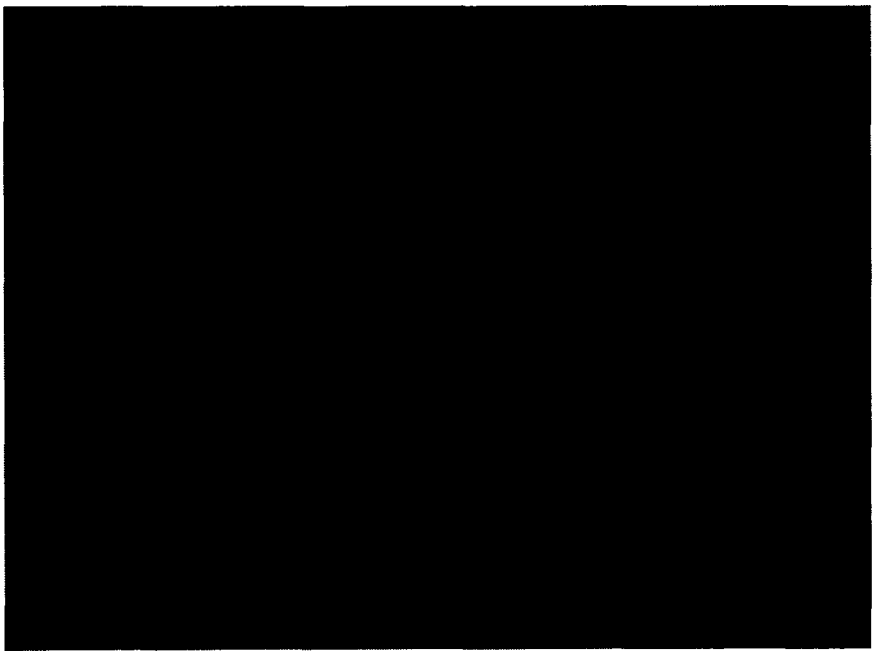

Figure A3.1. Dynamic image of periosteal callus (10x) illustrating areas of single calcein and tetracycline label as well as one bone surface on which double label has been incorporated into the tissue; MS would be calculated as the sum of the lengths of single label plus the length of double label normalized to the amount of bone surface in this ROI (the latter is measured in stained slides: MAR would be calculated by quantifying the average difference between surfaces on which both tetracycline and calcein label has been incorporated divided by the time difference (in days) between which those labels were administered; BFR in this ROI would be the product of the quantified MS and MAR (MS*MAR); as an example, the distance from 1-2 would be included as one of the lengths of double label in this ROI and used to quantify MS.

APPENDIX IV – SAS PROGRAM EDITORS FOR MECHANICS, RADIOGRAPHY & HISTOLOGY.

A.3.1. ONE-WAY ANOVA WITH DUNNETT'S POST-HOC MULTIPLE COMPARISON TEST. TORSIONAL BIOMECHANICS

```
options ls=74 ps=40 nodate;
data ultimatetorque;
input specimen $ treatment $ parameter $ torque (maxangle/stiffness/etc...)
datalines;
.
.
[ENTER DATA HERE]
.
.
;
proc glm data=ultimatetorque;
class treatment;
model torque = treatment;
lsmeans treatment/pdiff cl;
means treatment /lsd tukey snk regwq lines alpha = 0.05;
means treatment /dunnett ('A') alpha =0.05;
run;
```

A.3.2. ONE-WAY ANOVA WITH DUNNETT'S POST-HOC MULTIPLE COMPARISON TEST. RADIOGRAPHICAL ANALYSIS FOR COMPARISON OF CALLUS AREA QUANTIFIED WITH IMAGE J.

```
options ls=74 ps=40 nodate;
data callus;
input specimen $ treatment $ proxtot distaltot total;
datalines;
.
.
[ENTER DATA HERE]
.
.
;proc glm data=callus;
class treatment;
model proxtot = treatment;
lsmeans treatment/pdiff cl;
means treatment /lsd tukey snk regwq lines alpha = 0.05;
means treatment /dunnett ('A') alpha =0.05;
```

```
proc glm data=callus;
class treatment;
model distaltot = treatment;
lsmeans treatment/pdiff cl;
means treatment /lsd tukey snk regwq lines alpha = 0.05;
means treatment /dunnett ('A') alpha =0.05;

proc glm data=callus;
class treatment;
model total = treatment;
lsmeans treatment/pdiff cl;
means treatment /lsd tukey snk regwq lines alpha = 0.05;
means treatment /dunnett ('A') alpha =0.05;
run;
```

A.3.3. Initial Correlation Analysis. Correlating Torsional Biomechanics Data To Radiographical Callus Area Measurements.

```
options ls=74 ps=40 nodate;
data callus;
input specimen $ treatment $ proxtot distaltot total corticaldensity ultimatetorque angle
stiffness energy PCongruency DCongruency;
datalines;
.
.
[ENTER DATA HERE]
.
.
;
proc corr pearson;
var proxtot distaltot total corticaldensity ultimatetorque angle stiffness energy
PCongruency DCongruency;
run;
```

A.3.4. Uniaxial Compression/Diametral Compression One-Way ANOVA Followed By Post-Hoc Multiple Comparisons To Quantify Effects Of LAP Treatment On Graft Ultimate Force, Displacement and Strain At Failure.

```
data LAP;
input  trt $ force displacement strain;
datalines;
.
.
[ENTER DATA HERE]
.
.
;Proc print;
proc glm data=LAP;
class trt;
model force = trt;
means trt/lsd tukey snk regwq;
run;

proc glm data=LAP;
class trt;
model displacement = trt;
means trt/lsd tukey snk regwq;
run;
```

A.3.5. Decalcified Analysis. Non-Parametric Wilcoxon Test Comparing (-)CTL vs. (+)CTL. All Other Comparisons Use Same Code.

```
options ps=40 ls=74 nodate;
data histopath;
input  id Position $ trt $ Bridging CalType Interface PercCallus Vasc OBCHost
OBCGraft Inflam Viability;
cards;
.
.
[ENTER DATA HERE]
.
.
;
proc npar1way wilcoxon;
class trt;
var Bridging CalType Interface PercCallus Vasc OBCHost OBCGraft Inflam Viability;
run;
```

A.3.6. UNDECALCIFIED DYANAMIC ANALYSIS. ONE-WAY ANOVA FOLLOWED BY DUNNETT'S POST-HOC TEST COMPARING DYNAMIC PARAMETERS OF BONE FORMATION RATE (BFR), MINERALIZING SURFACE (MS) AND MINERAL APPOSITION RATE (MAR) QUANTIFIED IN PROXIMAL CALLUS. ALL OTHER COMPARISONS OF DYNAMIC PARAMETERS IN OTHER REGIONS OF INTEREST USE SAME CODE.

```
options ls=74 ps=40 nodate;
data dynamic;
input treatment $ ms mar bfr;
datalines;
.
.
[ENTER DATA HERE]
.
.
;
proc glm data=dynamic;
class treatment;
model bfr = treatment;
lsmeans treatment/pdiff cl;
means treatment /dunnett ('NegCTL') alpha =0.05;
run;
```

A.3.7. UNDECALCIFIED STATIC ANALYSIS. ONE-WAY ANOVA FOLLOWED BY DUNNETT'S POST-HOC TEST COMPARING STATIC PARAMETERS OF CALLUS AREA AND TRABECULAR THICKNESS.

```
data statichisto;
input animal trt $ location $   region $ calarea        trabth;
datalines;
.
.
[ENTER DATA HERE]
.
.
;
Proc print;
proc sort data=statichisto; by trt;
proc glm data=statichisto;
class location region ;
model calarea = location region location*region;
by trt;
lsmeans location*region/pdiff cl;
run;
```

```
proc sort data=statichisto; by trt location;
proc glm;
class region;
model calarea = region ;
by trt location;
run;

proc sort data=statichisto; by trt;
proc glm;
class region;
model calarea= region;
by trt;
run;
```

A.3.8. Final Correlation Analysis. Correlating Mechanical Parameters Quantified Using Torsional Biomechanics To Histological Analyses.

```
options ls=74 ps=40 nodate;
data callus;
input specimen $ treatment $ proxcallusarea distalcallusarea totalca corticaldensity
ultimatetorque maxangle stiffness energy PCongruency DCongruency PHMS PGMS
PCMS PHMAR PGMAR PCMAR PHBFR PGBFR PCBFR DHMS DGMS DCMS
DHMAR DGMAR DCMAR DHBFR DGBFR DCBFR;
datalines;
.
.
[ENTER DATA HERE]
.
.
;proc corr pearson;
var proxcallusarea distalcallusarea totalca corticaldensity ultimatetorque maxangle
stiffness energy PCongruency DCongruency PHMS PGMS PCMS PHMAR PGMAR
PCMAR PHBFR PGBFR PCBFR DHMS DGMS DCMS DHMAR DGMAR DCMAR
DHBFR DGBFR DCBFR;
run;
```

APPENDIX V – MTS TESTWARE-SX PROGRAM CODE.

A.4.1. TIBIAL TORSION –LEFT EXPERIMENTAL LIMBS.

PROCEDURE NAME = COUNTERCLOCKWISE (LEFT LIMBS) TORSION DEFAULT PROCEDURE
FILE SPECIFICATION = D:\TS2\TWSX\MTF_LIPUS_02-04\TIBIAL TORSION TESTING\COUNTERCLOCKWISE (LEFT LIMBS) TORSION.000
SOFTWARE VERSION = 4.0D
PRINTOUT DATE = 10/25/04 9:46:57 AM

DATA FILE OPTIONS
  FILE FORMAT = EXCEL TEXT FILE
  LOG EVENTS = YES
  INCLUDE PROCEDURE DESCRIPTION = NO

RECOVERY OPTIONS
  AUTOSAVE DISABLED.

TIBIAL TORSION_COUNTERCLOCKWISE(LT.) : STEP
  STEP DONE TRIGGER 1 = 12_DEGREES/S TORQUE

  PRE-TEST CHECK : OPERATOR EVENT
    START TRIGGER = STEP START
    END TRIGGER = ZERO TORQUE
    BUTTON ID = BUTTON 1
    SINGLE SHOT = YES
    BUTTON LABEL = CHECKLIST
    DESCRIPTION = HAVE YOU COMPLETED EVERYTHING ON THE CHECKLIST?
    GRAB FOCUS = YES

  ZERO TORQUE : OPERATOR EVENT
    START TRIGGER = PRE-TEST CHECK
    END TRIGGER = CORRECT PROGRAM
    BUTTON ID = BUTTON 1
    SINGLE SHOT = YES
    BUTTON LABEL = ZERO TQ.
    DESCRIPTION = HAVE YOU ZEROED THE TORQUE BEFORE STARTING?
    GRAB FOCUS = YES

  CORRECT PROGRAM : OPERATOR EVENT
    START TRIGGER = ZERO TORQUE
    END TRIGGER = TORQUE DATA COLLECTION
    BUTTON ID = BUTTON 2
    SINGLE SHOT = YES
    BUTTON LABEL = PROGRAM
    DESCRIPTION = ARE YOU RUNNING THE CORRECT PROGRAM? REMEMBER:
      CLOCKWISE = RIGHT LIMBS
      COUNTERCLOCKWISE = LEFT LIMBS
    GRAB FOCUS = YES

  TORQUE DATA COLLECTION : DATA ACQUISITION
    START TRIGGER = CORRECT PROGRAM
    END TRIGGER = <NONE>
    MODE = TIMED
    BUFFER TYPE = SINGLE

MASTER CHANNEL = TIME
SLAVE CHANNEL 1 = ANGLE
SLAVE CHANNEL 2 = TORQUE
DATA HEADER = TORGUE DATA @ 1000 HZ
TIME INCREMENT = 0.001 (SEC)
BUFFER SIZE = 16000

MAXIMUM ANGLE : DATA LIMIT DETECTOR
START TRIGGER = CORRECT PROGRAM
END TRIGGER = <NONE>
DATA CHANNEL = TORQUE
LIMIT VALUE = 50 N-M
LIMIT VALUE IS = ABSOLUTE
DETECTOR OPTIONS = GREATER THAN LIMIT VALUE
TRIGGER OPTION = TRIGGER ONCE

12_DEGREES/S TORQUE : MONOTONIC COMMAND
START TRIGGER = CORRECT PROGRAM
END TRIGGER = MAXIMUM ANGLE
SEGMENT SHAPE = RAMP
RATE = 12 (DEG/SEC)
TORSIONAL
CONTROL MODE = ANGLE SG
END LEVEL = -45 (DEG)

A.4.2. TIBIAL TORSION –RIGHT ICTL LIMBS.

PROCEDURE NAME = CLOCKWISE (RIGHT LIMBS) TORSION DEFAULT PROCEDURE
FILE SPECIFICATION = D:\TS2\TWSX\MTF_LIPUS_02-04\TIBIAL TORSION TESTING\CLOCKWISE (RIGHT LIMBS) TORSION.000
SOFTWARE VERSION = 4.0D
PRINTOUT DATE = 10/25/04 9:33:10 AM

DATA FILE OPTIONS
FILE FORMAT = EXCEL TEXT FILE
LOG EVENTS = YES
INCLUDE PROCEDURE DESCRIPTION = NO

RECOVERY OPTIONS
AUTOSAVE DISABLED.

TIBIAL TORSION_COUNTERCLOCKWISE(LT.) : STEP
STEP DONE TRIGGER 1 = 12_DEGREES/S TORQUE

PRE-TEST CHECK : OPERATOR EVENT
START TRIGGER = STEP START
END TRIGGER = ZERO TORQUE
BUTTON ID = BUTTON 1
SINGLE SHOT = YES
BUTTON LABEL = CHECKLIST
DESCRIPTION = HAVE YOU COMPLETED EVERYTHING ON THE CHECKLIST?
GRAB FOCUS = YES

ZERO TORQUE : OPERATOR EVENT

START TRIGGER = PRE-TEST CHECK
END TRIGGER = CORRECT PROGRAM
BUTTON ID = BUTTON 1
SINGLE SHOT = YES
BUTTON LABEL = ZERO TQ.
DESCRIPTION = HAVE YOU ZEROED THE TORQUE BEFORE STARTING?
GRAB FOCUS = YES

CORRECT PROGRAM : OPERATOR EVENT
START TRIGGER = ZERO TORQUE
END TRIGGER = TORQUE DATA COLLECTION
BUTTON ID = BUTTON 2
SINGLE SHOT = YES
BUTTON LABEL = PROGRAM
DESCRIPTION = ARE YOU RUNNING THE CORRECT PROGRAM? REMEMBER:
CLOCKWISE = RIGHT LIMBS
COUNTERCLOCKWISE = LEFT LIMBS
GRAB FOCUS = YES

TORQUE DATA COLLECTION : DATA ACQUISITION
START TRIGGER = CORRECT PROGRAM
END TRIGGER = <NONE>
MODE = TIMED
BUFFER TYPE = SINGLE
MASTER CHANNEL = TIME
SLAVE CHANNEL 1 = ANGLE
SLAVE CHANNEL 2 = TORQUE
DATA HEADER = TORGUE DATA @ 1000 HZ
TIME INCREMENT = 0.001 (SEC)
BUFFER SIZE = 16000

MAXIMUM ANGLE : DATA LIMIT DETECTOR
START TRIGGER = CORRECT PROGRAM
END TRIGGER = <NONE>
DATA CHANNEL = TORQUE
LIMIT VALUE = -5 N-M
LIMIT VALUE IS = ABSOLUTE
DETECTOR OPTIONS = LESS THAN LIMIT VALUE
TRIGGER OPTION = TRIGGER ONCE

12_DEGREES/S TORQUE : MONOTONIC COMMAND
START TRIGGER = CORRECT PROGRAM
END TRIGGER = MAXIMUM ANGLE

SEGMENT SHAPE = RAMP
RATE = 12 (DEG/SEC)
TORSIONAL
CONTROL MODE = ANGLE SG
END LEVEL = 45 (DEG)

A.4.3. UNIAXIAL COMPRESSION TO QUANTIFY EFFECTS OF LAP.

PROCEDURE NAME = PRELIMINARY_ALLOGRAFT_COMPRESSION DEFAULT PROCEDURE
FILE SPECIFICATION =
C:\WINNT\PROFILES\JNH22\DESKTOP\PRELIMINARY_ALLOGRAFT_COMPRESSION.000
SOFTWARE VERSION = 4.0D
PRINTOUT DATE = 3/17/06 5:41:40 PM

DATA FILE OPTIONS
  FILE FORMAT = EXCEL TEXT FILE
  LOG EVENTS = YES
  INCLUDE PROCEDURE DESCRIPTION = NO

RECOVERY OPTIONS
  AUTOSAVE DISABLED.

ALLOGRAFT COMPRESSION : STEP
  STEP DONE TRIGGER 1 = RAMP TO FAILRUE

  COLLECT COMPRESSION DATA : DATA ACQUISITION
    START TRIGGER = STEP START
    END TRIGGER = <NONE>
    MODE = TIMED
    BUFFER TYPE = CONTINUOUS
    MASTER CHANNEL = TIME
    SLAVE CHANNEL 1 = DISPLACEMENT
    SLAVE CHANNEL 2 = FORCE
    DATA HEADER = COLLECT COMPRESSION DATA (10 HZ)
    TIME INCREMENT = 0.1 (SEC)
    BUFFER SIZE = 16000

  RAMP TO FAILRUE : MONOTONIC COMMAND
    START TRIGGER = STEP START
    END TRIGGER = <NONE>
    SEGMENT SHAPE = RAMP
    RATE = 0.5 MM/MIN
    AXIAL
      CONTROL MODE = DISP SG
      END LEVEL = -5 (MM)

A.4.4. DIAMETRAL COMPRESSION TO QUANTIFY EFFECTS OF LAP/TAP.

PROCEDURE NAME = DIAMETRAL_ALLOGRAFT_COMPRESSION DEFAULT PROCEDURE
FILE SPECIFICATION = C:\WINNT\PROFILES\JNH22\DESKTOP\DIAMETRAL_ALLOGRAFT_COMPRESSION.000
SOFTWARE VERSION = 4.0D
PRINTOUT DATE = 3/17/06 5:41:13 PM

DATA FILE OPTIONS
  FILE FORMAT = EXCEL TEXT FILE
  LOG EVENTS = YES
  INCLUDE PROCEDURE DESCRIPTION = NO

RECOVERY OPTIONS
  AUTOSAVE DISABLED.

ALLOGRAFT COMPRESSION : STEP
STEP DONE TRIGGER 1 = RAMP TO FAILRUE

COLLECT COMPRESSION DATA : DATA ACQUISITION
START TRIGGER = STEP START
END TRIGGER = <NONE>
MODE = TIMED
BUFFER TYPE = CONTINUOUS
MASTER CHANNEL = TIME
SLAVE CHANNEL 1 = DISPLACEMENT
SLAVE CHANNEL 2 = FORCE
DATA HEADER = COLLECT COMPRESSION DATA (10 HZ)
TIME INCREMENT = 0.5 (SEC)
BUFFER SIZE = 16000

RAMP TO FAILRUE : MONOTONIC COMMAND
START TRIGGER = STEP START
END TRIGGER = <NONE>
SEGMENT SHAPE = RAMP
RATE = 0.5 MM/MIN
AXIAL
CONTROL MODE = DISP SG
END LEVEL = -5 (MM)